Wave propagation in non-uniform waveguides

Nielsen, Rasmus Bruus

Publication date:
2015

Document Version
Early version, also known as pre-print

Department of Mechanical and Manufacturing Engineering
Aalborg University, Denmark.

Wave propagation in non-uniform waveguides

Ph.D. Thesis

by

Rasmus Bruus Nielsen

Department of Mechanical and Manufacturing Engineering, Aalborg University
Fibigerstraede 16, DK-9220 Aalborg East, Denmark
e-mail: rn@m-tech.aau.dk

PREPRINT – April 11, 2015

ISBN 87-91200-78-4

Preface

This thesis has been submitted to the Faculty of Engineering and Science at Aalborg University in partial fulfilment of the requirements for the degree of Doctor of Philosophy in Mechanical Engineering. The underlying work has been carried out at the *Department of Mechanical and Manufacturing Engineering*, Aalborg University, during the period from September 2011 to December 2014. The work is a part of the research project entitled "Advanced Modelling of Wave Propagation in Spatially Curved Elastic Rods and Pipes" supported by the *The Danish Council for Independent Research, Technology and Production Sciences* (FTP) grant number UK 95 OS63822 PO83004. The financial support from FTP is gratefully acknowledged.

The project has been supervised by Professor, Ph.D., Dr. Sci., Sergey V. Sorokin to whom I owe my sincere gratitude. The endless number of discussions, hours of debugging, constructive criticism given to manuscripts, and the always enthusiastic attitude towards the work has been an absolutely essential support. A special thanks is addressed to Professor Nigel Peake and the *Waves Group* at *Department of Applied Mathematics and Theoretical Physics*, University of Cambridge, UK, where I spent three month as a visiting research student and who also appeared as a visiting professor on the project. The corporation with Professor Peake has resulted in a joint journal paper. Likewise, would I like to address my sincere gratitude to the two remaining visiting professors on the project: Professor Dmitrij Indejtsev (IPME RAS, Russia) and Professor Mike Brennan (UNEPS, Brazil) for the discussions during their stays, and in particular to Professor John Chapman for providing his expertise and the careful reading of manuscripts.

I would also like to thanks my fellow Ph.d. student and colleague Jonas Morsbøl for the joint journey through the land of wavenumbers, vibrations, Ph.D. courses, mathematics, etc. Also thanks to all other colleagues in the 3.2xx corridor for keeping a pleasant atmosphere over the last three years. To the rest of the colleagues at the m-tech department would I like to say thanks for the always entertaining lunch and coffee breaks, and department gatherings whether these have been Christmas or costume parties.

Finally, would I like to address my most sincere gratitude to my small family, Iben and Bodil, for their love and support which is appreciated beyond words.

Aalborg, January 2015

Rasmus Bruus Nielsen

Abstract

The purpose of the present work has been to investigate and develop methods for analysis and to gain understanding of wave propagation in non-uniform structures. The work is conducted with emphasis on extracting simple formulae predicting the wave propagation, to provide designers with simple tools applicable to achieve certain desired dynamic properties of a construction. Consequently, large parts of the project work have relied on asymptotic methods and perturbation techniques. The structures analysed are of slender geometries such as elastic beams and rods, and acoustic ducts.

The work is conducted within the framework of linear wave motion and apart from a minor study of transient effects is harmonic wave motion assumed throughout. Beams and rods are modelled by the plane cross section hypothesis, specifically have both the *Rayleigh model* and *Timoshenko model* been considered, and for simple axial wave motion is the *Bernoulli-Euler model* applied. These models are the low frequency (or long wave) asymptotic reduction of the elasto-dynamic model of a solid continuum, but of simpler mathematical form. The simplicity accompanying the plane cross section models are suited for gaining understanding of wave propagation.

Wave propagation in elastic beams and acoustic ducts of varying geometry is analysed by means of the *Wentzel-Kramers-Brillouin* (WKB) approximation which resolves the wave motion by summation of slowly varying modes. It is demonstrated how WKB solutions for modes experiencing a local cut-off break down in the vicinity of the cut-off location, and how a solution is established at this transition point. This analysis is conducted for acoustic waves in a circular flow duct with a smooth constriction. Floquet theory is employed to study periodicity effects of axial waves in a periodic Bernoulli-Euler rod. By perturbative investigation the locations of stop band borders are determined. Resonance criteria for a unit cell and its individual segments are formulated by means of the Phase-closure Principle, and these are compared to the location of stop bands borders.

Eigenfrequencies for straight and curved beams of varying diameter are determined by specialising the WKB solutions to various boundary conditions. A failure criteria linking wavelength to waveguide variation is established and the influence of modal participation is discussed. It is found that there is an appreciable overlap of validity ranges between the short wave WKB method and the long wave plane cross section hypothesis.

The analysis of wave cut-off in the acoustic flow duct yields the reflection

and transmission coefficient for waves reflecting and passing through the constriction. This enables the determination of the acoustic field at any location. Acoustic fields are provided with and without a mean flow.

The band gap structure determined from the Floquet analysis of the periodic rod is discussed and linked to the waveguide parameters. The explicit dependence of stop bands on impedance mismatch between the segments in a unit cell is demonstrated. It is furthermore demonstrated that several resonance criteria for a unit cell and its basic constituents corresponds directly to the location of features in the band gap structure. Some physical interpretations of the results are lastly discussed.

As concluding remarks the contributions and impact of the work is summarised and discussed. Direct extensions of the work presented in the papers as well as combination of methods presented in the papers are finally suggested in a future work section.

Dansk Resumé

Formålet med nærværende afhandling har været at undersøge og udvikle metoder til, at analysere og opnå forståelse for bølgeudbredelse i ikke-uniforme strukturer. Arbejdet er udført med fokus på at udlede simple formler til forudsigelse af bølgeudbredelse og derved opnå let anvendelige designredskaber til frembringelse af ønskede dynamiske egenskaber af en konstruktion. Af disse årsager har store dele af projektet været baseret på asymptotiske metoder og perturbations teknikker. Typen af konstruktioner der analyseres har alle slanke geometrier, såsom elastiske bjælker og stænger, samt akustiske kanaler.

Arbejdet er udført indenfor den lineær elasticitets teori og med undtagelse af et mindre studie af transiente effekter, antages harmonisk bølgebevægelse gennem hele afhandlingen. Bjælker og stænger modelleres ved hjælp af hypotesen for plane tværsnit, specifikt anvendes både *Rayleigh modellen* og *Timoshenko modellen*, og til simple aksiale bølger anvendes *Bernoulli-Euler modellen*. Disse er de lavfrekvente asymptotiske simplificerede modeller af den elasto-dynamiske model for et kontinuum, og de er af simplere matematisk karakter. Enkeltheden forbundet med disse plane tværsnits-modeller er velegnet til at opnå indblik i bølgeudbredelse.

Bølgeudbredelse i elastiske bjælker og akustiske kanaler med varierende geometri analyseres ved hjælp af *Wentzel-Kramers-Brillouin*-approksimationen hvorved bølgefeltet bestemmes ved summation af langsomt varierende modes. Det demonstreres hvorledes en sådan løsning bryder sammen i nærheden af en cut-off lokation, og yderligere hvorledes en løsning etableres ved denne lokation. Denne analyse gennemføres for akustiske bølger i en cylindrisk flow kanal med en glat indsnævring. Endvidere anvendes Floquet teori til analyse af periodicitetseffekter af aksiale bølger i en periodisk Bernoulli-Euler stang. Gennem en perturbations analyse explicitte udtryk for bestemmelse af stop bands grænserne. Resonanskriterier for en enkelt periodisk celle, samt dennes individuelle bestanddele, formuleres ved hjælp af *Phase-closure Princippet*, og disse sammenlignes med stop band grænserne.

Egenfrekvenser for lige og krumme bjælker med varierende diameter bestemmes ved, at specialisere WKB løsninger til forskellige randbetingelser. Et fejlkriterium der forener bølgelængde og bjælkens geometri etableres og betydningen af modalblanding diskuteres. Der observeres et tilfredsstillende overlap mellem pålidelighedsregimerne for den kortbølgede WKB metode og den langbølgede plane tværsnits-model.

Analysen af bølger med et cut-off i en akustisk flow kanal fører til bestem-

melse af refleksions- og transmissionskoefficienterne for bølger der passerer kanalens indsnævring. Ved hjælp af disse kan det akustiske felt bestemmes i et arbitrært punkt i kanalen. Eksempler på akustiske felter gives med og uden et middel flow.

Mønsteret af stop bands i frekvensbåndet bestemt fra Floquet analysen diskuteres og sammenhængen mellem dette mønster og stangens parametre forklares. Endvidere demonstreres det hvorledes disse stop bands afhænger af impedans forskellen mellem bestanddelene i en periodisk celle. Det demonstreres ligeså at adskillige resonanskriterier for en periodisk celle samt dennes individuelle bestanddele besidder en direkte sammenhæng med lokationen af forskellige karakteristika i frekvensbåndet. En fysisk fortolkning af resultaterne gives slutteligt.

Som konklusion opridses og diskuteres bidragene og deres potentielle betydning. Direkte udvidelser af analyserne præsenteret i artiklerne, og kombinationer af disse, uddybes slutteligt i et perspektiverende afsnit.

Mandatory pages

Thesis Title
Wave propagation in non-uniform waveguides

Name of Ph.D. Student
Rasmus Bruus Nielsen

Supervisor
Sergey V. Sorokin
Professor, Dr. Sci, Ph.D.
Department of Mechanical and Manufacturing Engineering
Aalborg University

Publications in refereed journals

- Nielsen R.B, Sorokin S.V. (2014): "The WKB approximation for analysis of wave propagation in curved rods of slowly varying diameter" *Proceedings of the Royal Society A*
- Nielsen R.B, Peake N. (*to be submitted*): "Tunnelling effects of waves in acoustic flow ducts" *Journal of Sound and Vibration*
- Nielsen R.B, Sorokin S.V. (*under review*): "Periodicity effects of axial waves in elastic compound rods" *Journal of Sound and Vibration*

Publications in proceedings and monographs with review

- Nielsen R., Sorokin S.V. (2012): "The WKB approximation for wave propagation in corrugated and spatially curved elastic rods", *Book of Abstracts, EUROMECH Colloquium 540*, Prague, Czech Republic, October, 2 pages
- Nielsen R., Sorokin S.V. (2013): The WKB approximation and periodicity effects for perturbed helical springs, *Book of Abstracts, 4th International Conference on Computational Methods in Structural Dynamics and Earthquake Engineering*, Kos, Greece, June, 1 page
- Nielsen R.B. (2013): "The WKB method for analysis of waves in curved rods", *Book of Abstracts, 11th International Conference on Vibration Problems*, Lisbon, Portugal, September, 1 page.

This thesis has been submitted for assessment in partial fulfillment of the PhD degree. The thesis is based on the submitted or published scientific papers which are listed above. Parts of the papers are used directly or indirectly in the extended summary of the thesis. As part of the assessment, co-author statements have been made available to the assessment committee and are also available at the Faculty. The thesis is not in its present form acceptable for

Contents

Chapter 1

Introduction

1.1 Waves and Vibrations

Vibrations and waves are unavoidable phenomena in everyday life and are as pleasant and enjoyable just as much as a source of problems, annoyance, and potentially danger. Mechanical vibrations is a topic which has interested mankind ever since the first stringed instruments were made around 3000 B.C. [Rao, 2004]. The development of knowledge about vibrations has throughout history involved many of the greatest scientists such as Galilei, Newton, Bernoulli, Euler, Lagrange, Rayleigh, etc. Today, the vast majority of technology driven companies producing parts of or complete mechanical systems are likely to have *Noise, Vibrations, Harshness-* or *NVH*-engineers employed. The tasks for a NVH-engineer span from detecting sources of vibrations and measuring vibration levels to provide design changes that eliminates the source or isolates it from the surroundings. To accomplish such tasks a continuous effort must be payed to develop high quality measurement equipment, easy-to-use and accurate computational methods to analysed structural vibrations and gain understanding of wave formation, interaction, and propagation.

The present work focusses on vibrations conveyed through slender waveguides such as beams, rods, and acoustic ducts. The main topic is to study the effect of non-uniformity on wave propagation and wave attenuation. Beams, rods, and ducts appear in various types of machinery where they serve some purpose, e.g. static, but meanwhile convey undesirable vibrations and noise.

Undesirable mechanical vibrations appear in machinery found almost everywhere in the modern world. Vibrations may be the source to disastrous structural failure caused by fatigue in, for instance, machinery with rotating imbalances like turbines, impellers, generators or shafts. Likewise is fatigue failure of oil and gas risers a challenge that occupy design engineers around the world. Some illustrations of vibration sensitive applications are provided in Figure 1.1. The aspect of undesirable noise transmission is relevant in a vast variety of every day situation. In civil transportation (cars, trains, planes etc.), domestic pumps and pipe systems, compressors in fridges and freezers, or ventilation ducts are well-known examples of such applications. Beams and rods play a central role in vibration and noise transmission in these kinds of applications as they are the basic constituents in many suspension systems, e.g. helical springs or spiralling springs. To account for noise transmission

Figure 1.1: Structures that usually involve vibrations. Top left: curved oil risers, [http://subseaworldnews.com/]. Top right, turbine wheel, [http://met-tech.com/]. Bottom row: a reciprocating compressor from a refrigerator shown with and without hermetic shell and a close up of the suspension on which the motor is resting, Courtesy of *Secop*.

and vibrations while designing such machinery it is essential for the designer to have simple and easily applied relations available to predict the structural response.

1.2 Methodology

With the advent of modern computers alongside with the powerful numerical analysis packages available, for instance those based on the Finite Element Method (FEM), detailed analysis of complex structures is possible and has been so for a few decades. Obvious advantages hereof are the ease, flexibility, accuracy and typically short analysis time needed to run a harmonic analysis of a complex construction. A disadvantage of this computational approach is the lack of insight in underlying mechanisms and physics involved in the problem. In particular is the influence of parameters to the solution typically not apparent. Consequently, the analyst is often left to parameter studies and intuition to iterate a design towards the goal.

For these reasons are the work presented in this dissertation conducted with an emphasis on more traditional analytical, 'pen&paper' approaches. The goal of this is to understand wave propagation, wave attenuation, and energy transportation, and to provide useful relations to design engineers that allow them to base a 'silent design' on simple formulae and insight, and thereby cut down on the amount of computation based analysis in the design process. Furthermore, it is of scientific interest to gain as much knowledge of the wave phenomenon in general.

A key feature of establishing analytical solutions, whether approximate or exact, is the availability of models appropriate for doing so. Thus, a model

should retain just the essentials in a problem and consequently neglect the non-essential and avoidable details. This concerns both the model of the problem as well as the method employed. Thus, this deliberation is conveniently summed up by stating that the overall approach should follow a "*Everything should be made as simple as possible, but not simpler*"-strategy. A quote typically attributed to Einstein.

Analysis of harmonic waves in beams, rods, and acoustic ducts traditionally fall into the category of 'manageable problems' in the framework of analytical methods. This is indeed the case when these are uniform. What is explored through the work presented in this thesis is, as mentioned already, the influence of non-uniformity on wave propagation. Unlike the uniform waveguides, dynamics of a non-uniform waveguide most often constitute a very difficult, if not impossible, problem or it may call for methods that only provide the desired result implicitly. The cause of the increased complexity is of mathematical nature and specifically pertains to the differential equation governing the problem. The increased complexity in solving a wave equation representing a non-uniform waveguide naturally leads to a solution with different properties compared to its uniform counterpart. Solutions of such wave equations involve wave modulations, multiple internal reflections, altered energy transmission properties, etc. All are examples of phenomena which are difficult to handle in the framework of traditional harmonic analysis, but also are they examples of desirable properties in the pursuit of gaining control over wave propagation as such. These matters are naturally discussed in much more detail throughout the thesis.

1.3 Categorisation of non-uniformity

Non-uniform waveguides can be thought of as waveguides having location dependent properties. The non-uniformity can be alterations in geometric features such as changes in cross sectional dimensions, changes in curvature, or it can be local inertial attachments, evenly spaced supports, and so on. Likewise, can a multi-material compositions constitute a non-uniform waveguide.

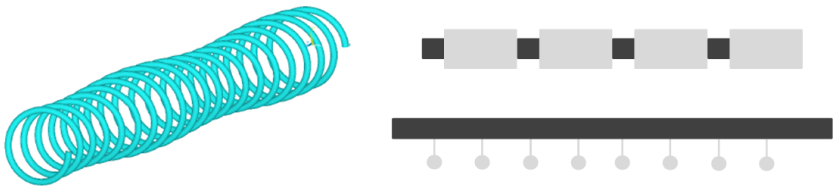

Figure 1.2: Examples of non-uniformity. Left: A helical spring with gradually changing diameter. Top right: Two component beam or duct. Bottom right: A uniform beam with local inertial attachments.

Whether the non-uniformity relates to geometrical or material changes there is another important aspect of its presence. Namely, if the variation is gradual, abrupt, or possibly a mix. I.e. does the change happen gradually and smoothly or is the transition sharp and abrupt? Some examples of non-uniform waveguides are shown in Figure 1.2. How the wave propagation is affected by the

non-uniformity, naturally depends highly on how the non-uniformity has been defined. It is this link between non-uniformity and effect on wave propagation which is studied throughout the thesis.

1.4 Overall Objectives

The overall goal of this Ph.D. project is to gain understanding of how wave propagation in slender waveguides is affected by non-uniformity and, ultimately, to gain some control over the wave propagation. The three following key objectives are selected as study cases:

1. Study methods to predict the propagation of waves in gradually changing waveguides and its physical significance, numerical performance and validity range.

2. Investigate how wave attenuation and reflection occurs in gradually changing waveguides.

3. Investigate the wave cancellation mechanism in abruptly changing periodic waveguides and how the presence of band gaps can be predicted.

It is expected that these three key objectives lead to a palette of useful knowledge, formulae and conclusions helpful to engineers and designers dealing with wave propagation in non-uniform structures.

1.5 Outline of thesis

The remaining part of the thesis is organised in three main chapters appended by the three journal papers.

Chapter 2 provides a brief overview of methods applicable to model wave propagation in gradually and abruptly changing waveguides. This overview is followed by three sections which give a more technical introduction to the techniques employed. Each of these three sections are closely related to the three objectives in section 1.4.

Chapter 3 briefly summarises the main findings and conclusions from the three papers.

Chapter 4 concludes the thesis and discusses aspects of future work.

The three scientific journal papers are included in the appendices.

Chapter 2

Introduction to the research area

In this chapter an overview and some introductory details of the topics employed in the project are given. The first sections of the chapter concerns two short reviews of the existing literature. This is followed by three more technical sections each are closely related to the three project objectives stated in the previous chapter. In each section is a short description of the background of the theory provided alongside with some essential details relating specifically to the application of the theory in the papers.

It is expedient firstly to discuss in a bit more detail the challenges of studying wave propagation in non-uniform waveguides. This shall be done within the framework of linear, stationary, time-harmonic problems, which is the setting for almost all of the work presented throughout the thesis. The root course of the difficulty in predicting waves in a non-uniform waveguide is due to non-constant coefficients in the governing differential equations. A canonical one-dimensional non-uniform wave equation represented in the frequency domain is:

$$\frac{d^2\phi}{dx^2} + p^2(x,\omega)\phi = 0 \tag{2.1}$$

where ω is the frequency. The non-uniformity presents itself through the x dependence of p. This equation represents a class of problems, for instance is the equations governing axial waves in a rod or flexural waves in a string reducible to this equation. Other problems in dynamics of non-uniform waveguides, like propagation of flexural waves in beams, are governed by higher order differential equations with varying coefficients as well. Despite, the fact that (2.1) is linear there exist no general way of finding an exact solution to it. The standard procedure to solve such an equation, i.e. by the exponential form $\phi \propto \exp(\mathrm{i}kx)$, fails because the constant k becomes x dependent, and therefore is not a solution. Consequently, large parts of the work presented in this thesis are concerned with describing the solution to this family of equations. Throughout the thesis is a temporal dependence $\exp(-\mathrm{i}\omega t)$ assumed, thus, positive wavenumbers represent positive going waves and negative wavenumbers represent negative going waves.

2.1 Overview

2.1.1 Gradually changing waveguides

The amount of literature existing on wave propagation in non-uniform beams, rods and ducts bear witness to the intense interest paid to this class of problems. A definite way of studying dynamics of non-uniform waveguides is by variational methods such as the *Ritz* or by *Galerkins* method. Whether conducted numerically by for instance the FE method or in some semi-analytical manner this is a versatile approach that typically performs well with regards to accuracy. It does not, however, constitute an appropriate setting to gain much understanding of wave propagation. The main focus is therefore turned to alternative methods.

An immediate approach is to state a problem which leads to a governing equation that can be solved exactly. I.e. to select the non-uniformity corresponding to some $p(x, \omega)$, in equation (2.1), which causes the equation to be exactly solvable. Such considerations are presented in [S.Abrate, 1995] who pursues potential cross sectional variation of rods and beams allowing for exact solutions. [Kumar and Sujith, 1997] identifies further variations allowing for exact solutions of axial vibrations of rods. In spite of the convenience of knowing the exact solution this approach is regarded as less attractive since it lacks a basic flexibility, as solutions must be derived for any possible variation of $p(x, \omega)$.

Various attempts on using asymptotic analysis to predict wave propagation in varying waveguides are likewise found in the literature. [Lenci et al., 2013] uses the Poincaré-Lindstedt technique to determine eigenfrequencies of tapered beams. [Krylov and Sorokin, 1997] used the *Method of Multiple Scaled* to study the modulations of wave amplitudes in a beam with spatial-temporal changing bending stiffness, and identified a dependence leading to wave attenuation. In acoustics similar approaches have been reported which typically employs the short wave based *Wentzel-Kramers-Brillouin* (WKB) approximation. In particular are the following references of interest: [Rienstra, 1999], [Rienstra, 2003], [Cooper and Peake, 2001], [Cooper and Peake, 2002], [Brambley and Peake, 2008], and [Ovenden, 2005]. These papers demonstrate how the WKB method may be used to predict wave propagation and internal wave reflection in ducts with and without flow, ducts of arbitrary cross section, ducts with swirling flow, and curved ducts with flow. The technique is therefore regarded attractive as a method in correlation to the project objectives stated in section 1.4.

Even though the WKB method originally was developed to celestial mechanics, it has gained its huge acceptance in quantum mechanics to predict motion and tunnelling of particles, see [Froman and Froman, 2004], [Heading, 2013], and [Bender and Orszag, 1978]. The method has become popular in acoustics due to its ability to handle waves in ducts of varying properties in the short wave limit. There is, however, only a small amount of literature on the WKB method applied to elasticity problems such as beams and rods. Pierce [1969] has derived WKB solution to slowly varying Bernoulli-Euler and Timoshenko beams in a somewhat untraditional fashion. [Rosenfeld and Keller, 1975] investigated a similar problem, but in the framework of elastodynamics. Common for these references is that they do not investigate the

numerical performance of the method. In a more recent publication [Firouz-Adabi et al., 2007] some focus is given to numerical accuracy of the WKB solutions when used to determine eigenfrequency of a tapered Bernoulli-Euler beam by comparing results to reference solution. It does not seem, however, that the authors acknowledge the basic assumption of the method being that the waveguide must be slowly varying.

The work presented in *Paper 1* and *Paper 2* are set out to apply the WKB methods to slowly varying beams and to study how the method predicts wave attenuation in a slowly varying acoustic duct.

2.1.2 Abruptly changing waveguides

Periodic structures are an important and much studied class of abruptly changing waveguides. The applicability of *Floquet theory* to dynamics of such structures allows for an efficient handling of the periodic non-uniformity. Moreover, it is known that periodicity in waveguide properties may lead to wave attenuation. Periodicity effects and periodic structures therefore constitute the main topic of this last part of the research area. The classical reference on wave propagation in periodic structures is the book by Brillouin [1946] who demonstrates the many possible realms of physics in which periodic waveguides have been studied. Brillouin [1946] also provides a historical survey of the topic starting from some of the very first mechanical and electrical periodic lines supporting wave propagation. The potential outcome of studying waves in periodic structure is the appearance of band gaps on the frequency axis. Band gaps are frequency ranges where waves cannot propagate through the structure and is consequently denoted *stop band*. Frequency ranges which are not stop bands are *pass bands*.

Periodic waveguides may consist of continuous segments, e.g. beams, rods, plates, and shells assembled in a periodic pattern, or it may consist of lumped constituents, e.g. point masses connected by springs and dampers. Lumped systems are likewise of relevance in electrical engineering as periodic series of capacitors, resistors, and coils, see [Brillouin, 1946], who also illustrates the relevance of periodicity in mechanical vibrations in rows of diatomic molecules which also are modelled by lumped constituents. [Jensen, 2003] investigated waves in rows and lattices of point masses and springs, and considers implications such as damping and imperfections. Continuous periodic systems have likewise received a lot of attention due to the many practical industrial applications. A comprehensive review of various periodic continuous structures is given in [Mead, 1996].

Some very interesting applications of periodicity effects have emerged in a combination with the modern numerical techniques. An example is Søe-Knudsen [2011] who uses numerical shape optimisation on a planar curved beam structure to design a mechanical filter with stop bands in a specified frequency range. A somewhat reversed study is reported by [Olhoff et al., 2012] who performed shape optimisation of simply supported and cantilevered beams to maximise eigenfrequency gaps (which is closely related to band gaps, see [Mead, 1970]) and observed how a periodic geometry resulted from the optimisation. In [Jensen and Pedersen, 2006] is the similar problem treated, but with the use of topology optimisation of multi-material rods.

In view of the above mentioned references it is deemed that introducing periodicity to a waveguide is an appealing way of gaining control over wave propagation and attenuation. The work presented in *Paper 3* is set out to identify simple ways of achieving this control.

2.2 The WKB approximation

As mentioned in subsection 2.1.1 the WKB approximation is applicable to equations like (2.1) provided that the properties of the waveguide is slowly varying. This is stated more formally as $p = p(\epsilon x, \omega)$ where x is a dimensionless coordinate and ϵ is a small parameter defined as the ratio of the local cross wise dimension and the length scale over which the properties of the waveguide varies appreciably. I.e. the local cross sectional length scale is small compared to the length scale over which the waveguide properties changes. Remark that such a statement does not necessitate small variations nor a specific functional form of p which is a huge advantage of the method.

The WKB solution can then be found by a summation of waves of the form, see Hinch [1991]:

$$\phi = \Phi(\epsilon x) \mathrm{e}^{\mathrm{i} \int_0^x k(\epsilon x') dx'} \tag{2.2}$$

It is noticed immediately that this is not a simple harmonic wave since the amplitude $\Phi(\epsilon x)$ and wavenumber $k(\epsilon x)$ are allowed to vary. To understand why (2.2) is a well suited solution guess a waveguide with slowly varying properties, as sketched in Figure 2.1, is considered. A number of adjacent segments are indicated in the figure. Since the waveguide varies slowly the properties within each of these segments are roughly constant and changes only by little from segment to segment. Consequently, a constant wavenumber, k_i, canbe attributed to each segment, and secondly, any reflections a wave experiences between two adjacent segments are neglected. Thus, a suitable exponential form of a wave propagating in such a waveguide can be stated by summation of the phase change in each segment, i.e.:

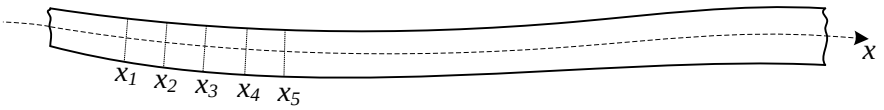

Figure 2.1: A waveguide, with curvilinear coordinate x, with slowly varying parameters such as cross section or curvature.

$$\mathrm{e}^{\mathrm{i}k_1(x_2-x_1)+\mathrm{i}k_2(x_3-x_2)+\cdots+\mathrm{i}k_m(x-x_{m-1})} = \mathrm{e}^{\sum_{i=1}^{m} \mathrm{i}k_i \Delta x_i} \tag{2.3}$$

It is clear that in the limit of thinner and thinner segments this can be stated as an integral:

$$\mathrm{e}^{\mathrm{i} \lim\limits_{\Delta x_i \to 0} \sum_{i=1}^{m} k_i \Delta x_i} = \mathrm{e}^{\mathrm{i} \int_0^x k(\epsilon x') dx'} \tag{2.4}$$

A similar interpretation is provided in Heading [2013]. This effectively demonstrates how the technique has earned its alternative name the *Phase-integral*

method. Notice, that in the above equation the wavenumber has been stated with the spatial dependence $k(\epsilon x)$. This must naturally be the case since the local waveguide properties varies with $p(\epsilon x)$.

In asymptotic or perturbation methods one usually employs a parameter, most often designated by ϵ, to keep track of the order of magnitude of the terms in an equation. So far has ϵ appeared in the argument of the waveguide parameters, and therefore is not a measure of the order of magnitude of terms, but rather is it a measure of the rate at which terms change. A convenient way of keeping track of what is large and what is small is by introducing the slow scale $X = \epsilon x$, see for instance [Hinch, 1991]. By the chain rule it is immediately obtained that $\frac{d}{dx} = \epsilon \frac{d}{dX}$, and therefore the governing equation should now be stated as:

$$\epsilon^2 \frac{\mathrm{d}\phi^2}{\mathrm{d}X^2} + p^2(X, \omega)\phi = 0 \tag{2.5}$$

The appropriate WKB anzats then have the form:

$$\phi(X) \sim \left(\Phi_0(X) + \epsilon\Phi_1(X) + O(\epsilon^2)\right) \mathrm{e}^{\frac{i}{\epsilon}\int_0^X k(X')dX'} \text{ as } \epsilon \to 0 \tag{2.6}$$

Here the amplitude Φ has been expanded in a series of ϵ. By introducing the concept of a slow scale X a WKB solution is derived by the formal procedure of perturbation methods. By inserting (2.6) into (2.5) and balance the largest terms, in this case order $O(1)$ terms, yields what in applied mathematics is commonly known as the *Eikonal equation* and in wave theory the *dispersion relation* which determines the slowly varying wavenumber $k(X)$:

$$\left(-k^2(X) + p^2(X, \omega)\right) \Phi_0 = 0 \tag{2.7}$$

and therefore $k(X) = \pm p(X, \omega)$. Proceeding to the next order, the $O(\epsilon)$ terms, yields

$$\left(-k^2(X) + p^2(X, \omega)\right) \Phi_1 = -2\mathrm{i}k(X)\frac{\mathrm{d}\Phi_0}{\mathrm{d}X} - \mathrm{i}\frac{\mathrm{d}k(X)}{\mathrm{d}X}\Phi_0 \tag{2.8}$$

The left hand side of this equation vanishes thanks to the dispersion relation, thus, Φ_0 is determined from a first order differential equation with variable coefficients:

$$-2\mathrm{i}k(X)\frac{\mathrm{d}\Phi_0}{\mathrm{d}X} - \mathrm{i}\frac{\mathrm{d}k(X)}{\mathrm{d}X}\Phi_0 = 0 \tag{2.9}$$

This is generally known as the *Transport Equation* and this particular equation has the simple solution $\Phi_0(X) = \frac{1}{\sqrt{k(X)}}$. Hence, the full solution is stated by a summation of right and left going waves:

$$\phi = \frac{\alpha}{\sqrt{p(X, \omega)}} \mathrm{e}^{\frac{\mathrm{i}}{\epsilon}\int_0^X p(X', \omega)dX'} + \frac{\beta}{\sqrt{p(X, \omega)}} \mathrm{e}^{-\frac{\mathrm{i}}{\epsilon}\int_0^X p(X', \omega)dX'} \tag{2.10}$$

where the constants α and β are to be determined from boundary conditions.

The first paper, *Paper 1*, treats the problem of wave propagation in non-uniform beams and discusses energy conservation properties of the WKB method. The

paper furthermore elaborates on the numerical performances and criterion for validity. Unlike the case considered in this section, i.e. a single second order wave equation with a varying coefficient, beams are governed by higher order differential equations, such as the Rayleigh beam, or systems of second order equation like the Timoshenko beam. This aspect of novelty is carefully addressed in the paper. Comments are given to details that have required special care in the work with the WKB method and non-uniform beams in the following subsection.

2.2.1 Notes on implementation and application

From the above example it is illustrated that a WKB solution presents itself as a linear combination of slowly varying modes. The constants appearing in front of these modes are to be determined from boundary conditions. Specialising a WKB solution to fulfil some boundary conditions is very similar to the uniform counterpart, and often involves taking derivatives of the solution. This is for instance the case when modelling zero bending moment or zero shear force. When taking derivatives a series of terms in increasing powers of ϵ is produced. It is important to notice that only those of $O(1)$ should be retained since the $O(\epsilon)$ terms has been neglected from the solution and therefore terms of such magnitude cannot be accounted for unless $O(\epsilon)$ terms were included in the solution as well.

The structure of the slowly varying amplitude typically involves $\sqrt{k(X)}$. This is indeed the case in the above example, but also the case in the problems treated in *Paper 1*. A potential complication arises when implementing such an expression and the dispersion relation is cumbersome. Even though such a cumbersome dispersion relation can be solved analytically the evaluation of wavenumbers may lead to small numerical errors. This causes problems when a wavenumber erroneous oscillates around the negative real axis with extremely small (say 10^{-10} or smaller) imaginary part. Due to the branch cut of the square root function along the negative real axis any such erroneous oscillation causes a sign change of the amplitude. A simple way of handling this problem is to replace imaginary parts of wavenumbers smaller than 10^{-10} by zero.

2.3 Asymptotic analysis of turning points

The WKB method as described in the previous section is based on the assumption of a small variation of the waveguide over a wavelength. It is clear that this assumption is violated if at some location the waveguide changes cause the wave to cut-off which corresponds to a local infinite wavelength. Such a cut-off location is called a *Turning Point* and can be analysed by asymptotic techniques. The turning point phenomenon has gained huge amount of attention from physicists since this is the quantum mechanical analogy to particle tunnelling. The following gives a short exposition of how a turning point is studied. This exposition follows directly from what is presented in the last subsection.

Consider a slowly varying waveguide governed by a wave equation like (2.5) and suppose that a wave is incident from left to the right, but cuts off at some

transition point designated by X_t. This means that $k^2 > 0$ for $X < X_t$ and vice versa. This situation is sketched in Figure 2.2. Away from this transition point, both up- and downstream, where the wavelength is sufficiently short the waves may be modelled by equation (2.10). These regions are indicated in Figure 2.2 as region *I* and region *III*, and the WKB solutions in these regions are:

$$\phi_I = \frac{\alpha_I}{\sqrt{k(X)}} \mathrm{e}^{\frac{\mathrm{i}}{\epsilon}\int_0^X k(X')dX'} + \frac{\beta_I}{\sqrt{k(X)}} \mathrm{e}^{-\frac{\mathrm{i}}{\epsilon}\int_0^X k(X')dX'} \tag{2.11}$$

$$\phi_{III} = \frac{\alpha_{III}}{\sqrt{k(X)}} \mathrm{e}^{\frac{\mathrm{i}}{\epsilon}\int_0^X k(X')dX'} \tag{2.12}$$

It is assumed that no wave is radiated from right in region *III* and furthermore that the amplitude of the incident wave α_I is known. In near proximity of the transition point, the WKB solutions break down. It is now demonstrated how to establish a solution valid close to X_t and how to knit this inner solution together with the outer WKB solutions by asymptotic matching. By matching are the coefficients β_I and α_{III} determined.

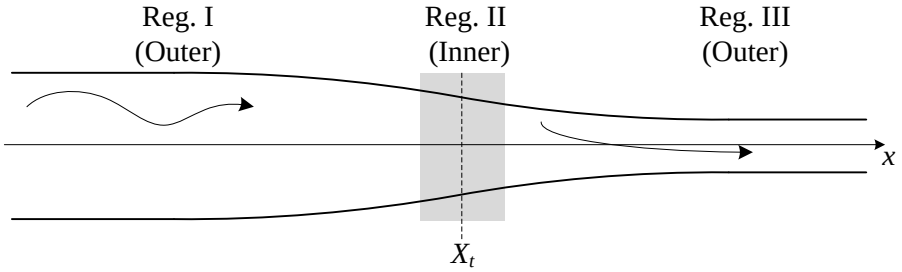

Figure 2.2: A waveguide of slowly varying properties with a cut-on/cut-off transitions point. A propagating wave is incident from left to right and becomes evanescent after the transition point X_t.

In the previous section the amplitude $\Phi_0(X)$ was determined from the transport equation and was found to be proportional to $1/\sqrt{k(X)}$ and consequently Φ_0 grows unboundedly as the wave approaches the cut-off location. The root cause of this problem is clearly seen from the transport equation:

$$2\mathrm{i}k(X)\frac{\mathrm{d}\Phi_0}{\mathrm{d}X} + \mathrm{i}\frac{\mathrm{d}k(X)}{\mathrm{d}X}\Phi_0 = 0 \tag{2.13}$$

Locations where $k(X_t) = 0$ changes the order of the transport equation and therefore is a singular point. This singular behaviour is due to the neglect of higher order terms that starts being significant as $k(X_t) \to 0$. Potential higher order terms are those of $O(\epsilon^2)$ obtained after inserting (2.6) into (2.5) and specifically reads:

$$\mathrm{i}\frac{\mathrm{d}k}{\mathrm{d}X}\Phi_1 + 2\mathrm{i}k(X)\frac{\mathrm{d}\Phi_1}{\mathrm{d}X} + \frac{\mathrm{d}^2\Phi_0}{\mathrm{d}X^2} \tag{2.14}$$

In order to regularise the transport equation one or more of these higher order terms must be introduced to it. This is an absolute key concept in turning

point studies, and therefore the following steps in the analysis are shown in detail. A scaled version of X is introduced and the scaling is selected such that some $O(\epsilon^2)$ terms are promoted to be as significant as the original terms in the transport equation. Before doing so, it is assumed that close to the turning point the wavenumber can be expanded by

$$k^2(X) \sim -c(X - X_t) \quad \text{as} \quad X \to X_t \tag{2.15}$$

where $c > 0$ is a constant. I.e. when $X < X_t$ $k(X)$ is real and the wave propagates and for $X > X_t$ $k(X)$ is imaginary so the wave is evanescent. A new scaled coordinate is now introduced:

$$\bar{X} = c^\gamma \epsilon^\alpha (X - X_t) \tag{2.16}$$

The strategy is to select α such that a higher order term from (2.14) is promoted to be of same order of magnitude as the $O(\epsilon)$ terms, i.e. the transport equation. Initially focus is given to the term $\frac{\mathrm{d}^2\Phi_0}{\mathrm{d}X^2}$. It will be shown later that the remaining terms in (2.14) in fact are negligible. For now this higher order term is added to the transport equation as it is:

$$2\mathrm{i}k(X)\frac{\mathrm{d}\Phi_0}{\mathrm{d}X} + \mathrm{i}\frac{\mathrm{d}k(X)}{\mathrm{d}X}\Phi_0 + \epsilon\frac{\mathrm{d}^2\Phi_0}{\mathrm{d}X^2} = 0 \tag{2.17}$$

Embedding (2.15) and (2.16) in this equation yields:

$$2\mathrm{i}c^{1/2+\gamma/2}\epsilon^{\alpha/2}(-\bar{X})^{1/2}\frac{\mathrm{d}\Phi_0}{\mathrm{d}\bar{X}} - \mathrm{i}c^{1/2+\gamma/2}\epsilon^{\alpha/2}(-\bar{X})^{-1/2}\Phi_0 + \epsilon^{1+2\alpha}c^{2\gamma}\frac{\mathrm{d}^2\Phi_0}{\mathrm{d}\bar{X}^2} = 0 \tag{2.18}$$

The important things to notice are that the first two terms, those originating from (2.13), are still of the same order, specifically $O(\epsilon^{\alpha/2})$. And furthermore, that these balance the latter term, which is $O(\epsilon^{1+2\alpha})$, provided that α is selected as:

$$\alpha/2 = 1 + 2\alpha \qquad \Leftrightarrow \qquad \alpha = -2/3 \tag{2.19}$$

It is furthermore noticed that selecting $\gamma = 1/3$ makes the c's cancel throughout the equation. What is left now is:

$$2\mathrm{i}(-\bar{X})^{1/2}\frac{\mathrm{d}\Phi_0}{\mathrm{d}\bar{X}} - \frac{\mathrm{i}}{2(-\bar{X})^{1/2}}\Phi_0 + \frac{\mathrm{d}^2\Phi_0}{\mathrm{d}\bar{X}^2} = 0 \tag{2.20}$$

I.e. on this new short inner scale $\bar{X} = \frac{c^{1/3}(X-X_t)}{\epsilon^{2/3}}$ the higher order term apparently is of the same order as the other terms in the transport equation. Remark, that the same rescaling applied to the terms containing Φ_1 in (2.14) leaves them at $O(\epsilon^{2/3})$ which is negligible compared to the terms in (2.20) being $O(\epsilon^{-1/3})$. This new version of the transport equation is further reducible with the help of an integrating factor $\Phi_0(\bar{X}) = B(\bar{X})\mathrm{e}^{g(\bar{x})}$ in order to eliminate first order derivatives. By choosing $g(\bar{X}) = -\mathrm{i}\int_0^{\bar{X}}\sqrt{-\bar{X}}d\bar{X}$ the equation conveniently reduces to:

$$\frac{\mathrm{d}^2B(\bar{X})}{\mathrm{d}\bar{X}^2} - \bar{X}B(\bar{X}) = 0 \tag{2.21}$$

This is *Airy's equation* and is one amongst the type of differential equations with non-constant coefficient to which exact solutions exist. Other examples of such equations are the *Bessel equation* and the *Parabolic Cylinder equation*. The general solution to the Airy equation is a linear combination of the two Airy function, see for instance [Bender and Orszag, 1978]:

$$B(\bar{X}) = c_1 \mathrm{Ai}(\bar{X}) + c_2 \mathrm{Bi}(\bar{X}) \tag{2.22}$$

So, apart from the two constants c_1 and c_2 the solution in the inner region is now known. These constants are determined from asymptotic matching to the outer WKB solutions, but before doing so the inner solution is simplified. The inner solution in terms of ϕ_{II} is:

$$\phi_{II} = \left(c_1 \mathrm{Ai}(\bar{X}) + c_2 \mathrm{Bi}(\bar{X})\right) \mathrm{e}^{g(\bar{X})} \mathrm{e}^{\frac{\mathrm{i}}{\epsilon}\int_0^X k(X')dX'} \tag{2.23}$$

It becomes evident that the eikonal part of the solution $\exp\left(\frac{\mathrm{i}}{\epsilon}\int_0^X k(X')dX'\right)$ cancels with the integration factor $\mathrm{e}^{g(\bar{X})}$ when the latter is expressed in terms of X rather than $\bar{X}$ and when the Taylor expansion in (2.15) is employed in place of $k(X)$. Furthermore, the function $\mathrm{Bi}(\bar{X})$ grows unbounded for large positive arguments which does not match the evanescent behaviour of the outer solution and consequently, $c_2 = 0$. What remains is simply:

$$\phi_{II} = c_1 \mathrm{Ai}(\bar{X}) \tag{2.24}$$

This must now be matched to the outer solution. The procedure for asymptotic matching is available from textbooks such as [Bender and Orszag, 1978] or [Hinch, 1991], and only a few details is given here. In short, the procedure is to write the inner solution in terms of the outer variable and expand it asymptotically for large arguments. Asymptotic expansions of special functions like the Airy functions are tabulated in compilations such as [Olver et al., 2010]. Expanding the inner solution, equation (2.24) yields:

$$\phi_{II} \sim \frac{c_1}{2\sqrt{\pi}} \frac{\epsilon^{1/6}}{c^{1/12}(X - X_t)^{1/4}} \mathrm{e}^{\frac{-2}{3}\frac{c^{1/2}}{\epsilon}(X - X_t)^{3/2}} \, , X \to \infty \tag{2.25}$$

Similarly, by taking the limit $X \to +X_t$ (i.e. approaching the turning point from the right) of ϕ_{III} the following is obtained:

$$\phi_{III} \sim \frac{\alpha_{III}\mathrm{e}^{-\mathrm{i}\pi/4}}{c^{1/4}(X - X_t)^{1/4}} \mathrm{e}^{\frac{-2}{3}\frac{c^{1/2}}{\epsilon}(X - X_t)^{3/2}} \, , X \to X_t \tag{2.26}$$

Apparently (2.25) and (2.26) has developed the same functional form and can be made exactly the same by selecting:

$$\alpha_{III} c^{-1/4} \mathrm{e}^{-\mathrm{i}\pi/4} = c_1 \frac{\epsilon^{1/6}}{2\sqrt{\pi} c^{1/12}} \tag{2.27}$$

In the exact similar fashion may two matching conditions be established by comparing terms after taking the limits of ϕ_{II} as $X \to -\infty$ and ϕ_I as $X \to -X_t$, respectively. From these two matching equations and (2.27) the unknown

constants can be determined:

$$\beta_I = \mathrm{e}^{\mathrm{i}\pi/2}\alpha_I \tag{2.28}$$

$$\alpha_{III} = \alpha_I \tag{2.29}$$

$$c_1 = \frac{2\pi^{1/2}\mathrm{e}^{\mathrm{i}\pi/4}}{\epsilon^{1/6}c^{1/6}}\alpha_I \tag{2.30}$$

This result admits the interpretation that the incident wave is fully reflected with a phase shift of $\pi/2$. Thus, the energy flux is blocked by the turning point. The example given here is amongst the simplest of its kind, but nevertheless outlines the approach in a turning point problem. Other kinds of turning point problems can be done by assuming another behaviour of k^2 around the transition point. This leads to another scaling of the inner region and consequently also another differential equation in the inner region.

Textbooks typically presents a slightly different approach for doing a turning point problem, see for instance [Bender and Orszag, 1978] and [Hinch, 1991]. Rather than attempting to promote higher order terms to the transport equation, they simply replace $p^2(X, \omega)$ in the differential equation (2.5) by its Taylor expansion around the turning point and from there arrive at Airy's equation. This approach appears somewhat simpler compared to the exposition given above, but this is only the case when tackling Schrödinger type equations, i.e. where the wavenumber appears directly in the governing differential equation. It is found through the work with more general problems such as turning points in beams and acoustic ducts that the approach presented in this section is by far the most instructive.

The second paper included in the thesis, *Paper 2*, treats the similar, but more advanced problem of acoustic waves travelling in a flow duct with a constriction and determines reflection and transmission coefficients, and a solution which is uniformly valid for all x. The waves undergo a cut-on/cut-off/cut-on transition, i.e. the waves tunnel through the constriction and become propagating again on the other side. In such a case it turns out that the inner region is governed by the *Parabolic Cylinder Equation*. Furthermore, the duct supports a slowly varying flow which also affects the acoustic field and consequently the wave equation to be solved includes convection.

2.3.1 Details on the matching procedure

Performing the asymptotic matching in the above turning point example did not require a lot of manipulations for the inner and outer solution to have the same functional form. This not the case in the two turning point problem studied in *Paper 2*. In the following it is demonstrated how an *intermediate variable* may be employed to identify negligible terms. The problem is specifically that the outer solution in the transmission region close to the rightmost turning point has a phase which is proportional to:

$$\frac{X}{2}\sqrt{X^2 - b} - \frac{b}{2}\ln\left(\frac{X - \sqrt{X^2 - b}}{\sqrt{b}}\right) \tag{2.31}$$

but the corresponding terms in the inner solution for large positive arguments is:

$$\frac{X^2}{2} - \frac{b}{2}\ln\left(\frac{2X}{\sqrt{b}}\right) \tag{2.32}$$

and therefore there is no apparent match between the two. The inner coordinate for the problem is denoted z and defined by $z = G\frac{X}{\epsilon^{1/2}}$ where G is some constant. An intermediate variable is now introduced $Y = \frac{X}{\epsilon^{\beta}}$ where $0 < \beta < 1/2$. I.e. Y lies between X and z and therefore helps estimating if any terms in (2.31) may be neglected. The outer solution with X replaced by Y and $b = \epsilon\bar{b}$, see *Paper 2* for details, is therefore:

$$\frac{Y^2\epsilon^{2\beta}}{2}\sqrt{1-\epsilon^{1-2\beta}\frac{\bar{b}}{Y^2}} - \frac{\epsilon\bar{b}}{2}\ln\left(\frac{Y\epsilon^{\beta}+Y\epsilon^{\beta}\sqrt{1-\epsilon^{1-2\beta}\frac{\bar{b}}{Y^2}}}{\sqrt{\epsilon\bar{b}}}\right) \tag{2.33}$$

By the binomial expansion this becomes

$$\frac{Y^2\epsilon^{2\beta}}{2} - \epsilon\frac{\bar{b}}{4} - \frac{\epsilon\bar{b}}{2}\ln\left(\frac{2Y\epsilon^{\beta}-\epsilon^{1-\beta}\frac{\bar{b}}{2Y}}{\sqrt{\epsilon\bar{b}}}\right) \tag{2.34}$$

Since β is strictly smaller $1/2$ then we notice that $2Y\epsilon^{\beta} >> \epsilon^{1-\beta}\frac{\bar{b}}{2Y}$ as $\epsilon \to 0$. Thus, (2.31) becomes:

$$\frac{X^2}{2} - \frac{b}{4} - \frac{b}{2}\ln\left(\frac{2X}{\sqrt{b}}\right) \tag{2.35}$$

which has the same X dependence as (2.32) and a matching condition can therefore be identified. The term $b/4$ corresponds to a constant phase shift.

As a last comment it is mentioned that to generate the results presented in *Paper 2* has it been necessary to implement the Parabolic Cylinder Function which have a few different definitions $U(a,z)$, $V(a,z)$, $D_\nu(z)$ and $W(a,x)$. The function $W(a,x)$ is the one needed. In the preferred software (*Mathematica*) the function $D_\nu(z)$ exists and by combining formulae from [Olver et al., 2010, ch. 12] a definition of $W(a,x)$ can be implemented.

2.4 Periodicity effects

The application of the theory of periodic waveguides employed is so limited that only very little introduction to this is needed. Consequently, is only a very short exposition of elementary Floquets theory given and focus is then turned to various other techniques employed in the research.

The theory of wave propagation in periodic structures typically concerns analysis of a structure composed of a number of segments of various structural members forming a *unit cell*. A number of consecutive unit cells form a periodic structure. If the individual segments are simple enough exact solutions are available to describe the wave motion in these. This is advantageous since a unit cell can be modelled by matching the individual segments at the internal

interfaces. The waveguide properties of the periodic structure are then obtainable by *Floquets theorem* which shall be introduced briefly in the following.

In short the Floquet theorem states that the solution to an ordinary differential equation with 2π periodic coefficients is, [Bender and Orszag, 1978]:

$$y(t) = \lambda y(t + 2\pi) \tag{2.36}$$

where λ is a propagation constant. It is the quantity λ that is of interest since it relates directly to wave attenuation. In the practical usage of the Floquet theorem waveguides of arbitrary period, say L, are typically studied.

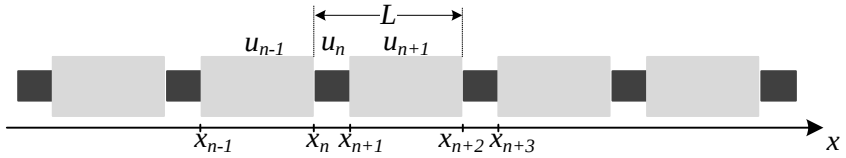

Figure 2.3: A periodic rod consisting of a number of unit cells of length L.

The work on periodicity effects in this thesis is applied to simple axial waves in a Bernoulli-Euler rod consisting of unit cells with segments of different properties. An illustration is provided in Figure 2.3. The result of applying the periodicity conditions is an eigenvalue problem leading to a characteristic equation which links the propagation constant λ to the frequency ω.

The simplicity of the model facilitates understanding the underlying mechanisms behind stop bands. Consequently, have much effort been given to establish relations between the propagation constant λ, waveguide parameters and frequency. It turns out that the use of non-dimensional scaling condenses the waveguide parameters to just two principal parameters, both having a clear physical meaning. These are the ratio of impedances and the ratio of propagation times of the two segments in a unit cell.

Parts of the study have been conducted as asymptotic analysis where expressions for stop band borders are derived by perturbing the impedance mismatches between the segments in the unit cell. This relies on the methodology of finding solution to algebraic equation containing a small parameter. A selection of illustrative examples on such problems are provided in [Hinch, 1991] and in [Bender and Orszag, 1978].

An important aspect of the dynamics of periodic structures is the link between the stop band borders and eigenfrequencies of the symmetric unit cell. This fact is discussed in [Mead, 1970] and it is recognised that the eigenfrequencies of the symmetric unit cell with borders fully fixed or free are located on the borders of the stop bands. This correspondence has been observed and commented on by other authors, but it does not appear to be very well understood. The work on periodicity effects applied to axial waves attempts to utilise this observation in the search for simple formulae useful to predict the band gap structure. To study this and other coherencies between resonances and periodicity effects have the *Phase-closure Principle* been utilised and found well suited. In the following is a simple exposition of the phase closure principle given. A more complete demonstration is provided by Mead [1994], who demonstrates how to derive eigenfrequencies of Bernoulli-Euler

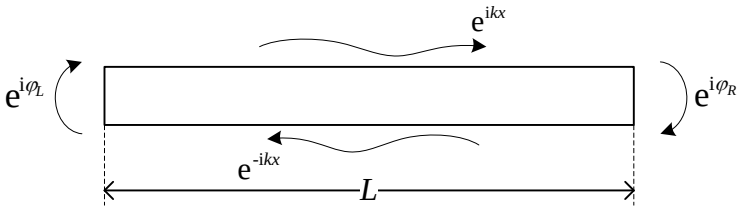

Figure 2.4: A finite length rod with indication of right and left going waves and reflections at the boundaries.

beams with various boundary conditions. By the phase closure principle the resonance condition is formulated via the phase change a wave experiences after completing a circuit in a finite length rod like the one shown in Figure 2.4. For simplicity the rod is assumed to support axial waves only. The complete phase change is found by summation of the phase change caused by traversing forth and back in the rod, which amounts to $2kL$, and the phase shifts from the reflections at the right and left boundaries, φ_R and φ_L, respectively. When the total phase change adds up to an integral multiple of 2π resonance occurs. Physically this corresponds to the wave returns back perfectly in phase with itself. Thus, we may state:

$$2kL + \varphi_R + \varphi_L = n2\pi \tag{2.37}$$

By designating the plane stress wave speed as c_0 and assuming free-free boundaries, i.e. $\varphi_R = \varphi = L = 0$, the above equation becomes:

$$2\frac{\omega}{c_0}L = n2\pi \quad \Rightarrow \quad \omega = \frac{n\pi c_0}{L} \text{ with } n = 0, 1, 2, 3, \ldots \tag{2.38}$$

This is also the expression given in [Rao, 2004]. In case either one or both of the boundaries were fixed φ_L and/or φ_R would be $-\pi$, and the eigenfrequencies would change accordingly. The phase closure principle is expedient in the case where the wave motion and the reflection at the boundaries are given by relatively simple expressions. I.e. where the frequency does not appear in the argument of, say, a trigonometric function in the expression for the phase change at the boundaries. It is demonstrated in [Mead, 1994] how the neglect of evanescent waves in a fully fixed Bernoulli-Euler beam leads to a very simple, yet very accurate, explicit formula for natural frequencies. Mead [1994] also demonstrates that with account of evanescent waves the well-known transcendental equation for eigenfrequencies quoted in standard textbooks are obtained by the phase closure principle.

Paper 3 is initiated from considerations about the fundamental cancellation mechanism behind stop bands, and a wish to establish some simple relations between waveguide properties and locations of stop and pass bands. It is for these reasons the very simple Bernoulli-Euler model for axial waves has been selected as the focal point of the paper. In the pursuit of these simple relations that perturbative analysis and the phase closure principle have been used. The results from here lead to the main conclusions in the paper. The paper lastly presents an analysis of steady-state and transients of a finite length

periodic rod. It is demonstrated how energy accumulates develops depending on whether excitation is done in a stop band, in a pass band, or at an eigenfrequency.

Chapter 3

Summary of results

This chapter gives a brief discussion of the main findings from each of the three journal papers that are part of the thesis. To each paper are reflections of potential extensions discussed and important limitations of the work are provided. This leads to reasoning on why the topic of the subsequent paper has been selected.

3.1 Paper 1

In this paper WKB solutions are derived in a systematic manner for a hierarchy of beam models of slowly varying diameter. The models are the Rayleigh beam, the Timoshenko beam, and a planar curved Timoshenko beam, governed by one, two, and three differential equations, respectively. The numerical performance of the solutions is tested by comparison to reference solutions and a validity criterion is presented.

It is found that apart from the location dependence of parameters the wavenumber is the same as in the unperturbed waveguide, and therefore this will typically be known in advance. This is a major advantage of the method since only little derivation is needed. Another important confirmation in the paper is that the variation of wavenumber and amplitude corresponds to energy conservation. I.e. a wave propagates with constant energy even though the wavenumber and amplitude varies.

From the approach demonstrated in the paper it is quite obvious how to derive WKB solutions for other beam structures such as beams of constant cross section, but with for instance slowly varying planar or spatial curvature. Such results are potentially of direct practical relevance in modelling of vibrations of suspension systems. The paper also demonstrates that the WKB method does not immediately lead to any wave attenuation. It merely gives a modulation of the wave. This is mainly the reason why the concepts of turning point analysis and tunnelling effects have been included as topics to be studied.

3.2 Paper 2

In this paper tunnelling of acoustic waves in a flow duct with a constriction is analysed. By asymptotic matching between outer WKB type solutions valid away from the constriction and an inner solution valid in the near vicinity of

the constriction expressions for reflections and transmissions coefficients are determined. A uniformly valid solution is furthermore derived and its correspondence to the composite solution is demonstrated.

The results are potentially important to engineers designing aero-craft engines since the results presented further enhance the opportunity to use multiple scales methods to determine the sound field through the duct. The response to any sound source can be determined by modal expansion and with the results presented in this paper the effect of modes tunnelling in the engine duct can now be accounted for.

The technique readily suggests how to tackle turning point problems in elasticity. In line with the models treated in *Paper 1* could this be cut-off of flexural waves in varying Bernoulli-Euler beams resting on an elastic foundation, shear wave cut-off in a varying Timoshenko beam, or turning points in beams of varying curvature. It is generally found that the technique behind turning point studies is advanced, but the results are general and therefore can be directly applied to various acoustic duct problems and moreover do they have a clear physical meaning. The methodology is, however, still considered as having limited potential as regards gaining control over wave propagation, since wave reflection or attenuation relies on the presence of cut-on/cut-off transition points. Thus, all modes of higher frequencies than that of the cut-on/cut-off mode will propagate past the transition point. Additional turning points should therefore be introduced to the waveguide to prevent these higher frequency modes from propagating. For these reasons, attention is turned to periodicity effects in the third paper.

3.3 Paper 3

In this paper various studies on axial waves in a periodic Bernoulli-Euler rod have been conducted. The focus is to understand the cancellation mechanism behind stop bands. This has been done by perturbative analysis of the eigenvalue problem from the Floquet analysis. The principle of phase closure is furthermore adopted and relations between resonance criteria and stop band locations are identified.

The results presented provide an easily understood overview of where stop bands are located depending on waveguide parameters, and consequently how parameters should be chosen to have stop bands in desired frequency ranges. The explanation of the stop band pattern and the formulae describing stop and pass band locations are considered so simple that these can be used actively in a design process. Despite these motivating findings should it be remembered that the similar knowledge for dispersive flexural waves is not available and therefore the results are likely insufficient for more general excitation condition. As a last comment should it also be noticed that if steel is selected as the material and the individual segment length are at maximum the order of a few meters then the first stop band is found at least at the kHz-level. In many practical applications this would indeed be a very high frequency, and there would likely be an interest to have stop bands at much lower frequencies.

3.4 Contribution and impact

The use of the WKB method to study curved Timoshenko beams of varying diameters and identifying the combination of validity criterion for multi-modal problems are definite contributions. To the authors knowledge no studies are reported treating such complex elastic beams which also contains a presentation of numerical performance. The generalised criterion for validity presented in the paper where both the small parameter ϵ and amount of variation of the waveguide also appears to be new. This leads to the key finding that an overlap of validity ranges exists between the plane cross section models and the WKB approximation. Consequently, it is confirmed that the WKB method is available to the analyst.

The research on tunnelling effects of acoustic waves propagating in flow ducts contributes to the pool of solutions available to predict noise transmission in for instance aero-craft engines. Thus, the results will potentially help engine designers to apply multiple scales methods to estimate the noise pollution, detect resonance from reflected waves, etc. The result may furthermore serve as an important benchmark solution to computational aero-acoustic codes. Finally, does the numerical result serve as an illustrative demonstration of tunnelling.

In paper 3 are explicit expressions given that very accurately describe the location of stop band borders at small and large impedance mismatches. To the author's knowledge this is the first time such a result have been presented for periodic waveguides consisting of continuous structural segments. The model is likely to primitive for the results to be practically applicable, but the methodology and the nature of the results may impact how periodic structures are analysed. In particular, similar results obtained for more complex waveguides will contribute to the ability to easily tailor the dynamic properties of a construction.

Chapter 4

Concluding remarks

The objectives of this work has been to investigate methods to predict wave propagation in various kinds of non-uniform waveguides, to gain insight in the underlying mechanism behind wave attenuation, and to identify simple relations between wave propagation and waveguide parameters. This has been done with a bias to use asymptotic and perturbative methods to retrieve dominant terms in solutions to wave equations. The work has been carried out within the framework of linear dynamics and specifically have acoustic flow ducts, non-uniform beams and periodic rods been considered.
A methodology to study waves in slowly varying beams is investigated with a subsequent test of numerical accuracy, and a criterion for validity is established. The special case of acoustic waves diminishing by tunnelling through narrow regions of evanescent wave motion in flow ducts is studied and reflection and transmission coefficients depending on tunnelling distance are derived. Finally, the cancellation mechanism behind stop bands is studied for axial waves in a periodic rod. It is discovered how resonance criteria for a unit cell and the individual segments correlate to the location of stop and pass bands. It is demonstrated how these locations can be found simply by the application of the phase closure principle.

Consequently, the overall objective of increasing the understanding of the effect of non-uniformity on wave propagation in slender waveguides is fulfilled.

4.1 Future works

An obvious extension on the topic of slowly varying beams would be to derive solutions similar to those presented in *Paper 1*, but for planar or spatial curvature in order to predict vibrations in for instance suspension systems made from curved beams of perturbed helical shape. In order to account for internal reflection of waves in such waveguides turning point analysis should be conducted. This will provide some, but limited options to control the wave propagation.

The analysis provided in *Paper 2* is an extension of the numerous studies of the one turning point problems handled in papers on flow duct acoustics published over the last few decades. These papers have advanced on several other fronts

compared to the setup up in *Paper 2*. For instance, the following challenging features are accounted for: arbitrary cross sectional shape of duct, transition from annular to hollow shape, and inclusion of a significant mean swirl. These extensions are as relevant to the two turning point problem as they are to the one turning point problem.

The concept behind turning point analysis presented in 2.3 is just as well applicable to varying beams and rods. A natural problem to study could be that of turning points of flexural waves in a Bernoulli-Euler rod resting on a Winkler foundation.

The work presented in *Paper 3* suggests many aspects of future work. An immediate extension would be to carry out the similar analysis for a unit cell of three or four different segments. This will likely lead to a more complex stop band pattern compared to that of *Paper 3*. The subsequent analysis of stop band borders, stop band pattern, and application of the phase closure principle will therefore be more challenging. It may, however, provide an option to push the first stop bands towards lower frequencies. A central assumption in *Paper 3* is the sole existence of non-dispersive waves and extending the analysis to included dispersive waves, such as flexural waves, is therefore highly relevant. In line with the suggestions for extensions made to *Paper 1*, it is certainly of interest to extend the results from *Paper 3* to unit cells with curved segments that conveys flexural, axial and torsional waves. The accessibility of results similar to those presented in *Paper 3* valid to such complicated periodic beams will likely provide a very powerful and relative easily applied tool to design of mechanical filters.

An interesting aspect of analysing periodic beam structures partly consisting of segments of gradually varying properties is now suggested. By the quite efficient approach to predict wave propagation in gradually varying beams presented in *Paper 1* and with the knowledge of internal reflection in line with the results presented in *Paper 2* these gradually varying segments can be analysed with relative ease. In particular, the phase changes the various waves experience when travelling in a segment are obtainable from the slowly varying dispersion relation. In *Paper 3* it is shown that this phase change is essential in the prediction of stop and pass band. If the analysis is extended successfully to study waveguides of such complexity, it will likely serve as a very powerful alternative to computational methods such as the FE method with an associated numerical optimisation routine.

References

C. M. Bender and S. A. Orszag. *Advanced Mathematical Methods for Scientists and Engineers*. Springer, 1978. ISBN 0-387-98931-5.

E. Brambley and N. Peake. Sound transmission in strongly curved slowly varying cylindrical ducts with flow. *Journal of Fluid Mechanics*, 596:387–412, 2008.

L. Brillouin. *Wave propagation in periodic structures*. Dover Publications, 1946.

A. J. Cooper and N. Peake. Propagation of unsteady distubances in slowly varying duct with mean swirling flow. *Journal of Fluid Mechanics*, 445:207–234, 2001.

A. J. Cooper and N. Peake. The stability of a slowly diverging swirling jet. *Journal of Fluid Mechanics*, 473:389–411, 2002.

R. D. Firouz-Adabi, H. Haddadpour, and A. B. Novinzadeh. An asymptotic solution to transverse free vibrations of variable-section beams. *Journal of Sound and Vibration*, 304:530–540, 2007.

N. Froman and P. O. Froman. *Physical Problems Solved by the Phase-Integral Method*. Cambridge University Press, 2004. ISBN 0-511-02995-0.

J. Heading. *An Introduction to Phase-Integral Methods*. Dover Publications, Inc, 2013. ISBN 0 486 49742 9.

E .J. Hinch. *Perturbation Methods*. Cambridge University Press, 1991. ISBN 0 521 37310 7.

J. S. Jensen. Phononic band gaps and vibrations in one- and two-dimensional mass-spring structures. *Journal of Sound and Vibration*, 266:1053–1078, 2003. doi: 10.1016/S0022-460X(02)01629-2.

J. S. Jensen and N. L. Pedersen. On maximal eigenfrequency separation in two-material structures: the 1d and 2d scalar cases. *Journal of Sound and Vibration*, 289:967–986, 2006.

V. Krylov and S. V. Sorokin. Dynamics of elastic beams with controlled distributed stiffness parameters. *Smart. Mater, Struct*, 6:573–582, 1997.

B. M. Kumar and R. I. Sujith. Exact solutions for the longitudinal vibration of non-uniform rods. *Journal of Sound and Vibrations*, 207:721–729, 1997.

S. Lenci, F. Clementi, and C.E.N. Mazzilli. Simple formulas for the natural frequencies of non-uniform calbes and beams. *International Journal of Mechanical Sciences*, 77:155–163, 2013.

D. J. Mead. Free wave propagation in periodically supported, infinite beams. *Journal of Sound and Vibration*, 11:181–197, 1970. doi: 10.1016/S0022-460X(70)80062-1.

D. J. Mead. Waves and modes in finite beams: Application of the phase-closure principle. *Journal of Sound and Vibration*, 171:695–702, 1994. doi: 10.1006/jsvi.1994.1150.

D. J. Mead. Wave propagation in continuous periodic structures: Research contributions from southampton, 1964-1995. *Journal of Sound and Vibration*, 190:495–524, 1996. doi: 10.1006/jsvi.1996.0076.

N. Olhoff, B. Nui, and G. Cheng. Optimum design of band-gap beam structures. *International Journal of Solids and Structures*, 49:3158–3169, 2012. doi: 10.1016/j.ijsolstr.2012.06.014.

F. W. J. Olver, D. W. Lozier, R. F. Boisvert, and C. W. Clark, editors. *NIST Handbook of Mathematical Functions*. Cambridge University Press, New York, NY, 2010.

N. C. Ovenden. A uniformly valid multiple scales solution for cut-on cut-off transition of sound in flow ducts. *Journal of Sound and Vibration*, 286:403–416, 2005.

A. D. Pierce. Physical interpretation of the wkb or eikonal approximation for waves and vibrations in inhomogeneous beams and plates. *Acoustical Society of America*, pages 275–284, 1969.

S. S. Rao. *Mechanical Vibrations*. PEARSON, Prentice Hall, 2004. ISBN 0-13-120768-7.

S. W. Rienstra. Sound transmission in slowly varying circular and annular lined ducts with flow. *Journal of Fluid Mechanics*, 380:279–296, 1999.

S. W. Rienstra. Sound propagation in slowly varying lined flow ducts of arbitrary cross-section. *Journal of Fluid Mechanics*, 495:157–173, 2003.

G. Rosenfeld and J. B. Keller. Wave propagation in nonuniform elastic rods. *Acoustical Society of America*, pages 1094–1096, 1975.

S.Abrate. Vibration of non-uniform rods and beams. *Journal of Sound and Vibrations*, 184:703–716, 1995.

A. Søe-Knudsen. Design of stop-band filter by use of curved pipe segments and shape optimization. *Struct Multidisc Optim*, 44:863–874, 2011. doi: 10.1007/s00158-011-0691-2.

Paper 1

Nielsen R.B, Sorokin S.V. (2014): "The WKB approximation for analysis of wave propagation in curved rods of slowly varying diameter", *Proceedings of the Royal Society A* **470**

PROCEEDINGS OF THE ROYAL SOCIETY A

rspa.royalsocietypublishing.org

The WKB approximation for analysis of wave propagation in curved rods of slowly varying diameter

Rasmus Nielsen and Sergey Sorokin

Department of Mechanical and Manufacturing Engineering, Aalborg University, Fibigerstraede 16, 9220 Aalborg, Denmark

Research

CrossMark click for updates

Cite this article: Nielsen R, Sorokin S. 2014 The WKB approximation for analysis of wave propagation in curved rods of slowly varying diameter. *Proc. R. Soc. A* **470**: 20130718. http://dx.doi.org/10.1098/rspa.2013.0718

Received: 29 October 2013
Accepted: 25 March 2014

Subject Areas:
mechanical engineering, applied mathematics

Keywords:
WKB approximation, asymptotic analysis, wave propagation, non-uniform rods

Author for correspondence:
Rasmus Nielsen
e-mail: rn@m-tech.aau.dk

The Wentzel–Kramers–Brillouin (WKB) approximation is applied for asymptotic analysis of time-harmonic dynamics of corrugated elastic rods. A hierarchy of three models, namely, the Rayleigh and Timoshenko models of a straight beam and the Timoshenko model of a curved rod is considered. In the latter two cases, the WKB approximation is applied for solving systems of two and three linear differential equations with varying coefficients, whereas the former case is concerned with a single equation of the same type. For each model, explicit formulations of wavenumbers and amplitudes are given. The equivalence between the formal derivation of the amplitude and the conservation of energy flux is demonstrated. A criterion of the validity range of the WKB approximation is proposed and its applicability is proved by inspection of eigenfrequencies of beams of finite length with clamped–clamped and clamped-free boundary conditions. It is shown that there is an appreciable overlap between the validity ranges of the Timoshenko beam/rod models and the WKB approximation.

1. Introduction

The Wentzel–Kramers–Brillouin (WKB) approximation is a well-established and recognized tool in theoretical physics in general, and in quantum mechanics in particular. Its application for solving the Schrödinger equation provides simple-structured solutions that describe the motion of particles and phenomena such as tunnelling. Examples can be readily found in classical compilations and textbooks such as Fröman & Fröman [1] or Bender & Orszag [2]. The fundamental feature of the WKB method is its ability to approximate the solutions of

Royal Society Publishing

linear differential equations with varying coefficients. This unique characteristic of the method immediately suggests its suitability for describing wave motion in inhomogeneous media and consequently the method has found its way to the field of acoustics. For problems of wave propagation in non-uniform acoustic ducts the method has been applied by for instance Rienstra [3], Cooper & Peake [4] and Brambley & Peake [5]. The method has also been applied in elastodynamics and, more specifically, for analysis of wave motion of planar curved elastic strips by Scott & Woodhouse [6], guided waves in a circular elastic annulus by Gridin *et al.* [7], and straight non-uniform rods in plane stress by Rosenfeld & Keller [8].

Another class of problems in elasticity where the WKB method is applicable, but, to the best of the authors knowledge has not yet been used profoundly, is the wave propagation in non-uniform rods in the framework of the classical 'plane cross-sectional' model. The pioneering work along these lines has been done by Pierce [9], who used the WKB method to determine the wavenumbers in straight inhomogeneous Bernoulli–Euler and Timoshenko beams. However, the amplitude variation was determined from the energy conservation condition, rather than by means of the formal WKB approximation. An expression for the eigenfrequencies of a cantilevered Bernoulli–Euler beam is presented in the paper, with no numerical results being reported. In a paper by Langley [10], the propagation of flexural waves in a straight Bernoulli–Euler beam was studied by deriving a short-wave perturbation solution similar to a WKB solution. The short-wave perturbation solution found in Langley [10] was derived after recasting the governing equation to a first-order matrix vector system and transform this to 'wave coordinates' based on the eigenvectors and eigenvalues of the system. More specifically the case analysed was the reflection and transmission coefficients for a non-uniform pre-compressed beam resting on an elastic foundation with non-uniform properties.

A relatively low interest in the WKB approximations in the classical rod theories can be explained by an obvious contradiction between the limitations of the two. Namely, the WKB approximation is, in essence, a short-wave or high-frequency method, whereas the classical rod theories are formulated for long-wave or low-frequency wave motion. More specifically, the Timoshenko beam model may be regarded as accurate up to and slightly above the shear wave cut-on [11], whereas the validity range for the Bernoulli–Euler beam model is much narrower. This naturally raises the question on whether there is an appreciable overlap of frequencies, where both the plane cross-sectional hypothesis and the WKB approximation are valid. To answer this question, results determined by the WKB method should be compared with results determined by a substantially different method, for example, by numerical solutions. In the above-mentioned references on rods, such a comparison has not been done and one of the goals of this paper is to accomplish this. This is done by comparing eigenfrequencies determined by the WKB method and numerical methods for various rods when specialized to different boundary conditions. Determining eigenfrequencies of non-uniform beams as done in this paper is, however, not the main motivation of using the WKB method, but rather eigenfrequencies are regarded as a convenient measure to assess the accuracy of the WKB method when applied to plane cross-sectional problems.

Analysis of elastic waves in non-uniform beams by the WKB approximation is useful in many practical aspects. Asymptotic analysis is, in general, known as a powerful tool to reveal the underlying physics of complicated problems and to provide some approximate yet simple and useful relationships between the parameters of a given problem and its solution. These insights can greatly facilitate the engineer during the design process of, say, a suspension system composed of non-uniform beams. The important information on wave propagation, cut-on/cut-off frequencies, etc., of a non-uniform waveguide, available from the WKB method is quite unique as no standard numerical method provides that.

The classical application of the WKB approximation in quantum mechanics (or in linear acoustics) is concerned with solving a single partial differential equation of the second order with varying coefficients. In elastodynamics, the approximation is applied to solve a system of two differential equations, which are of the second order each. The motion of curved rods in the framework of Timoshenko formulation are generally governed by six coupled differential

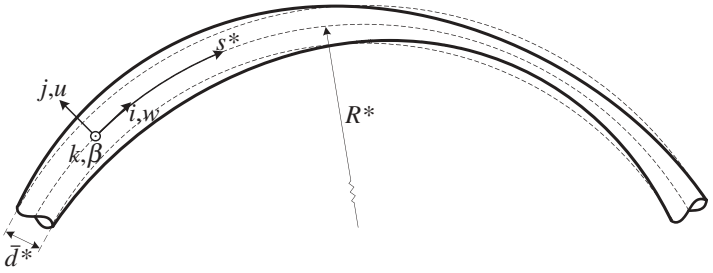

Figure 1. Curved corrugated rod.

equations with varying coefficients and therefore the WKB solution of three coupled equations, representing a planar curved corrugated Timoshenko rod, reported in this paper contains aspects of novelty in its own right.

The study presented in this paper is devoted to demonstrate how the WKB method is generalized to, in a formal manner, solve systems of differential equations with slowly varying coefficients and to demonstrate that there is an appreciable overlap between the high-frequency WKB method and the low-frequency theory of rods, which employs the plane cross-sectional hypothesis. The application of the WKB approximation will be exemplified on the following non-uniform elastic members: (i) *straight Rayleigh rod*, (ii) *straight Timoshenko rod* and (iii) *curved Timoshenko rod*. This choice of increasingly advanced models will accomplish the demonstration of how simple and systematic the WKB approximation in fact is. In §4, the accuracy of the WKB solutions when applied to elasticity problems based on the plane cross-sectional hypothesis is gauged. This is done by the aforementioned comparison of eigenfrequencies.

2. Models of non-uniform beams

Consider a rod with a circular cross section with a varying diameter and define the axial length scale of inhomogeneity as l^* (* denotes dimensional quantities), i.e. this is the length over which the diameter changes significantly. More specifically, the diameter may be defined as

$$d^*(s^*) = \bar{d}^* + d'^* \sin\left(\frac{s^*}{l^*}\right), \tag{2.1}$$

where $\bar{d}^*$ is the mean diameter, as indicated in figure 1, d'^* is the change in diameter and s^* is the axial coordinate. By scaling lengths using $\bar{d}^*$, the non-dimensional diameter can be stated as $d(s) = 1 + r\sin(\epsilon s)$, where $r = d'^*/\bar{d}^*$ and $\epsilon = \bar{d}^*/l^*$. The requirement for slow variation of the cross section is then $\epsilon \ll 1$. Thus, the diameter is dependent on a slow coordinate $d^*(\epsilon s)$, and likewise are the area and moment of inertia: $A^*(\epsilon s) = (\pi/4)d^{*2}(\epsilon s)$, $I^*(\epsilon s) = (\pi/64)d^{*4}(\epsilon s)$. This is the typical way of stating the requirement of slow variation of a waveguide even though nothing, at this stage, is said about the wavelength. It will be shown later on that stating $\epsilon \ll 1$ is not by itself sufficient to ensure accuracy of the WKB approximation.

The key assumption in classical rod theories is the assumption that a cross section remains plane in the course of deformation. The simplest of these models is the classical Bernoulli–Euler model, in which the cross section is additionally assumed to remain perpendicular to the middle axis during deformation [12]. This has the immediate consequence that the deformation of the beam is completely given by the lateral deflection $u^*(s^*, t^*)$ of the centreline. Owing to this assumption, the elastic energy stems only from the deflection caused by the bending moment, which is given by $Q^*(s^*, t^*) = -E^*I^*(s)(\partial^2 u^*(s^*, t^*)/\partial s^{*2})$, where E^* is Young's modulus, thus the elastic energy density is $v^* = \frac{1}{2}Q^*(s^*, t^*)(-\partial^2 u^*(s^*, t^*)/\partial s^{*2})$. So the elastic energy of a Bernoulli–Euler beam is

$$V^* = \frac{1}{2}\int_0^{L^*} E^*I^*(s^*)\left(\frac{\partial^2 u^*(s^*, t^*)}{\partial s^{*2}}\right)^2 \mathrm{d}s^*, \tag{2.2}$$

where L^* is the length of the beam. The kinetic energy of a beam under deformation is

$$T^* = \frac{1}{2}\int_0^{L^*}\left[\rho^* A^*(s^*)\left(\frac{\partial u^*(s^*,t^*)}{\partial t^*}\right)^2 + \rho^* I^*(s^*)\left(\frac{\partial^2 u^*(s^*,t^*)}{\partial s^* \partial t^*}\right)^2\right] \mathrm{d}s^*, \tag{2.3}$$

where ρ^* is the mass density. The first term in (2.3) is the conventional Bernoulli–Euler inertia term and the second term is the rotary inertia correction term introduced by Rayleigh [13]. For that reason, this model will henceforth be referred to as the Rayleigh beam model. The governing equation of such a beam can be found by setting up the action integral and using Hamilton's principle

$$\begin{aligned} 0 = \delta\int_{t_1^*}^{t_2^*}(T^* - V^*)\,\mathrm{d}t^* = \int_{t_1^*}^{t_2^*}\int_0^{L^*}\Bigg[&\rho^* A^*(s^*)\frac{\partial u^*(s^*,t^*)}{\partial t^*}\delta\frac{\partial u^*(s^*,t^*)}{\partial t^*} \\ &+ \rho^* I^*(s^*)\frac{\partial^2 u^*(s^*,t^*)}{\partial s^* \partial t^*}\delta\frac{\partial^2 u^*(s^*,t^*)}{\partial s^* \partial t^*} \\ &- E^* I^*(s^*)\frac{\partial^2 u^*(s^*,t^*)}{\partial s^{*2}}\delta\frac{\partial^2 u^*(s^*,t^*)}{\partial s^{*2}}\Bigg]\mathrm{d}s^*\,\mathrm{d}t^*. \end{aligned} \tag{2.4}$$

Integrating by parts the first term once, the second and the third term twice, and omitting the corresponding boundary terms one arrives at the following governing equation:

$$\begin{aligned} 0 = &\rho^* A^*(s^*)\frac{\partial^2 u^*(s^*,t^*)}{\partial t^{*2}} - \rho^*\frac{\partial}{\partial s^*}\left(I^*(s^*)\frac{\partial^3 u^*(s^*,t^*)}{\partial s^* \partial t^{*2}}\right) \\ &+ E^*\frac{\partial^2}{\partial s^{*2}}\left(I^*(s^*)\frac{\partial^2 u^*(s^*,t^*)}{\partial s^{*2}}\right). \end{aligned} \tag{2.5}$$

Let the temporal dependency throughout this paper be given by $\mathrm{e}^{-\mathrm{i}\omega^* t^*}$ and then scale lengths by $\bar{d}^*$ and frequency by $\sqrt{E^*/\rho^*}/\bar{d}^*$. Applying this yields the following ordinary differential equation:

$$0 = -\omega^2 A(s)u(s) + \omega^2\frac{\mathrm{d}}{\mathrm{d}s}\left(I(s)\frac{\mathrm{d}u(s)}{\mathrm{d}s}\right) + \frac{\mathrm{d}^2}{\mathrm{d}s^2}\left(I(s)\frac{\mathrm{d}^2 u(s)}{\mathrm{d}s^2}\right). \tag{2.6}$$

Unlike the Rayleigh beam model, the Timoshenko beam model does not assume the cross section to remain perpendicular to the centreline during deformation and therefore introduces a new variable that measures the cross-sectional rotation $\beta(s^*,t^*)$. Thus, the shear force in a Timoshenko beam cannot be determined only from the deflection of the centreline, but rather by the difference between the slope of the centreline and the rotation of a cross section

$$P^* = \lambda G^* A^*(s^*)\left(\frac{\partial u^*(s^*,t^*)}{\partial s^*} - \beta(s^*,t^*)\right), \tag{2.7}$$

where λ is the shear correction factor, which is dimensionless, and G^* is the shear modulus, which is rewritten by $G^* = E^*/(2(1+\nu))$ where ν is Poisson's ratio which is also dimensionless. The internal moment is given by

$$Q^* = -E^* I^*(s^*)\frac{\partial\beta(s^*,t^*)}{\partial s^*}. \tag{2.8}$$

The elastic and kinetic energy is then

$$V^* = \frac{1}{2}\int_0^{L^*}\left[E^* I^*(s^*)\left(\frac{\partial\beta(s^*,t^*)}{\partial s^*}\right)^2 + \kappa G^* A^*\left(\frac{\partial u^*(s^*,t^*)}{\partial s^*} - \beta(s^*,t^*)\right)^2\right]\mathrm{d}s^* \tag{2.9}$$

and

$$T^* = \frac{1}{2}\int_0^{L^*}\left[\rho^* A^*(s^*)\left(\frac{\partial u^*(s^*,t^*)}{\partial t^*}\right)^2 + \rho^* I^*(s^*)\left(\frac{\partial\beta(s^*,t^*)}{\partial t^*}\right)^2\right]\mathrm{d}s^*. \tag{2.10}$$

The equations governing the motion of a Timoshenko beam is then found by setting up the action integral and apply Hamilton's principle by performing variations with respect to $u^*(s^*,t^*)$ and

$\beta^*(s^*, t^*)$, so contrary to the Bernoulli–Euler and Rayleigh beam models the Timoshenko beam model is governed by two equations. Again by adopting the temporal dependence $e^{-i\omega^* t^*}$ and perform non-dimensional scalings the following equations are found:

$$0 = \omega^2 A(s)u(s) + p\frac{d}{ds}\left(A(s)\left(\frac{du(s)}{ds} - \beta(s)\right)\right) \tag{2.11a}$$

and

$$0 = \omega^2 I(s)\beta(s) + \frac{d}{ds}\left(I(s)\frac{d\beta(s)}{ds}\right) + pA(s)\left(\frac{du(s)}{ds} - \beta(s)\right). \tag{2.11b}$$

Here, $p = \lambda/(2(1+\nu))$ has been introduced for convenience. A complete derivation of these equations is available in Shames & Dym [12]. The curved Timoshenko beam is naturally based on the same kinematic hypothesis as the straight Timoshenko beam, but due to the curvature it couples to axial motion denoted by $w(s,t)$. A formal derivation requires the involvement of differential geometry and the use of Hamilton's principle. In non-dimensional form, the governing equations in the frequency domain are given by

$$\begin{aligned} 0 = {} & \omega^2 A(s)u(s) + p\frac{d}{ds}\left(A(s)\left(\frac{du(s)}{ds} - \beta(s)\right)\right) - \kappa A(s)\frac{dw(s)}{ds} \\ & - \kappa p\frac{d}{ds}(w(s)A(s)) + \kappa^2 A(s)u(s), \end{aligned} \tag{2.12a}$$

$$0 = \omega^2 I(s)\beta(s) + \frac{d}{ds}\left(I(s)\frac{d\beta(s)}{ds}\right) + pA(s)\left(\frac{du(s)}{ds} - \beta(s)\right) + \kappa pA(s)w(s) \tag{2.12b}$$

and

$$\begin{aligned} 0 = {} & \omega^2 A(s)w(s) + \frac{d}{ds}\left(A(s)\frac{dw(s)}{ds}\right) - \kappa\frac{d}{ds}(u(s)A(s)) \\ & + \kappa pA(s)\left(\beta(s) - \frac{du(s)}{ds}\right) - \kappa^2 pA(s)w(s). \end{aligned} \tag{2.12c}$$

Here, κ is the non-dimensional curvature found from the radius of curvature R^* indicated in figure 1.

In the limit of $\epsilon \to 0$, all of the above problems are exactly solvable since the coefficients become constants. More specifically, the dispersion relations for the unperturbed rods with spatial–temporal dependence taken as $e^{iks - i\omega t}$ are;

Rayleigh rod

$$-\omega^2 A - \omega^2 Ik^2 + Ik^4 = 0, \tag{2.13}$$

Timoshenko rod

$$p\omega^2 A - I(\omega^2 - k^2)(\omega^2 - pk^2) = 0 \tag{2.14}$$

and curved Timoshenko rod

$$\begin{aligned} & -p\omega^2 A(\kappa^2 - \omega^2 + k^2) - (\omega^2 - k^2)((\kappa^2 - \omega^2)(p\kappa^2 - \omega^2) \\ & - (\omega^2 + p(2\kappa^2 + \omega^2))k^2 + pk^4)I = 0. \end{aligned} \tag{2.15}$$

How the non-uniform equations are solved by the WKB method is exemplified in the following section.

A preliminary justification of whether an overlap exists between the short-wave WKB method applied to long-wave beam models is now given. In Chapman & Sorokin [14], it is demonstrated that the beam model formulation for uniform beams effectively corresponds to neglecting $O(h^2/\lambda^2)$ terms, where h is the local cross-wise dimension and λ is the wavelength. Denoting $\mu = h/\lambda$ and by introducing the relation $\mu = \epsilon^q$, it can be shown that for $1/2 < q < 1$ both the long-wave beam assumption, $\mu \ll 1$, and short-wave WKB assumption, $\lambda/l \ll 1$, are fulfilled when $\epsilon \ll 1$. Meanwhile does it ensure that the largest neglected term in the beam model is smaller than the smallest term accounted for in the WKB method.

3. Asymptotic solutions

The WKB solutions to the above-mentioned problems are derived by the formal procedure of asymptotics. It should be mentioned that when solving systems of coupled equations the transport equation is found by imposing orthogonality between the resonant terms of the $O(\epsilon)$ terms and the eigenvector of the $O(1)$ terms. Details are given in the following sections.

(a) The non-uniform Rayleigh beam

The WKB approximation takes its point of departure in a scaling of the axial coordinate

$$S = \epsilon s \quad \Rightarrow \quad \frac{\mathrm{d}}{\mathrm{d}s} = \epsilon \frac{\mathrm{d}}{\mathrm{d}S}. \tag{3.1}$$

This is embedded in the governing equations. The insertion of the WKB ansatz $u_j(S) = (U_{0,j}(S) + \epsilon U_{1,j}(S) + O(\epsilon^2))\,\mathrm{e}^{(\mathrm{i}/\epsilon)\int_0^S k_j(\xi)\,\mathrm{d}\xi}$ [15], in equation (2.6) and collecting the $O(1)$ terms yields

$$0 = -\omega^2 A(S) - \omega^2 I(S) k_j^2(S) + I(S) k_j^4(S) \quad \Rightarrow \tag{3.2}$$

$$k_{1,2,3,4}(S) = \pm \sqrt{\frac{1}{2}\omega^2 \pm \sqrt{\frac{A(S)}{I(S)}\omega^2 + \frac{1}{4}\omega^4}}. \tag{3.3}$$

Thus, this dispersion relation only differs from the one for the uniform Rayleigh beam by the presence of the spatial dependence of $A(S)$ and $I(S)$. Collecting the $O(\epsilon)$ terms yields

$$\begin{aligned}&(-\omega^2 A(S) + \omega^2 I(S) k_j^2(S) + I(S) k_j^4(S)) U_{1,j}(S) \\ &\quad = -2\mathrm{i}\sqrt{I(S) k_j(S)(2k_j^2(S) - \omega^2)}\,\frac{\mathrm{d}}{\mathrm{d}S}(U_{0,j}(S)\sqrt{I(S) k_j(S)(2k_j^2(S) - \omega^2)}).\end{aligned} \tag{3.4}$$

To ensure that the right-hand side of the above equation does not have any forcing on the left-hand side, the right-hand side must be set to zero. This has a very simple solution that, apart from a multiplicative constant, is

$$U_{0,j}(S) = \frac{1}{\sqrt{I(S) k_j(S)(2k_j^2(S) - \omega^2)}}. \tag{3.5}$$

The full solution is then given as the sum of four waves

$$u(S) = \sum_{j=0}^{4} c_j U_{0,j}(S)\,\mathrm{e}^{(\mathrm{i}/\epsilon)\int_0^S k_j(\xi)\,\mathrm{d}\xi}. \tag{3.6}$$

By neglecting the rotary inertia, the results perfectly match those found by Pierce [9] for the non-uniform Bernoulli–Euler beam model, namely

$$k_{1,2,3,4}(S) = \{\pm 1, \pm \mathrm{i}\}\sqrt{\omega}\left(\frac{A(S)}{I(S)}\right)^{1/4} \tag{3.7}$$

and

$$U_0(S) = \frac{1}{\sqrt{I(S) k_j^3(S)}} = A^{-3/8}(S) I^{-1/8}(S). \tag{3.8}$$

(b) The non-uniform Timoshenko beam

The results in this section can either be found by following the procedure demonstrated in §3*c* or alternatively by a deduction of the results presented in §3*c* involving the limit $\kappa \to 0$. In any case,

the asymptotic solution turns out to be

$$k_{1,2,3,4}(S) = \pm\sqrt{\frac{\omega^2(p+1) \pm \sqrt{4p^2\omega^2(A(S)/I(S)) + (p-1)^2\omega^4}}{2p}} \tag{3.9}$$

and

$$U_{0,j}(S) = \sqrt{\frac{k_j(S)}{p^2\omega^2 A(S) + I(S)(\omega^2 - pk_j^2(S))^2}}. \tag{3.10}$$

Again the wavenumbers are the same as for the unperturbed waveguide, but with a dependence on the slow coordinate. Furthermore, both the wavenumbers and amplitude can be shown to merge with the ones for the Bernoulli–Euler beam as $\omega \to 0$.

(c) The curved non-uniform Timoshenko beam

The derivation of this problem is shown in some detail in the following. Firstly, the axial coordinate s is scaled to S and the WKB ansatz can be put down as

$$\begin{bmatrix} u_j(S) \\ \beta_j(S) \\ w_j(S) \end{bmatrix} = \left(\begin{bmatrix} U_{0,j}(S) \\ B_{0,j}(S) \\ W_{0,j}(S) \end{bmatrix} + \epsilon \begin{bmatrix} U_{1,j}(S) \\ B_{1,j}(S) \\ W_{1,j}(S) \end{bmatrix} + O(\epsilon^2) \right) \mathrm{e}^{(\mathrm{i}/\epsilon)\int_0^S k_j(\xi)\,\mathrm{d}\xi}. \tag{3.11}$$

By inserting this in the governing equations and collecting $O(1)$ terms leads to

$$[L] \begin{bmatrix} U_{0,j}(S) \\ B_{0,j}(S) \\ W_{0,j}(S) \end{bmatrix} = 0, \tag{3.12}$$

where

$$[L] = \begin{bmatrix} (\omega^2 - k_j(S)^2)\dfrac{I(S)}{A(S)} - p & \mathrm{i}pk_j(S) & p\kappa \\ \mathrm{i}pk_j(S) & \kappa^2 - \omega^2 + pk_j(S)^2 & -\mathrm{i}\kappa(p+1)k_j(S) \\ p\kappa & -\mathrm{i}\kappa(p+1)k_j(S) & -p\kappa^2 + \omega^2 - k_j(S)^2 \end{bmatrix}. \tag{3.13}$$

Taking the determinant of this and performing some simplification leads to the dispersion relation

$$\begin{aligned} &-p\omega^2 A(S)(\kappa^2 - \omega^2 + k_j(S)^2) - (\omega^2 - k_j(S)^2)((\kappa^2 - \omega^2)(p\kappa^2 - \omega^2) \\ &-(\omega^2 + p(2\kappa^2 + \omega^2))k_j(S)^2 + pk_j(S)^4)I(S) = 0. \end{aligned} \tag{3.14}$$

This polynomial equation is of the sixth order in $k(S)$, with no odd powers and therefore has a closed form solution, that in the interest of brevity is omitted here. The wavenumbers come in pairs of left and right going waves denoted by $\pm k_u(S)$, $\pm k_\beta(S)$ and $\pm k_w(S)$, where the indices designate the dominant type of deformation. This can be analysed by inspection of the components of the eigenvector v_j for a certain wavenumber $k_j(S)$. In the limit of small κ, i.e. when the rod is straightened out, the dispersion relation factorizes itself into those for plane axial waves in a corrugated rod and the flexure and shear waves in a corrugated Timoshenko rod

$$\underbrace{(\omega^2 - k_j(S)^2)}_{\text{plane wave}} \underbrace{(p\omega^2 A(S) - I(S)(\omega^2 - k_j(S)^2)(\omega^2 - pk_j(S)^2))}_{\text{flexural and shear waves}} = 0. \tag{3.15}$$

The modal coefficients linking $B_0(S)$ and $W_0(S)$ to $U_0(S)$ determined from (3.12) are

$$M_j^{B_0}(S) = \frac{\mathrm{i}pA(S)(k_j(S)^2 - \kappa^2 + \omega^2)}{k_j(S)(pA(S) - (p+1)I(S)(\omega^2 - k_j(S)^2))} \tag{3.16}$$

and

$$M_j^{W_0}(S) = -\frac{\mathrm{i}(pA(S)(\kappa^2 - \omega^2) + I(S)(\omega^2 - k_j(S)^2)(-pk_j(S)^2 - \kappa^2 + \omega^2))}{\kappa k_j(S)(pA(S) - (p+1)I(S)(\omega^2 - k_j(S)^2))}. \tag{3.17}$$

Collecting the terms of $O(\epsilon)$ in the governing equation after inserting the WKB ansatz yields an inhomogeneous version of (3.12)

$$[L]\begin{bmatrix} U_{1,j}(S) \\ B_{1,j}(S) \\ W_{1,j}(S) \end{bmatrix} = \begin{bmatrix} F_{1,j}(S) \\ F_{2,j}(S) \\ F_{3,j}(S) \end{bmatrix}, \tag{3.18}$$

where

$$F_{1,j}(S) = pA(S)U'_{0,j}(S) + 2\mathrm{i}\sqrt{I(S)k_j(S)}\frac{\mathrm{d}}{\mathrm{d}S}\left(\sqrt{I(S)k_j(S)}B_{0,j}(S)\right), \tag{3.19a}$$

$$F_{2,j}(S) = -\mathrm{i}p2\sqrt{k_j(S)A(S)}\frac{\mathrm{d}}{\mathrm{d}S}\left(\sqrt{k_j(S)A(S)}U_{0,j}(S)\right) - p\kappa\frac{\mathrm{d}}{\mathrm{d}S}(A(S)W_{0,j}(S)) + p\frac{\mathrm{d}}{\mathrm{d}S}(A(S)B_{0,j}(S)) - \kappa A(S)W'_{0,j}(S) \tag{3.19b}$$

and

$$F_{3,j}(S) = -\kappa\frac{\mathrm{d}}{\mathrm{d}S}(A(S)U_{0,j}(S)) + 2\mathrm{i}\sqrt{A(S)k_j(S)}\frac{\mathrm{d}}{\mathrm{d}S}\left(\sqrt{A(S)k_j(S)}W_{0,j}(S)\right) - \kappa pA(S)U'_{0,j}(S). \tag{3.19c}$$

As is seen this forcing vector contains the three amplitudes and their first-order derivatives. The modal coefficients can now be used to eliminate $B_{0,j}(S)$ and $W_{0,j}(S)$ in (3.19) and to construct an eigenvector $\boldsymbol{v}_j = [1, M_j^{B_0}(S), M_j^{W_0}(S)]^{\mathrm{T}}$. After taking the dot product $\boldsymbol{F}_j \cdot \boldsymbol{v}_j = 0$ the transport equation for the present problem emerges. Solving it provides the following amplitude:

$$U_{0,j}(S) = \frac{\sqrt{k_j(S)}(pA(S) - (1+p)(\omega^2 - k_j(S)^2)I(S))}{\sqrt{A(S)}\sqrt{Z_1 + pA(S)(Z_2 - Z_3)I(S) + (\omega^2 - k_j(S)^2)^2 Z_4 I(S)^2}}, \tag{3.20}$$

where

$$Z_1 = p^2\omega^2(-\kappa^2 + \omega^2)A(S)^2,$$

$$Z_2 = (\kappa^2 - \omega^2)(2\omega^4 + p\kappa^2(\kappa^2 + \omega^2)),$$

$$Z_3 = 2(\kappa^2 - \omega^2)(\omega^2 + p(2\kappa^2 + \omega^2))k_j(S)^2 + p(3\kappa^2 - 2\omega^2)k_j(S)^4$$

and

$$Z_4 = -(\kappa^2 - \omega^2)(2p\kappa^2 + p^2\kappa^2 + \omega^2) + 2p(\kappa^2 - \omega^2)k_j(S)^2 + p^2k_j(S)^4.$$

It is easily verified that in the limit $\kappa \to 0$ the solution of the transport equation matches the one in equation (3.10).

(d) Energy flux

It is remarkable that the transport equation in all of the above cases turns out as

$$C(S)U'_0(S) + C'(S)U_0(S) = 0. \tag{3.21}$$

Thus, the derivative of the product $C(S)U_0(S)$ must vanish. This has the immediate consequence that an explicit expression for $U_0(S)$ can be determined with no further problems and, furthermore, that the quantity $C(S)U_0(S)$ is conserved over S, i.e. this is an adiabatic invariant. This was recognized by Pierce [9] as it can be proved that conservation of energy flux to the leading order leads to exactly the same requirement for the amplitude function. This can be exemplified by considering the straight Timoshenko beam. The energy flux is

$$E_{\mathrm{flux}} = \tfrac{1}{2}\Re[\dot{\beta}_j^\star(S)Q_j(S) - \dot{u}_j^\star(S)P_j(S)], \tag{3.22}$$

where * denotes complex conjugate. The above expression can be rewritten to

$$E_{\text{flux}} = \tfrac{1}{2}\Re[\mathrm{i}\omega U_{0,j}^2(S)pA(S)(\mathrm{i}k_j(S) - M_j^{(B_0)}(S)) + \omega U_{0,j}^2(S)M_j^{(B_0)}(S)I(S)k_j(S)]. \tag{3.23}$$

One of the two modal coefficient that relates $B_0(S)$ to $U_0(S)$ is

$$M_j^{(B_0)} = \frac{-\mathrm{i}\omega^2 + \mathrm{i}pk_j^2(S)}{pk_j(S)}. \tag{3.24}$$

By using this, the expression for energy flux simplifies to

$$E_{\text{flux}} = \frac{1}{2}\frac{-\omega}{p^2}\Re\left[U_{0,j}^2(S)\frac{A(S)\omega^2p^2 + I(S)(\omega^2 - pk_j^2(S))^2}{k_j(S)}\right]. \tag{3.25}$$

Then by requiring a constant energy flux yields the following expression for the amplitude:

$$U_{0,j}(S) = \sqrt{\frac{k_j(S)}{p^2\omega^2A(S) + I(S)(\omega^2 - pk_j^2(S))^2}}. \tag{3.26}$$

This expression identically matches that found in equation (3.10), thus the amplitude found via the WKB method corresponds to conserving the energy flux to the leading order.

4. Determination and comparison of eigenfrequencies

In this section, it is tested how the solutions obtained in the previous section perform numerically when compared to reference solutions. The reference solutions are obtained by the finite element (FE) method as this can be regarded as a reliable and easily applied tool as far as free and forced vibrations of beams of finite length are concerned and therefore is ideal for the comparison. Another advantage is that the FE method is most accurate at low frequencies and therefore is expected to be accurate where the WKB method is expected to be least accurate. For the WKB solutions this requires, however, that these are elaborated to predict standing waves in a beam and thereby match an FE model. Eigenfrequencies, which can be determine via the FE method with no further difficulty, are chosen as the result for the actual comparison. Thus, the WKB method must be specialized to fulfil certain boundary conditions and thereafter the eigenfrequencies can be determined and compared to those of the FE method. Here, clamped–clamped and clamped-free boundary conditions are considered.

A clamped boundary condition is stated as $u(s) = u'(s) = 0$ for a Rayleigh beam and as $u(s) = \beta(s) = w(s) = 0$ for the Timoshenko beam. At a free end, the Rayleigh boundary conditions are $u''(s) = u'''(s) = 0$ corresponding to zero bending moment and zero shear force, respectively. For a curved Timoshenko beam, the conditions at a free end are

$$\frac{\mathrm{d}w}{\mathrm{d}s} - \kappa u = 0, \tag{4.1a}$$

$$\frac{\mathrm{d}\beta}{\mathrm{d}s} = 0 \tag{4.1b}$$

and

$$\frac{\mathrm{d}u}{\mathrm{d}s} - \beta + \kappa w = 0. \tag{4.1c}$$

These are zero axial force, zero shear force and zero bending moment, respectively. In the case of the straight Timoshenko beam, κ is simply set to zero in (4.1). It is stressed that taking the derivatives related to the boundary equations produces a series of $O(1)$, $O(\epsilon)$, $O(\epsilon^2)$, ... terms and to be consistent with the WKB solutions found only the $O(1)$ terms are retained.

Table 1. First six eigenfrequencies for a clamped–clamped Rayleigh beam along with the deviation in brackets of the WKB approximations and the value of Φ_u.

	ω_n (Hz)		
n	FE	WKB	Φ_u
1	14.3	15.4 (8%)	4.4
2	40.8	42.3 (4%)	7.4
3	80.8	82.3 (2%)	10.4
4	133.1	134.7 (1%)	13.4
5	197.2	198.7 (1%)	16.4
6	272.0	273.6 (1%)	19.4

Table 2. First six eigenfrequencies for a clamped-free Rayleigh beam. Notations are similar to table 1.

	ω_n (Hz)		
n	FE	WKB	Φ_u
1	1.7	2.4 (40%)	1.8
2	13.8	15.2 (10%)	4.4
3	41.1	42.3 (3%)	7.4
4	80.9	82.3 (2%)	10.4
5	132.8	134.7 (1%)	13.4
6	196.1	198.7 (1%)	16.4

The cross section is defined as circular which immediately suggests a standard choice of shear correction factor

$$\lambda = \frac{6(1+\nu)}{7+6\nu}, \tag{4.2}$$

which is due to [12]. Furthermore, let the following quantities be defined initially:

$$\epsilon = 0.1, \qquad r = 0.5, \qquad \kappa = 0.1, \qquad \nu = 0.3,$$

$$\bar{d}^* = 1\,\mathrm{m}, \quad L^* = 20\,\mathrm{m}, \quad \rho^* = 7830\frac{\mathrm{kg}}{\mathrm{m}^3}, \quad E^* = 210\,\mathrm{GPa},$$

where L^* is the length of the beam. These parameters correspond to a length scale of inhomogeneity of $l^* = 10\,\mathrm{m}$. The first six eigenfrequencies can be found in tables 1 and 2 for the Rayleigh beam model, tables 3 and 4 for the Timoshenko beam model, and tables 5 and 6 for the curved Timoshenko beam model. Along with the FE and WKB eigenfrequencies, their mutual deviations determined as $(\omega_n^{\mathrm{WKB}} - \omega_n^{\mathrm{FE}})/\omega_n^{\mathrm{FE}}$ are shown in brackets. The FE analysis have been conducted in ANSYS 13.0 using the Timoshenko-based beam element *BEAM189* that allows for tapering. This way of modelling ensures that the plane cross-sectional hypothesis is preserved and consequently it is the governing differential equations presented in (2.6), (2.11) and (2.12) that are approximated numerically. When modelling the Rayleigh beam the shear deformation has simply been suppressed. The results reported in the tables have been generated with 60 elements in the axial direction. Eigenfrequencies of the same models have also been conducted with 20, 30, 40 and 50 elements and their convergence towards the results reported has been observed.

A common way of defining the wave regime in which the WKB approximation is valid is by

$$kl \gg 1, \tag{4.3}$$

Table 3. First six eigenfrequencies for a clamped–clamped Timoshenko beam. Notations are similar to table 1 with the addition of Φ_β.

	ω_n (Hz)			
n	FE	WKB	Φ_u	Φ_β
1	14.0	15.1 (8%)	1.8	0
2	39.1	40.6 (4%)	2.8	0
3	75.3	77.0 (2%)	4.0	0
4	120.5	122.4 (2%)	5.0	0
5	172.9	175.1 (1%)	6.0	0
6	231.2	233.7 (1%)	6.8	0

Table 4. First six eigenfrequencies for a clamped-free Timoshenko beam. Notations are similar to table 3.

	ω_n (Hz)			
n	FE	WKB	Φ_u	Φ_β
1	1.6	2.4 (50%)	0.8	0
2	13.6	15.0 (10%)	1.8	0
3	39.9	41.0 (3%)	2.8	0
4	76.9	77.8 (1%)	4.0	0
5	123.0	124.0 (1%)	5.0	0
6	176.5	177.8 (1%)	6.0	0

Table 5. First six eigenfrequencies for a clamped–clamped Timoshenko beam with constant curvature. Notations are similar to table 1 with the addition Φ_β and Φ_w.

	ω_n (Hz)				
n	FE	WKB	Φ_u	Φ_β	Φ_w
1	32.6	34.4 (6%)	7.2	0	0
2	53.9	55.0 (2%)	9.2	0	0
3	87.1	88.0 (1%)	11.4	0	0.8
4	108.1	111.5 (3%)	12.8	0	1.8
5	146.5	152.5 (4%)	15.2	0	3.2
6	169.9	171.7 (1%)	16.2	0	3.6

see, for instance Gridin *et al.* [7]. This basically requires the wavelength to be short compared with the length scale of inhomogeneity. Remark here the identity $kl = k/\epsilon$. An alternative to the above criteria, equation (4.3), is now proposed based on the fact that the WKB approximation is concerned with the change of the waveguide over one wavelength. Firstly, the change of the waveguide can be stated as the spatial derivative of the diameter

$$d'(s) = r\epsilon \cos(\epsilon s). \tag{4.4}$$

Table 6. First six eigenfrequencies for a clamped-free Timoshenko beam with constant curvature. Notations are similar to table 5.

	ω_n (Hz)				
n	FE	WKB	Φ_u	Φ_β	Φ_w
1	1.8	2.7 (54%)	2.8	1.0	1.0
2	9.5	10.8 (14%)	4.4	0	0
3	33.4	35.6 (6%)	7.4	0	0
4	67.5	70.8 (5%)	10.2	0	0
5	92.7	98.9 (7%)	12.0	0	1.4
6	122.4	123.3 (1%)	13.6	0	2.2

So it is the product $r\epsilon$ that is the controlling factor in the change of waveguide and not ϵ alone. Thus, an alternative version of the failure criteria is likely related to the quantity $k/r\epsilon$. Define

$$\Phi_x = \min \left| \Re \left(\frac{k_x(\xi)}{\epsilon r} \right) \right|, \tag{4.5}$$

where $\xi \in]0, L[$ and $x = u,\ \beta$, or w. These subscripts again designate the dominant type of deformation for the given wavenumber. It is stressed here that none of the wavenumbers corresponds solely to either flexural, axial or shear motion, but by inspection of the modal coefficients it can be seen that they do correspond dominantly to the indicated type of deformation. The expression in (4.5) is a convenient quantity to track for each eigenmode to assess how much larger than unity Φ_x is required to be for the WKB method to work well. This criteria can be interpreted as consisting of two conditions: a mild slope condition of the waveguide walls, i.e. ϵr must be small, and a short-wave condition, i.e. k/ϵ must be large, and together these form a criteria that requires only small changes of the waveguide over one wavelength. The values of Φ_x are given in tables 1–6.

In the following, some comments and observations pertaining to the results are given. From tables 1–4, it is clear, first of all, that the results are in general much better captured for the clamped–clamped model than the clamped-free model of the same length which naturally follows from the fact that the length of the standing wave is shorter in the clamped–clamped model. As a general trend, it is clear that the results improve for large values of Φ_u. The deviations for the WKB method compared to the FE method are 10%, the value of ϵ, when Φ_u is about 4 for the Rayleigh beam and a threshold $\Phi_u < 2$ confines the errors of the Timoshenko model by as little as 4%.

From tables 5 and 6, it broadly holds that the results agree for large values of Φ_x, with the exception of a minor increase around the fifth eigenfrequency. In table 6, it is seen that in the transition between the fourth and the fifth mode Φ_w has changed from being zero to be larger than zero, but smaller than one. Thus, this eigenfrequency is the first one where the axial wave has cut on, and therefore can have a global impact in the motion of the beam, but the value of Φ_w is not large enough for the asymptotics to work very well and therefore the result is determined with some deviation. As Φ_w is determined from the minimum value of $k(S)$, there is no cut-on/cut-off location at this frequency in the beam, but there will be so at a slightly lower frequency.

It is worth considering if an eigenmode that is associated with several different valued Φ_x is reasonably accurate and how this can be assessed. Thus, the question is whether an eigenfrequency compares well to the exact result even though its associated values of Φ_x do not collectively indicate accuracy of the result. The following dispute demonstrate the relevance of such a consideration. Mode one in table 6 is found with a large deviation and has one component,

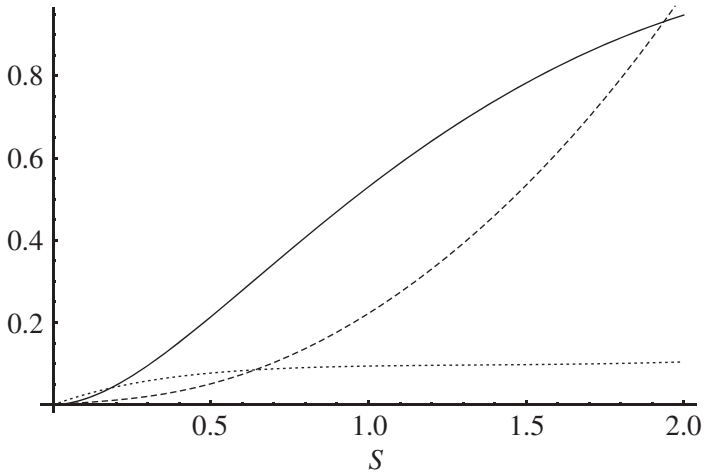

Figure 2. Mode shapes for clamped-free curved Timoshenko beam, first mode. Solid line, $u(S)$; dotted line, $\beta(S)$; dashed line, $w(S)$.

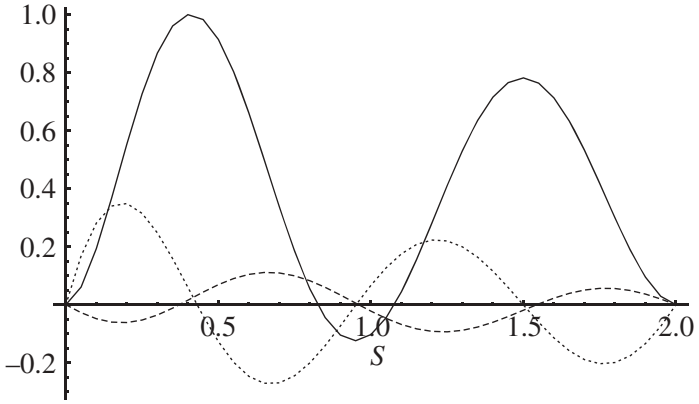

Figure 3. Mode shapes for clamped–clamped curved Timoshenko beam, third mode. Solid line, $u(S)$; dotted line, $\beta(S)$; dashed line, $w(S)$.

$\Phi_u > 2$, which suggests that it is probably accurate, whereas the two others, $\Phi_\beta < 2$ and $\Phi_w < 2$, suggest that it is not very accurate. Contrary, mode three in table 5 is found with a small deviation, but Φ_w suggests that it is wrong while Φ_u suggests that it is correct. The disagreement has a simple explanation that becomes evident by plotting the actual mode shapes. These are seen in figures 2 and 3. Here, it is seen in figure 3 that mode three is dominated by flexural motion, $u(S)$, and the fact that the value of Φ_w suggests the mode is outside the WKB validity range is therefore not relevant. From figure 2, it is clear that axial motion cannot be neglected when compared with flexural motion and therefore the approximation fails. In other words, the measure of 'asymptoticness', Φ_x, needs to be accompanied by an assessment of the involvement of modes for multi-modal problems. This involvement of modes can possibly be further quantified by the modal participation factor known from forced vibration [16]. Finally, it is seen that clamping both ends of the curved Timoshenko beam drastically increases the first eigenfrequency when compared with its cantilevered counterpart. This has a simple physical explanation: the bending couples to stretching due to the curvature, but stretching resistance is high since the beam is clamped at both ends.

A comparison of dispersion relationships is shown in appendix A in which the Rayleigh and Timoshenko rod theories are compared to the Pochhammer–Chree elastodynamics solution for waves in a straight elastic rod with circular cross section. The comparison demonstrates that Timoshenko theory for the parameters chosen can be expected to work well until about 8 kHz,

Table 7. Percentage deviations between WKB and FE of the first eigenfrequency for a clamped–clamped Rayleigh beam in the ϵ–r parameter space. Short dashed lines bounds $\Phi_u < \pi$, medium dashed lines bounds $\Phi_u < 2$ and long dashed lines bounds $\Phi_u < 1$.

	ϵ (%)									
r	0.001	0.01	0.02	0.03	0.04	0.05	0.06	0.07	0.08	0.09
0.001	0	0	0	0	1	0	1	0	0	0
0.1	0	0	0	0	0	0	1	1	1	2
0.2	0	0	0	0	1	0	1	2	2	3
0.3	0	0	0	0	0	1	1	2	3	4
0.4	0	0	0	0	0	1	2	3	4	5
0.5	0	0	0	0	1	1	2	3	4	6
0.6	0	0	0	0	1	1	2	3	5	7
0.7	0	0	0	0	1	1	2	4	5	7
0.8	0	0	0	0	1	1	2	4	6	8
0.9	0	0	0	0	1	1	3	4	6	9

	ϵ (%)									
r	0.1	0.2	0.3	0.4	0.5	0.6	0.7	0.8	0.9	1
0.001	0	0	1	0	0	1	0	0	0	0
0.1	2	7	2	−5	1	3	−6	−5	2	−2
0.2	4	13	4	−10	2	4	−10	−9	7	0
0.3	5	19	7	−15	4	4	−12	−11	17	5
0.4	6	25	10	−18	5	5	−14	−13	34	18
0.5	8	32	13	−21	5	6	−14	−12	63	40
0.6	9	39	17	−23	7	11	−11	−11	114	77
0.7	10	47	17	−23	11	22	−2	−6	185	162
0.8	11	56	11	−27	28	58	22	11	422	354
0.9	12	69	159	76	324	612	464	378	3429	14 042

whereas the Rayleigh theory breaks down at a much earlier stage. In fact, it can be observed from the results in tables 1 and 3 that already at the sixth eigenfrequency the Rayleigh theory diverges by 17% from the Timoshenko theory.

The attention is now turned to an inspection of how the results compare in the $\epsilon - r$ parameter space—the two parameters free to choose in the modulation of the waveguide with the given functional form of $d(s)$. In table 7 is the deviation between WKB method and FE method shown for the first eigenfrequency for a clamped–clamped Rayleigh beam at various combination of ϵ and r. Level curves are drawn in the table that bounds Φ_u less than π, 2, and 1. It can be observed from the results in table 7 that none of the level curves perfectly captures the incorrect results. Thus, it is not possible to state a minimum value of Φ_u, but only require that $\Phi_u \gg 1$. It is observed, however, that in many cases $\Phi_u > 3$ is actually sufficient. Additionally, it is pointed out that the measure for validity proposed in this paper, equation (4.5), correctly predicts that, results based on a large value of ϵ, but a small value of r, and vice versa, can be determined correctly. This is an improvement compared to the more traditional measure in (4.3).

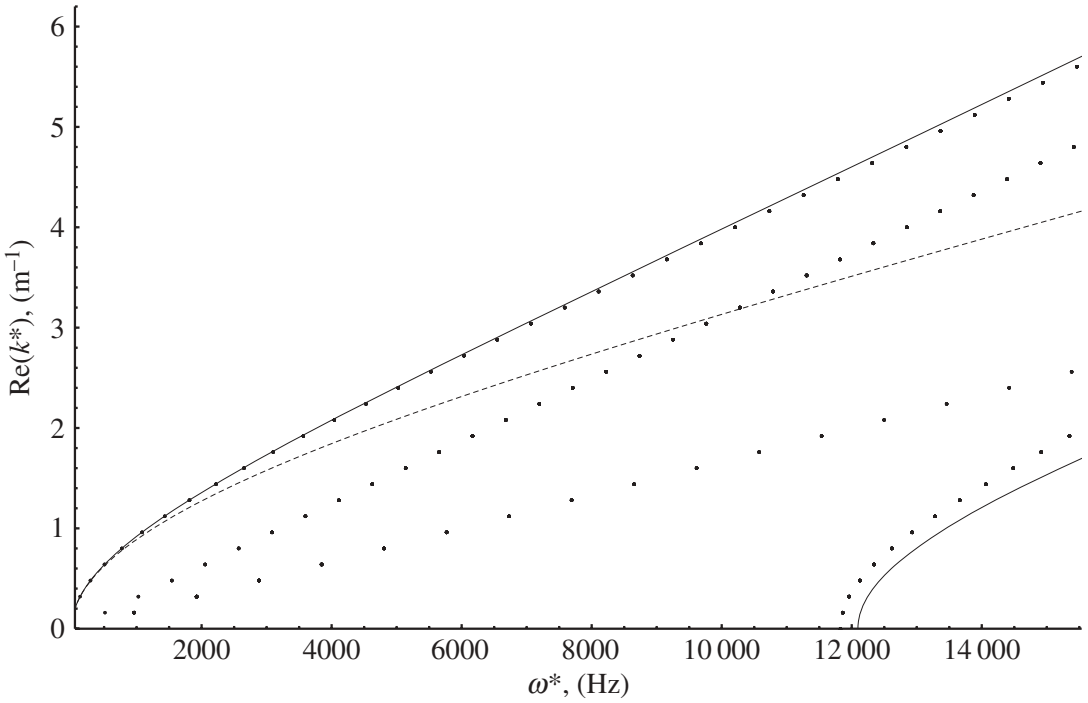

Figure 4. Dispersion diagram for straight rod with circular cross section. Dotted curves, Pochhammer–Chree solution of elastodynamics; solid lines, Timoshenko theory; dashed lines, Rayleigh theory. The plot is generated with the parameters introduced in §4, but for a constant cross section, i.e. $r = 0$. The two Pochhammer–Chree branches that are not accompanied by a Rayleigh or a Timoshenko branch corresponds to axial and torsional wave motion.

5. Conclusion

In the work presented in this paper, the WKB method is applied to approximate the solution of the wave propagation problem in non-uniform beams. It is demonstrated that the leading order WKB approximation corresponds to conservation of energy flux. The solutions are specialized to clamped–clamped and clamped-free boundary conditions, and a number of eigenfrequencies are determined and compared to those determined by the FE method. A parameter study is conducted and the validity range of the WKB method and the plane cross-sectional hypothesis are discussed. It is found that $\min|\Re(k(\xi)/\epsilon r)| \gg 1$ is a conservative criterion for accurate determination of an eigenfrequency by the WKB method. It is furthermore illustrated that often $\min|\Re(k(\xi)/\epsilon r)| > 3$ is sufficient. For multi-modal problems, this criterion needs to be accompanied by an assessment of what kind of motion is dominant for a given mode. This can be conducted by investigating the mode shape.

It is found that there is an appreciable overlap of validity between the WKB method and Timoshenko beam theory, the overlap with Rayleigh (or Bernoulli–Euler) beam theory is found to be much more narrow.

The simplicity of the WKB approximation, and the fact that the dispersion relation matches that of the unperturbed waveguide, illustrates the power of the method in the analysis of non-uniform rods. This is fortunate as the wavenumbers often will be known *a priori*; these are just the same as the wavenumbers found for the corresponding uniform waveguide. It seems natural to extend the analysis to waveguides with constant cross section, but varying curvature. These kind of structures are of practical interest in the analysis of the linear time harmonic dynamics of suspension systems, pipes, curved rails, etc., where one would be concerned with noise transmission and energy flux. Since the 'standard' WKB approximations reported in this paper, as is shown, conserves the energy flux it seems obvious to propose to analyse turning point problems. Doing so allows to study problems where the net energy flux is zero because of the wave reflection at a turning point. This will give detailed information on the internal reflection

of waves in a non-uniform beam structure and can potentially be used to analyse asymptotically stop and pass bands in rods with periodic curvature.

Acknowledgements. The authors address their sincere gratitude to Prof. C. J. Chapman for the many discussions on the topic.

Funding statement. The research is funded by *The Danish Council for Independent Research, Technology and Production Sciences*.

Appendix A. Comparison of rod theories and elastodynamics

Here, the validity ranges of the Rayleigh beam theory and the Timoshenko beam theory are demonstrated and discussed briefly. In figure 4, the dispersion diagram for a beam in terms of the Rayleigh beam model, the Timoshenko beam model and the Pochhammer–Chree exact solution of elastodynamics is shown. For details on the Pochhammer–Chree solution, see Chree [17]. The plot illustrates how well the first branch of the Timoshenko model compares to the Pochhammer–Chree solution in a large frequency range (until $\omega^* \approx 14$ kHz corresponding to $\omega \approx 3$), whereas the Rayleigh model compares well only at much lower frequencies. There is an obvious mismatch between Timoshenko theory and Pochhammer–Chree when it comes to the second branch (the shear wave). This is not of any great importance for frequencies lower than this cut-on frequency as the shear wave in this regions is evanescent. It should be mentioned that the cut-on can be perfectly matched with a proper selection of λ. For the non-uniform Timoshenko beams, the lowest cut-on is found to be $\omega^* \approx 8$ kHz for both the straight and curved beam model with the parameters in §4. The disagreement between Rayleigh and Timoshenko model can even be observed by comparing the results in, for instance, tables 1 and 3. Here, the deviation between the Rayleigh results and the Timoshenko results is about 17% already at the sixth eigenfrequency.

References

1. Fröman N, Fröman PO. 2004 *Physical problems solved by the phase-integral method*. Cambridge, UK: Cambridge University Press.
2. Bender CM, Orszag SA. 1978 *Advanced mathematical methods for scientists and engineers*. New York, NY: McGraw-Hill.
3. Rienstra SW. 1999 Sound transmission in slowly varying circular annular lined ducts with flow. *J. Fluid Mech.* **380**, 279–296. (doi:10.1017/S0022112098003607)
4. Cooper AJ, Peake N. 2001 Propagation of unsteady disturbances in a slowly varying duct with mean swirling flow. *J. Fluid Mech.* **445**, 207–234. (doi:10.1017/S0022112001005559)
5. Brambley EJ, Peake N. 2008 Sound transmission in strongly curved slowly varying cylindrical ducts with flow. *J. Fluid Mech.* **596**, 387–412. (doi:10.1017/S0022112007009603)
6. Scott JFM, Woodhouse J. 1992 Vibration of an elastic strip with varying curvature. *Phil. Trans. R. Soc. Lond. A* **339**, 587–625. (doi:10.1098/rsta.1992.0052)
7. Gridin D, Craster RV, Fong J, Lowe MJS, Beard M. 2003 The high-frequency asymptotic analysis of guided waves in circular elastic annulus. *Wave Motion* **38**, 67–90. (doi:10.1016/S0165-2125(03)00002-7)
8. Rosenfeld G, Keller JB. 1975 Wave propagation in nonuniform elastic rods. *Acoust. Soc. Am.* **57**, 1094–1096. (doi:10.1121/1.380558)
9. Pierce AD. 1970 Physical interpretation of the WKB or eikonal approximation for waves and vibrations in inhomogeneous beams and plates. *Acoust. Soc. Am.* **48**, 275–284. (doi:10.1121/1.1912125)
10. Langley R. 1999 Wave evolution, reflection, and transmission along inhomogeneous waveguides. *J. Sound Vib.* **227**, 131–158. (doi:10.1006/jsvi.1999.2337)
11. Sorokin SV, Chapman CJ. 2011 A hierarchy of rational Timoshenko dispersion relations. *J. Sound Vib.* **330**, 5460–5473. (doi:10.1016/j.jsv2011.06.004)

12. Shames IH, Dym CL. 1991 *Energy and finite element methods in structural mechanics*. London, UK: Taylor & Francis.
13. Rayleigh JWS. 1945 *The theory of sound*. New York, NY: Dover Publications.
14. Chapman CJ, Sorokin SV. 2010 The finite-product method in the theory of waves and stability. *Proc. R. Soc. A* **466**, 471–491. (doi:10.1098/rspa.2009.0255)
15. Hinch EJ. 1991 *Perturbation methods*. Cambridge, UK: Cambridge University Press.
16. Rao S. 2004 *Mechanical vibrations*. Englewood Cliffs, NJ: Prentice Hall.
17. Chree C. 1889 The equations of an isotropic elastic solid in polar and cylindrical coordinates, their solutions and applications. *Trans. Camb. Philos. Soc.* **14**, 250–309.

Paper 2

Nielsen R.B, Peake N. (*to be submitted*): "Tunnelling effects of waves in acoustic flow ducts" *Journal of Sound and Vibration*

Tunnelling effects of acoustic waves in slowly varying axisymmetric flow ducts

R.B. Nielsen[a], N. Peake[b]

[a]*Department of Mechanical and Manufacturing Engineering, Aalborg University, Fibigerstraede 16, 9220 Aalborg, Denmark*
[b]*Department of Applied Mathematics and Theoretical Physics, University of Cambridge, Wilberforce Road, CB3 0WA, United Kingdom*

Abstract

The multiple-scales Wentzel-Kramers-Brillouin (WKB) approximation is applied to model the propagation of acoustic waves in an axisymmetric flow duct with a constriction. An analysis of the reflection/transmission process of modes tunnelling through the constriction is conducted. The resulting piecewise solution consists of WKB solutions in regions away from the constriction and a solution valid in the near vicinity of it. A complementary approach is demonstrated hereafter and a uniformly valid solution is derived. The solutions are demonstrated through two test cases, one with and one without a mean flow. The effect of tunnelling is illustrated and the correspondence between the piecewise and the uniform solution is shown.

Keywords: Non-uniform acoustic duct, tunnelling effects, turning point analysis, uniformly valid solution

1. Introduction

The interest in reducing noise emission from machinery such as aircraft engines have resulted in a considerable effort payed to study sound transmission through slowly varying flow ducts. Consequently, a vast number of alterations of such waveguide studies are currently available. A small selection of these are: Circular lined ducts with a mean flow [1], ducts of arbitrary cross section with a mean flow [2], ducts with a mean swirling flow

Email address: rn@m-tech.aau.dk (R.B. Nielsen)

[3], and strongly curved ducts [4]. In these papers formulae for wavenumbers and amplitudes are derived using the Wentzel-Kramers-Brillouin (WKB) approximation which is applicable when the duct variation is small over a wave length. An analysis of modes undergoing a transition from cut-on to cut-off in the duct is often included and reveals that an incident wave is fully reflected with a phase shift $-\pi/2$ at the transition point. Consequently only an evanescent wave is transmitted beyond the transition point and the net energy flux of the mode therefore vanishes. This effect of internal wave reflection is advantageous from a noise reduction perspective and is the main focus of this paper.

The singular transition points in acoustics are analog to the turning points occurring in solutions to the Schrödingers equation which have been studied intensively. A parabolic potential with two turning points is treated in [5] and expressions for reflection and transmission coefficients depending on the distance between the turning points was derived. Keller [5] furthermore derived a uniformly valid approximation for a general potential with two turning points.From this uniformly valid solution reflection and transmission coefficients can be extracted. By such a solution one avoids the tedious process of matching inner and outer solutions in overlap regions which contrasts the more traditional procedure available from [6] or [7].

The concept of uniformly valid solutions have been employed in flow duct acoustics before. In [8] a uniformly valid solution for modes undergoing a cut-on cut-off transition in a hard-walled acoustic duct of arbitrary cross section with a irrotational mean flow was derived. It does not seem, however, that the acoustic duct analogy of the work by Keller [5] has been attempted. The focus of this paper is specifically to apply the WKB method to model the wave propagation in an acoustic duct with two turning points and thereby determine the inner and outer solution and the corresponding uniform solution.

The description of the acoustic field using eigenmodes is attractive since these form a complete basis from where any solution may be represented by summation of these eigenmodes. The results from previous publications allow only modes that remains cut-on through out the duct and those that is fully reflected at a transition point to be accounted for. The effect of a mode that cuts off and cuts on again slightly further downstream can therefore not be accounted for yet. Having such results available would help engineers in the design process of aircraft engines when analysing the noise transmission from the fan to the surroundings. The result may furthermore serve as benchmark

solutions for computational aeroacoustic codes.

This paper focuses on the reflection and transmission of modes tunnelling through a *cut-on cut-off cut-on* region of a slowly varying cylindrical hard-walled duct with an irrotational mean flow. The analysis is presented in the following order. In Section 2 the equations governing the flow and acoustic field are presented. The slowly varying modes, i.e. those that are either well cut-on or those far away from the transition points are derived in Section 3. In Section 4 the wave motion through the neck of the duct is studied and by asymptotic matching to the outer solution reflection and transmission coefficients are determined. Lastly, a uniform approximation is derived which is valid both far up- and downstream as well as in close proximity of the transition points. This derivation is presented in Section 5. The results are finally presented through a collection of test cases in Section 6. Here the effect of tunnelling is illustrated and the correspondence between the uniform solution and the piecewise solution is shown.

2. Problem formulation

The setup of the problem largely follows that of [8] and the similar notation is therefore adopted. The duct is defined as hard-walled and circular, and the flow and sound field enters the duct from each side as indicated in Figure 1. The acoustic medium is assumed to be a compressible inviscid isentropic irrotational gas. In what follows we non-dimensionalise distances by the far upstream radius R_∞, speeds and density by c_∞ and ρ_∞, respectively. Let,

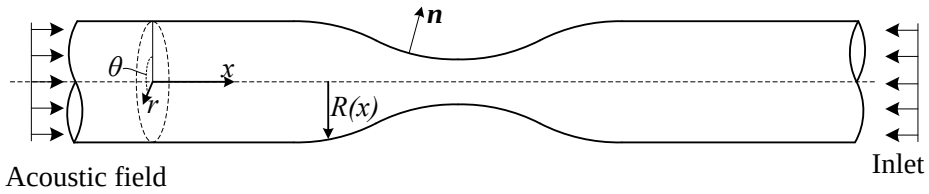

Figure 1: Illustration of a duct with a constriction. The flow is assumed to enter the duct from the right hand side and the acoustic field is assumed to enter from the left hand side.

with no loss of generality, the neck of the duct be located symmetrically about $x = 0$ for convenience. The duct is assumed to be slowly varying, that is the ratio between the local crosswise length scale R_∞, compared to the length scale over which the duct geometry changes l is small, i.e. $\epsilon = R_\infty/l << 1$. Thus, on a slow scale defined as $X = \epsilon x$ the radius varies like $R(X)$.

The flow field is split into a stationary mean flow and small time-harmonic perturbations [1]

$$[\tilde{\mathbf{v}}, \tilde{\rho}, \tilde{p}, \tilde{c}] = [\mathbf{V}, D, P, C] + [\nabla\phi, \rho, p, c]\,\mathrm{e}^{-\mathrm{i}\omega t} \tag{1}$$

where $\tilde{\mathbf{v}}$ designate the velocity field and $\tilde{p}$ is the pressure. The equations governing the flow field are [9]

$$0 = \frac{\partial\tilde{\rho}}{\partial t} + \nabla\cdot(\tilde{\rho}\tilde{\mathbf{v}}) \tag{2}$$

$$0 = \tilde{\rho}\left(\frac{\partial\tilde{\mathbf{v}}}{\partial t} + \tilde{\mathbf{v}}\cdot\nabla\tilde{\mathbf{v}}\right) + \nabla\tilde{p} \tag{3}$$

$$\tilde{c}^2 = \tilde{\rho}^{\gamma-1} \tag{4}$$

$$\gamma\tilde{p} = \tilde{\rho}^{\gamma} \tag{5}$$

where γ is the ratio of specific heats. With the introduction of the velocity potential ϕ pressure and density perturbations can be eliminated and the convected wave equation emerges

$$\nabla\cdot(D\nabla\phi) - D\left(-\mathrm{i}\omega + \mathbf{V}\cdot\nabla\right)\left[\frac{1}{C^2}\left(-\mathrm{i}\omega + \mathbf{V}\cdot\nabla\right)\phi\right] = 0 \tag{6}$$

A time dependence $\mathrm{e}^{-\mathrm{i}\omega t}$ has been adopted. For a hard-walled duct with outward pointing normal $\mathbf{n}$ the boundary conditions are

$$\nabla\phi\cdot\mathbf{n} = 0 \tag{7}$$

The steady mean flow component can according to [1] be expanded by

$$\mathbf{V}(X, r, \theta) = U_0(X)\mathbf{e}_x + \epsilon V_1(X, r)\mathbf{e}_r + O(\epsilon^2) \tag{8}$$

$$D(X, r) = D_0(X) + O(\epsilon^2) \tag{9}$$

$$C(X, r) = C_0(X) + O(\epsilon^2) \tag{10}$$

$$P(X, r) = P_0(X) + O(\epsilon^2) \tag{11}$$

where V_1 denotes a radial flow. The leading order mean flow components can be determined from Bernoulli's equation, mass flux conservation, and equation (4) and (5). A slowly varying solution to equation (6) is derived in the following subsection.

3. The slowly varying modes

Due to the circular cross-section the solution will be of Fourier-WKB form, specifically we assume

$$\phi \sim \left(\Phi_0 + \epsilon\Phi_1 + O(\epsilon^2)\right) \mathrm{e}^{\frac{\mathrm{i}}{\epsilon}\int^X k(X')\mathrm{d}X' - \mathrm{i}m\theta}, \text{ as } \epsilon \to 0 \tag{12}$$

Inserting this in (6) and collecting terms of $O(1)$ yields the Bessel equation

$$\frac{\partial^2\Phi_0}{\partial r^2} + \frac{1}{r}\frac{\partial\Phi_0}{\partial r} + \left(\frac{(\omega - kU_0)^2}{C_0^2} - k^2 - \frac{m^2}{r^2}\right)\Phi_0 = 0 \tag{13}$$

where m and k are the circumferential and axial wavenumbers, respectively. The $O(1)$ boundary condition becomes

$$\frac{\partial\Phi_0}{\partial r} = 0 \quad \text{on} \quad r = R(X) \tag{14}$$

with the introduction of $\Phi_0 = N(X)\psi(r;X)$ we have

$$\psi = b_1 J_m(\alpha r) \tag{15}$$

where b_1 is an arbitrary constant to be determined from the sound source and $\alpha = \frac{\mu_j}{R(X)}$ with μ_j being a root of $J'_m(\mu_j) = 0$. A term proportional to the Bessel function of the second kind has been omitted in (15) to remove the singularity at $r = 0$. From the $O(1)$ boundary condition the axial wavenumber is determined

$$k = \frac{-\omega U_0}{C_0^2 - U_0^2} \pm \frac{\omega C_0 \sigma}{C_0^2 - U_0^2} \tag{16}$$

in which σ is the reduced wavenumber

$$\sigma = \sqrt{1 - (C_0^2 - U_0^2)\frac{\alpha^2}{\omega^2}} \tag{17}$$

The unknown axially varying amplitude $N(X)$ is obtainable from a solvability condition determined from the $O(\epsilon)$ terms in the convected wave equation. After some manipulation and the application of the steady mass conservation condition

$$\frac{\partial}{\partial X}(D_0 U_0) = -\frac{D_0}{r}\frac{\partial}{\partial r}(rV_1) \tag{18}$$

one arrives at the following $O(\epsilon)$ terms

$$\frac{\partial^2\Phi_1}{\partial r^2}+\frac{1}{r}\frac{\partial\Phi_1}{\partial r}+\left(\frac{(\omega-kU_0)^2}{C_0^2}-k^2-\frac{m^2}{r^2}\right)\Phi_1=$$
$$-\frac{\mathrm{i}}{\Phi_0}\left\{\frac{\partial}{\partial X}\left[\left(\frac{(\omega-kU_0)U_0}{C_0^2}+k\right)D_0\Phi_0^2\right]+\frac{1}{r}\frac{\partial}{\partial r}\left[rV_1\frac{\omega-kU_0}{C_0^2}D_0\Phi_0^2\right]\right\} \quad (19)$$

with $O(\epsilon)$ boundary conditions

$$\frac{\partial\Phi_1}{\partial r}+\mathrm{i}kR'\Phi_0=0 \quad \text{on} \quad r=R(X) \quad (20)$$

To leave the solvability condition on Φ_0 only multiply (19) with Φ_0 and integrate over the duct cross section. After the use of the $O(\epsilon)$ boundary condition, the mean flow equations to eliminate V_1, and Leibniz rule one arrives at the adiabatic invariant

$$\frac{\mathrm{i}}{N}\frac{\mathrm{d}}{\mathrm{d}X}\left[\frac{\omega\sigma D_0R^2}{C_0}N^2\right]=0 \quad (21)$$

Thus, we conclude that, apart from a multiplicative constant, $N(X)$ is

$$N(X)=\sqrt{\frac{C_0(X)}{\omega\sigma(X)D_0(X)R^2(X)}} \quad (22)$$

The outer solution, i.e. away from prospective transition points, is found by summation of modes of the following form

$$\phi_j=\sqrt{\frac{C_0(X)}{\omega\sigma(X)D_0(X)R^2(X)}}J_m\left(\frac{\mu_k}{R(X)}r\right)\mathrm{e}^{-\mathrm{i}m\theta}\mathrm{e}^{-\frac{\mathrm{i}}{\epsilon}\int^{X'}\frac{\omega U_0}{C_0^2-U_0^2}\mathrm{d}X'}$$
$$\left\{\beta_1\mathrm{e}^{\frac{\mathrm{i}}{\epsilon}\int^{X'}\frac{\omega C_0\sigma}{C_0^2-U_0^2}\mathrm{d}X'}+\beta_2\mathrm{e}^{-\frac{\mathrm{i}}{\epsilon}\int^{X'}\frac{\omega C_0\sigma}{C_0^2-U_0^2}\mathrm{d}X'}\right\} \quad (23)$$

With the designations $\mathcal{T}$, $\mathcal{I}$ and $\mathcal{R}$ representing transmitted, incident, and reflected waves, respectively, the solutions are stated as: $\beta_1=\mathcal{T}$ and $\beta_2=0$ to the right of the neck, and by: $\beta_2=\mathcal{I}$ and $\beta_1=\mathcal{R}$ to the left of the neck. We note, furthermore, that at a turning point, i.e. when $\sigma(X)$ is zero $N(X)$, becomes infinite and the solution breaks down. This case is treated in the next section.

4. Turning point analysis

The singular behavior of the transport equation (21) at a turning point is due to the neglect of higher order terms that become significant when $\Phi_0(X)$ changes rapidly. The most rapidly varying $O(\epsilon^2)$ term is

$$D_0 \left(1 - \frac{U_0^2}{C_0^2}\right) \frac{\partial^2 \Phi_0}{\partial X^2} \tag{24}$$

Thus, promoting this term to the transport equation removes the singular behavior. First, add (24) to (19), multiply with $\Phi_0(X)$, and then integration over the cross section yields

$$\mathrm{i}\frac{\mathrm{d}}{\mathrm{d}X}\left[\frac{\omega\sigma D_0 R^2}{C_0} N^2(X)\right] + \epsilon R^2 D_0 \left(1 - \frac{U_0^2}{C_0^2}\right) N(X) \frac{\mathrm{d}^2 N(X)}{\mathrm{d}X^2} = 0 \tag{25}$$

We shall now consider the behavior of the reduced wavenumber in order to introduce an appropriate inner scale that balances the terms in (25) as $\epsilon \to 0$. Close to the neck we expand the reduced wavenumber by

$$\sigma^2 \sim A^2(X^2 - b) \quad \text{as} \quad X \to 0 \tag{26}$$

The parameter b is real, but may be positive, zero or negative representing the cases of two real turning points, a double turning point, or two complex turning points, respectively. Now we introduce a scaled inner coordinate $\bar{X} = \epsilon^q X$. Selecting $q = -1/2$ ensures that the higher order term in (25) becomes as significant as the original terms in the transport equation. Furthermore, do we introduce a scaled version of b, $b = \epsilon\bar{b}$, which ensures b is as significant as X^2 in the expansion of σ^2. Thus, the turning points ($X_t = \pm\sqrt{b}$) are necessarily located on $\bar{X}$. The transport equation becomes

$$\frac{\mathrm{d}^2 B}{\mathrm{d}\bar{X}^2} + \left(\frac{\omega C_0}{C_0^2 - U_0^2}\right)^2 A^2 \left(\bar{X}^2 - \bar{b}\right) B = 0 \tag{27}$$

Where the following substitution has been made

$$N(X) = B(X)\mathrm{e}^{-\frac{\mathrm{i}}{\epsilon}\int_0^X \frac{\omega c_0 \sigma}{C_0^2 - U_0^2}\mathrm{d}X'} \tag{28}$$

to reduce the equation to standard form. One may remark that derivatives of any slowly varying quantity (U_0, C_0, D_0, or R) are roughly constant on

the inner scale and therefore should be ignored. Further reduction of (27) is done by the two parameters

$$z = \bar{X}\sqrt{2A\frac{\omega C_0}{C_0^2 - U_0^2}} \tag{29}$$

$$a = \frac{A\bar{b}}{2}\frac{\omega C_0}{C_0^2 - U_0^2} \tag{30}$$

we then arrive at

$$\frac{\mathrm{d}^2 B}{\mathrm{d}z^2} + \left(\frac{z^2}{4} - a\right) B = 0 \tag{31}$$

This is the *Parabolic Cylinder Equation* and has the solution [10]

$$B = c_1 W(a, z) + c_2 W(a, -z) \tag{32}$$

where c_1 and c_2 are arbitrary constants to be determined from matching which is done by comparing the inner and outer solutions when these are expanded in the appropriate limits. The outer solution in the transmission region when X approaches the transition point is written as:

$$\phi_{\mathcal{T}} \sim \left[\sqrt{\frac{C_0}{\omega D_0 R^2}}\right]_{X=X_t} \frac{\mathcal{T}}{A^{1/2}X^{1/2}} \mathrm{e}^{\frac{\mathrm{i}}{\epsilon}\frac{\omega C_0}{C_0^2-U_0^2}\frac{A}{2}X^2 - \mathrm{i}\frac{a}{2} - \mathrm{i}a\ln\left(\frac{2X}{\sqrt{b}}\right)} \qquad \text{as} \quad X \to \sqrt{b} \tag{33}$$

Here we have omitted the Bessel-Fourier and convected part of the solution as this appear similarly on both inner and outer solution. This result is obtainable through the application of an intermediate variable $Y = X/\epsilon^\eta$ with $0 < \eta < 1/2$ to neglect small phase shifts due to the smallness of ϵ.

The appropriate expansions of $W(a, z)$ for large positive and negative arguments are available in [10]. For $z \to \infty$ the result is

$$\phi_{inner} \sim \left[c_1\sqrt{\frac{\bar{k}}{2z}} - \mathrm{i}c_2\sqrt{\frac{1}{2\bar{k}z}}\right]\mathrm{e}^{\mathrm{i}\Omega} + \left[c_1\sqrt{\frac{\bar{k}}{2z}} + \mathrm{i}c_2\sqrt{\frac{1}{2\bar{k}z}}\right]\mathrm{e}^{-\mathrm{i}\Omega} \tag{34}$$

where

$$\Omega = \tfrac{1}{4}z^2 - a\ln(z) + \tfrac{1}{4}\pi + \tfrac{1}{2}\phi_2 \tag{35}$$

$$\phi_2 = \angle\Gamma\left(\tfrac{1}{2} + \mathrm{i}a\right) \tag{36}$$

$$\bar{k} = \sqrt{1 + \mathrm{e}^{2\pi a}} - \mathrm{e}^{\pi a} \tag{37}$$

At this intermediate step we are in a position to choose $c_2 = \mathrm{i}\bar{k}c_1$ to eliminate the left going wave. Rewriting the inner solution in terms of the outer variable X yields

$$\phi_{inner} \sim \frac{c_1 \bar{k} 2^{1/4}}{\left(\frac{\omega C_0}{C_0^2 - U_0^2}\right)^{1/4} \left(\frac{A}{\epsilon}\right)^{1/4} X^{1/2}} \mathrm{e}^{\frac{\mathrm{i}}{\epsilon} \frac{\omega C_0}{C_0^2 - U_0^2} \frac{A}{2} X^2 - \mathrm{i}a \ln\left(\frac{2X}{\sqrt{b}}\right) - \mathrm{i}\frac{a}{2}\ln(|a|) + \mathrm{i}\frac{\pi}{4} + \mathrm{i}\frac{\phi_2}{2}} \tag{38}$$

$$\text{as} \quad X \to \infty \tag{39}$$

By comparing terms in the inner and outer solutions and perform the similar expansions upstream from the constriction three additional matching conditions are found. The solutions to these are:

$$\frac{\mathcal{T}}{\mathcal{I}} = \frac{\mathrm{e}^{\mathrm{i}a - \mathrm{i}a\ln|a| + \mathrm{i}\phi_2}}{\sqrt{1 + \mathrm{e}^{2a\pi}}} \tag{40}$$

$$\frac{\mathcal{R}}{\mathcal{I}} = \frac{\mathrm{e}^{\pi a}\mathrm{e}^{\mathrm{i}a - \mathrm{i}a\ln|a| + \mathrm{i}\phi_2 - \mathrm{i}\pi/2}}{\sqrt{1 + \mathrm{e}^{2a\pi}}} \tag{41}$$

$$\frac{c_1}{\mathcal{I}} = \left[\sqrt{\frac{C_0}{\omega D_0}} \left(\frac{\omega C_0}{C_0^2 - U_0^2}\right)^{1/4}\right]_{X=X_t} \left(\frac{8}{\epsilon A}\right)^{1/4} \frac{\bar{k}^{1/2}}{\mathrm{i}\left(1 + \bar{k}^2\right)} \mathrm{e}^{\mathrm{i}\left(-\frac{a}{2}\ln|a| + \frac{a}{2} + \frac{\pi}{4} + \frac{\phi_2}{2}\right)} \tag{42}$$

$$c_2 = \mathrm{i}\bar{k}c_1 \tag{43}$$

The velocity potential in the inner region is finally given by

$$\phi_{inner} = \left(c_1 W(a, z) + c_2 W(a, -z)\right) J_m\left(\frac{\mu}{R(X)} r\right) \mathrm{e}^{\frac{\mathrm{i}}{\epsilon}\int_0^\infty \frac{-\omega U_0}{C_0^2 - U_0^2} \mathrm{d}X' - \mathrm{i}m\theta} \tag{44}$$

The solution derived in the this section consists of WKB solutions in the outer regions and the above solution in the inner region shall henceforth be referred to as a *composite solution*. In the next section we derive a solution valid at any location, i.e. a uniform solution.

5. Uniform solution

The derivation of a uniformly valid solution can be conducted from the leading order terms of (6) when the mean flow is assumed to be slowly varying. These are, see [2]:

$$\left(1 - \frac{U_0}{C_0}\right) \frac{\partial^2 \phi}{\partial x^2} + \frac{2\mathrm{i}\omega U_0}{C_0^2} \frac{\partial \phi}{\partial x} + \left(\frac{\omega^2}{C_0^2} - \alpha^2\right) \phi = O(\epsilon) \tag{45}$$

Again this is reducible to:

$$\frac{\partial^2 \tilde{\phi}}{\partial x^2} + k_2^2 \tilde{\phi} = O(\epsilon) \tag{46}$$

with the substitution:

$$\phi = \tilde{\phi} \mathrm{e}^{-\mathrm{i} \int \frac{U_0 \omega}{C_0^2 - U_0^2} \mathrm{d}x} \tag{47}$$

and $k_2 = \frac{\omega C_0 \sigma}{C_0^2 - U_0^2}$. Guided by [5] and [8] we shall seek a solution of the form

$$\tilde{\phi} = \Phi(X, r, \theta) \frac{G(\zeta)}{(\zeta_x)^{1/2}} \tag{48}$$

where $\zeta(x)$ is a function to be determined. We assume initially that its derivative ζ_x varies slowly. Immediately it is noticed that due to the neglect of higher order terms the second derivative of $\tilde{\phi}$ is

$$\frac{\partial^2 \tilde{\phi}}{\partial x^2} = G'' (\zeta_x)^{3/2} \Phi(X, r, \theta) \tag{49}$$

where primes denote derivatives wrt. ζ. Applying this in (46) yields

$$\left(G'' + \frac{k_2^2}{\zeta_x^2} G \right) \Phi(X, r, \theta) = 0 \tag{50}$$

By dropping the slowly varying Φ this becomes the parabolic cylinder equation provided that we select

$$\zeta_x^2 \left(\frac{\zeta^2}{4} - \eta \right) = k_2^2 \tag{51}$$

with ζ as the argument and η as a parameter corresponding to a in equation (31). Once again, the solution can be stated by summation of parabolic cylinder functions:

$$G(\zeta) = h_1 W(\eta, \zeta) + h_2 W(\eta, -\zeta) \tag{52}$$

but the relation between ζ and x remains unknown at this stage. To determine this relation we eliminate ζ_x in (51) which can be done by integration. At two real turning points located at $x = x_{0,1}$ we have $k_2^2 = 0$ corresponding

to $\zeta(x_0) = -2\sqrt{\eta}$ and $\zeta(x_1) = 2\sqrt{\eta}$ with $\eta > 0$. So equation (51) in the downstream region $x > x_1$ becomes

$$\frac{\zeta}{4}\sqrt{\zeta^2 - 4\eta} - \eta \ln\left[\frac{\zeta + \sqrt{\zeta^2 - 4\eta}}{2\eta}\right] = \int_{x_1}^{x} k_2 \mathrm{d}x \tag{53}$$

In the tunnelling region $x_0 < x < x_1$ we find

$$\frac{\zeta}{4}\sqrt{4\eta - \zeta^2} + \eta \sin^{-1}\left(\frac{\zeta}{2\sqrt{\eta}}\right) + \frac{\pi\eta}{4} = \int_{x_0}^{x} |k_2| \mathrm{d}x \tag{54}$$

By selecting $\zeta(x_1) = 2\sqrt{\eta}$ in this equation yields

$$\pi\eta = \int_{x_0}^{x_1} |k_2| \mathrm{d}x \tag{55}$$

Which determines η. In the upstream region $x < x_0$ we get:

$$\frac{\zeta}{4}\sqrt{\zeta^2 - 4\eta} + \eta \ln\left[\frac{-\zeta + \sqrt{\zeta^2 - 4\eta}}{2\eta}\right] = \int_{x_0}^{x} k_2 dx \tag{56}$$

Similarly, when $\eta < 0$ the turning points are complex and we have $k_2^2 = 0$ at $x_{0,1}$ where $\mathrm{Im}(x_{0,1}) \neq 0$, so at these locations $\zeta(x_0) = -2\mathrm{i}|\eta|^{1/2}$ and $\zeta(x_1) = 2\mathrm{i}|\eta|^{1/2}$. By eliminating ζ_x in equation (51) yields:

$$\frac{\zeta}{4}\sqrt{\zeta^2 + 4|\eta|} + |\eta| \ln\left(\frac{\zeta + \sqrt{\zeta^2 + 4|\eta|}}{2|\eta|^{1/2}}\right) = \int_{0}^{x} k \mathrm{d}x \tag{57}$$

for any x. Furthermore, do we find:

$$\pi|\eta| = \int_{\mathrm{Im}(x_0)}^{\mathrm{Im}(x_1)} k(\mathrm{i}s) \mathrm{d}s \tag{58}$$

The unknown η can now be determined from equation (55) and (58), while ζ is obtained by solving equation (53), (54), and (56) for $\eta > 0$ and equation (57) for $\eta < 0$, at each axial station. This naturally entails numerical integration of k in these equation and subsequent numerically solving for ζ which is straight forward in all cases. ζ_x is subsequently determined from equation (51).

The constants h_1 and h_2, and the function $\Phi(X, r, \theta)$ can now be determined. Similar to the analysis in section 4 do we require no left going wave downstream from the constriction and therefore $h_2 = \mathrm{i}\bar{k}h_1$. To fix the incident wave to be the same as the upstream WKB solution we select:

$$h_1\Phi(X, r, \theta) = \frac{2\sqrt{\bar{k}}\mathcal{I}}{\bar{k}^2 + 1}\sqrt{\frac{C_0^2}{D_0(C_0^2 - U_0^2)R^2}}\mathrm{e}^{-\mathrm{i}m\theta}J_m(\alpha r)\mathrm{e}^{-\frac{\mathrm{i}\eta}{2}\ln(\eta)+\frac{\mathrm{i}\eta}{2}-\frac{\mathrm{i}\pi}{4}+\frac{\mathrm{i}\phi_2}{2}} \tag{59}$$

This result is obtainable by expanding the parabolic cylinder functions in equation (52) for large negative arguments and compare to (23). This concludes the derivation of the uniform solution.

6. Results

Before turning to specific test cases the behaviour of $\mathcal{T}$ and $\mathcal{R}$ as $a \to \pm\infty$ and $a \to 0$ is examined. From *Stirling's formula* is it found that $\phi_2 \sim a\ln|a| - a \quad \text{as} \quad a \to \infty$. For large tunnelling distances it is found from (40) and (41) that $\left|\frac{\mathcal{T}}{\mathcal{I}}\right| \to 0$ and $\left|\frac{\mathcal{R}}{\mathcal{I}}\right| \to 1$. In the $a \to -\infty$ these are reversed. The phase changes are $\angle\frac{\mathcal{T}}{\mathcal{I}} \to 0$ and $\angle\frac{\mathcal{R}}{\mathcal{I}} \to \frac{-\pi}{2}$ as $a \to \pm\infty$. I.e. for large tunnelling distances the result becomes what is known from the well-known one turning point problem, namely a fully reflected wave with a $\frac{-\pi}{2}$ phase shift. If $a = 0$ then $\left|\frac{\mathcal{T}}{\mathcal{I}}\right| = \left|\frac{\mathcal{R}}{\mathcal{I}}\right| = \frac{1}{\sqrt{2}}$. Thus, when the two transitions points merge half the energy of the incident wave is transmitted and the other half is reflected.

6.1. Test cases

The radius of the acoustic duct is defined as:

$$R(X) = 1 - 0.3\,\mathrm{sech}(X) \tag{60}$$

We select furthermore $\epsilon = 0.1$, $\gamma = 1.4202$, and $\mathcal{I} = 1$. The results are demonstrated in two test cases, one with zero mean flow and one with a non-zero mean flow.

In the first test case is the mean flow zero. The circumferential wave number is $m = 21$ and the fourth radial mode is studied. This parametric choice replicates the zero mean flow test case in [8]. The axial variation of ϕ for three different frequencies is shown in Figure 2. The location of the

turning points are indicated to each plot in brackets in the figure caption. A comparison between the composite and the uniform solution is provided in Figure 3 and a contour map is found in Figure 4. The effect of tunnelling can be observed as the transition of a rapid decay of ϕ in the inner region, Figure 2a), to a harmonic shape of ϕ in Figure 2c). Inspection of the graphs also reveals a decrease in the peak value of ϕ of about 10% corresponding to a smaller acoustic pressure. The location of the peak also drifts from just ahead of the left most turning point to the center of the constriction. From Figure 3 is it demonstrated that the composite and the uniform solutions compare extremely well.

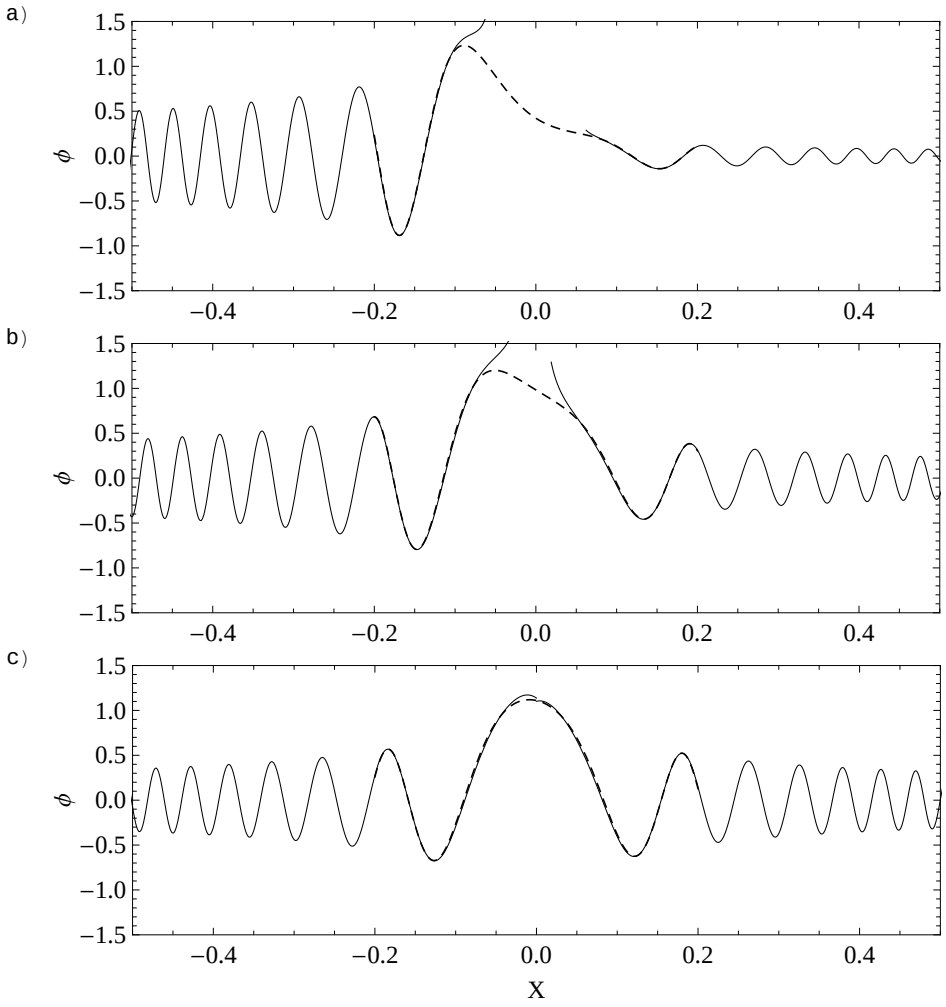

Figure 2: First test case: Axial variation of ϕ, solid lines: outer solution, dashed line: inner solution. *a)* at $\omega = 52.9$ ($X_t = \pm 0.052$), *b)* at $\omega = 52.93$ ($X_t = \pm 0.009$), *c)* at $\omega = 52.95$ ($X_t = \pm \mathrm{i}0.041$).

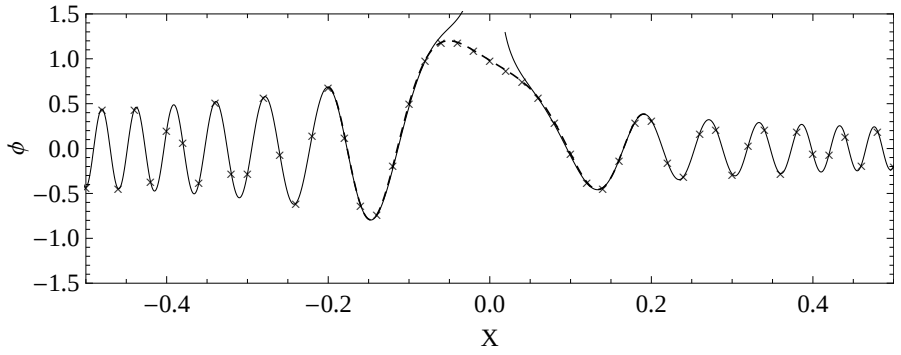

Figure 3: First test case: Comparison of composite and uniform solution, first test case at $\omega = 52.93$. Solid-Dashed curve: composite solution, crosses: Uniformly valid solution.

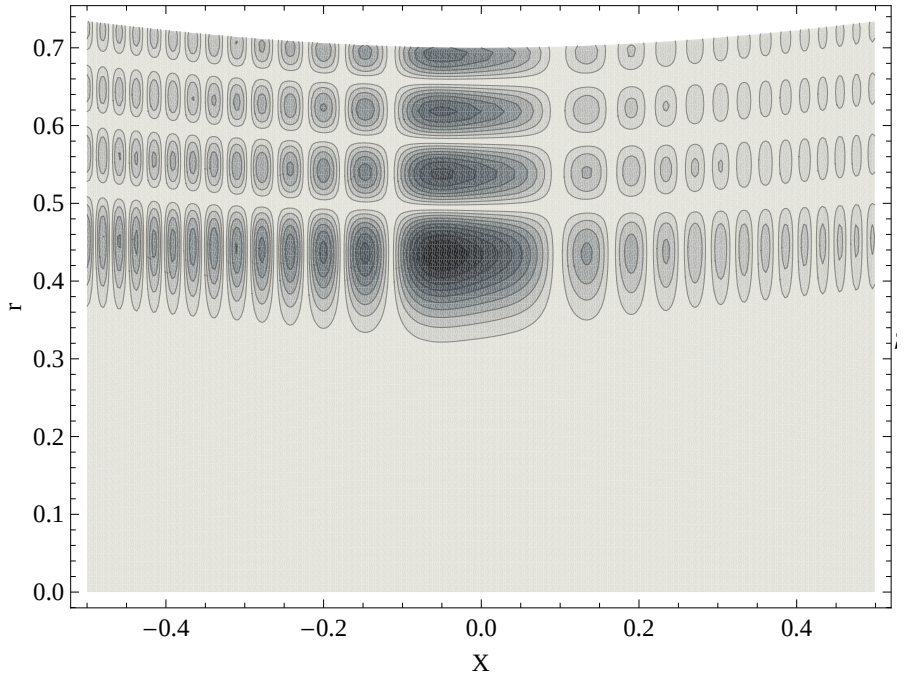

Figure 4: First test case: Contour map of upper half plane of $|\phi/\max(\phi)|$ at $\omega = 52.93$ with no mean flow, $m = 21$, fourth radial mode. Contour levels at intervals of 0.1.

The second test case has a mean flow of $U_0 = 0.2$, the circumferential wavenumber is $m = 4$ and the results are for the second radial mode. The axial variation of ϕ is found in Figure 5 for increasing frequencies. The distorted wave form to the left of the constriction arise due to the presence of the reflected wave of longer wave length interfering with the incident wave of shorter wave length. The uniformly valid solution and the composite solution are compared in Figure 6 where a very appreciable match between them is observed. In this plot a significant reflected wave is observed despite the fact that the mode remains cut-on throughout the duct. Specifically is $|\mathcal{R}/\mathcal{I}| \approx 0.43$.

The results demonstrate that the flow field is equally well obtainable by a uniform solution and by the more standard composite representation. The composite solution have the advantages due to its simple nature in the outer regions, whereas the uniform solution require evaluations is the parabolic cylinder function.

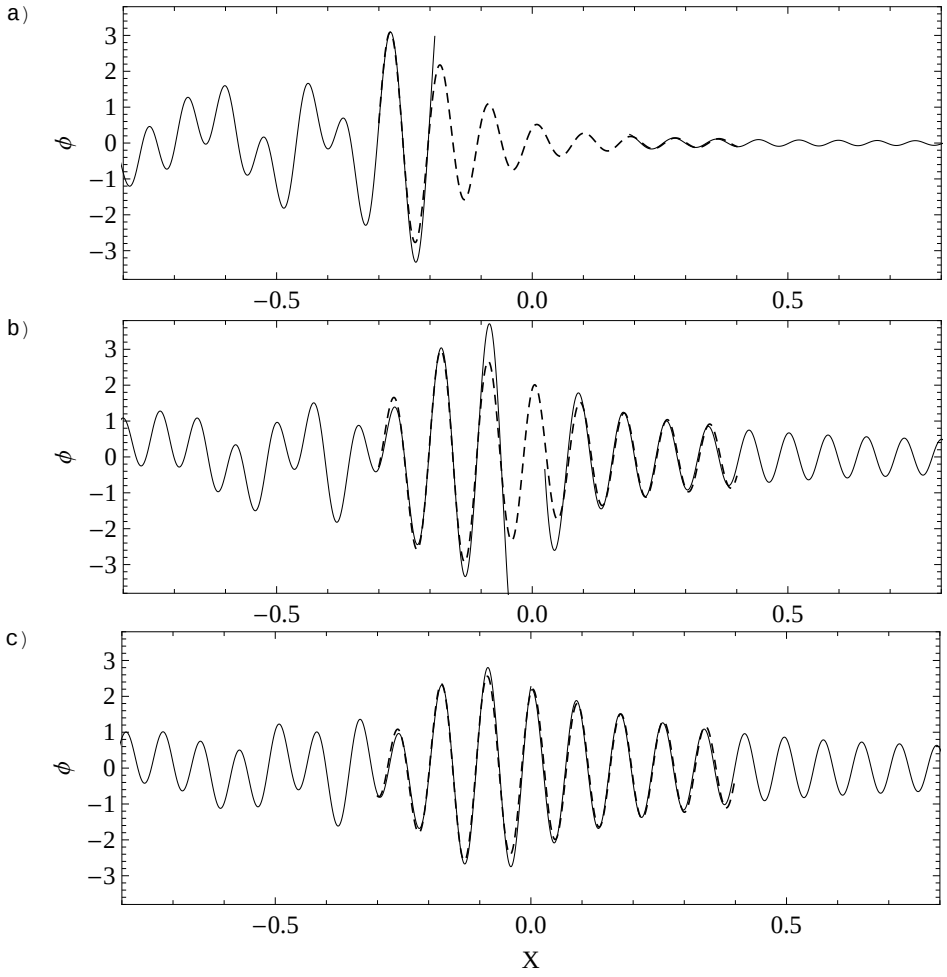

Figure 5: Second test case: Axial variation of ϕ, solid lines: outer solution, dashed line: inner solution. *a)* at $\omega = 11.635$ ($X_t = \pm 0.18$), *b)* at $\omega = 11.654$ ($X_t = \pm 0.015$), *c)* at $\omega = 11.66$. ($X_t = \pm \mathrm{i}0.10$)

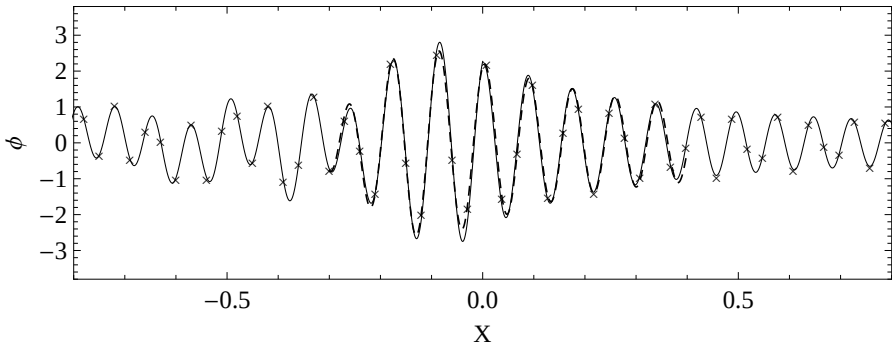

Figure 6: Second test case: Comparison of composite and uniform solution, second test case at $\omega = 11.66$. Solid-Dashed curve: composite solution, crosses: Uniformly valid solution.

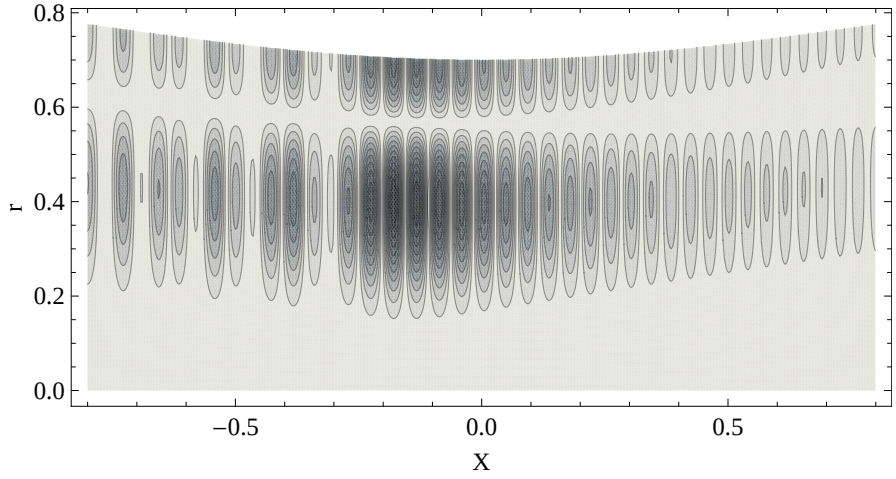

Figure 7: Second test case: Contour map of upper half plane of $|\phi/\max(\phi)|$ at $\omega = 11.654$. Contour levels at intervals of 0.1.

7. Conclusions

In this paper a cylindrical flow duct of slowly varying diameter has been considered and the WKB method has been employed to determine the slowly varying acoustic modes. An analysis of waves tunnelling through a narrow region of evanescent wave motion is conducted and the explicit dependence of the reflection and transmission coefficients on the tunnelling parameter is obtained. The results agree with the well known ones for large tunnelling distances, and for the tunnelling distance decreasing to zero. By use of the reflection and transmission coefficients the acoustic field is represented by a composite solution consisting of WKB solutions away from the tunnelling region and by parabolic cylinder functions in the vicinity of the tunnelling region. A uniformly valid solution is also derived which is valid at any location in the duct. This solution uses parabolic cylinder functions in conjunction with coordinate stretching.

The effect of tunnelling is demonstrated at various frequencies for a zero mean flow test case and a test case with a mean flow. Through the test cases are a very accurate match between the composite and the uniform solution demonstrated. The test cases also show how an incident mode that remains propagating throughout the duct causes a reflection from the constriction.

It seems natural to extend the results to include annular ducts which would allow the results to be directly applicable to study more realistic aircraft engine geometries similar to [11]. The results can furthermore serve as important reference solutions when numerical techniques, such as computational aero-acoustic codes, are employed to capture the details of waves passing through a neck of a waveguide. The results generally enhance the option to remain using multiple-scales methods to estimate the noise pollution from aircraft engines and the relatively simple expression for reflection and transmission coefficients should likewise help detecting if internal resonances builds up.

Acknowledgement

The research is funded by *The Danish Council for Independent Research, Technology and Production Sciences* Grant number: UK 95 OS63822 PO83004.

References

[1] S. W. Rienstra, Sound transmission in slowly varying circular and annular lined ducts with flow, Journal of Fluid Mechanics 380 (1999) 279–296, doi: 10.1017/S0022112098003607.

[2] S. W. Rienstra, Sound propagation in slowly varying lined flow ducts of arbitrary cross-section, Journal of Fluid Mechanics 495 (2003) 157–173, doi: 10.1017/S0022112003006050.

[3] A. J. Cooper, N. Peake, Propagation of unsteady distubances in slowly varying duct with mean swirling flow, Journal of Fluid Mechanics 445 (2001) 207–234, doi: 10.1017/S0022112001005559.

[4] E. Brambley, N. Peake, Sound transmission in strongly curved slowly varying cylindrical ducts with flow, Journal of Fluid Mechanics 596 (2008) 387–412, doi: 10.1017/S0022112007009603.

[5] J. B. Keller, Uniform solutions for scattering by a potential barrier and bound states of a potential well, Am. J. Phys. 54 (6) (1986) 546–550, doi: 10.1119/1.14560.

[6] E. J. Hinch, Perturbation Methods, Cambridge University Press, 1991.

[7] C. M. Bender, S. A. Orszag, Advanced Mathematical Methods for Scientists and Engineers, McGraw-Hill, 1978.

[8] N. C. Ovenden, A uniformly valid multiple scales solution for cut-on cut-off transition of sound in flow ducts, Journal of Sound and Vibration 286 (2005) 403–416, doi: 10.1016/j.jsv.2004.12.009.

[9] A. D. Pierce, Acoustics, an Introduction to its Physical Principles and Applications, McGraw-Hill, 1981.

[10] F. W. J. Olver, D. W. Lozier, R. F. Boisvert, C. W. Clark, NIST Handbook of Mathematical Functions, Cambridge University Press, 2010.

[11] S. W. Rienstra, W. Eversman, A numerical comparison between the multiple-scales and finite-elelment solution for sound propagation in lined flow ducts, Journal of Fluid Mechanics 437 (2001) 367–384, doi: 10.2514/6.1999-1821.

Paper 3

Nielsen R.B, Sorokin S.V. (*under review*): "Periodicity effects of axial waves in elastic compound rods" *Journal of Sound and Vibration*

Periodicity effects of axial waves in elastic compound rods

R.B. Nielsen, S.V. Sorokin

Department of Mechanical and Manufacturing Engineering, Aalborg University, Fibigerstraede 16, 9220 Aalborg, Denmark

Abstract

Floquet analysis is applied to the Bernoulli-Euler model for axial waves in a periodic rod. Explicit asymptotic formulae for the stop band borders are given and the topology of the stop band pattern is explained. Eigenfrequencies of the symmetric unit cell are determined by the *Phase-closure Principle*, and their correspondence with stop band formation is shown. Steady-state and transient dynamics of a periodic rod of finite length are analysed numerically and the difference in structural response when excitation is done in either stop- or pass bands is demonstrated. A physical interpretation of the underlying mechanisms of stop bands is proposed.

Keywords: Periodicity effects, Axial waves, Phase-closure Principle, Transient effects, Band gaps

1. Introduction

Analysis of wave propagation in periodic structures is a classical topic in theory of guided waves and has been studied for centuries. The classical textbook on this topic is [1] which demonstrates the diversity of possible realms of physics in which the periodicity phenomenon is of interest. Acoustic and electromagnetic (in particular, optical) waveguides have gained much attention from this viewpoint [2], [3], [4], [5], and [6]. Periodicity effects arising in the theory of elastodynamics and in vibroacoustics have been studied in [7] and [8], surface waves in periodic plates in [9], and surface waves on periodic elastic half spaces are for instance studied by [10] and [11].

A variety of methods has been employed in the abovementioned references. The choice of a method to analyse the problem depends upon

Email address: rn@m-tech.aau.dk (R.B. Nielsen)

whether a three-, two- or one-dimensional formulation is used. For analysis of three- and two-dimensional waveguides, the method of multiple scales and Floquet's theorem appear to be the preferred choices [2]-[6], although alternative methods, such as null field approach [12], have also been used. A common explanation of the band gap phenomenon is the so-called *Bragg resonance* which originates from constructive interference of the multiple reflections occurring from the periodic perturbation of the waveguide, although an alternative *non-Bragg* resonance mechanism of generation of stop bands in two-dimensional waveguides has been discussed in [5].

In structural dynamics, a canonical and much studied model is an idealised lumped parameter system consisting of point masses and massless springs, see for instance [1]. Similarly, wave propagation in one- and two-dimensional lattices composed of masses and springs is treated in [13]. Continuous one-dimensional structures such as beams with periodic supports have been considered amongst others in [14] and [15]. Numerous papers are concerned with analysis of more complex one-, two-, and three-dimensional elastic structures such as fluid filled curved pipes [16], elastic plates with periodic inclusions of rigid pins in [17], and elastic waves in a medium with periodically spaced spheres in [18], where the dependence between impendence mismatch and existence of band gaps is also discussed. A rather extensive review of periodicity studies can be found in [19] encompassing various structures like beams, rib-skin structures, periodically stiffened cylinders, etc.

It is natural to conclude from the abovementioned references, that the periodicity phenomenon may be employed for tailoring dynamic characteristics, such as insertion losses and eigenfrequencies, of non-uniform structures, as has been done, for example, in [20] and [21]. To guide such a tailoring, it is expedient to have simple formulae relating waveguide parameters to band gap locations and shapes. Despite the variety of areas and diversity of specific problems in wave propagation in periodic waveguides, not much attention has been given to pursue such formulae. The present paper is aimed to fill in this gap by means of rigorous asymptotic analysis of characteristic equations and consistent use of the Phase-closure Principle. To exercise these tasks, a model, which is as simple as possible and as complicated as necessary should be chosen.

The mass-spring structures, compared to the continuous structures, lack the basic wave motion in the constituents which to the authors opinion is an essential ingredient in the understanding of stop and pass bands in continuous structures. Continuous structures such as beams considered by [14], however, add further complexities which are not directly related to the ex-

istence of stop bands, more specifically evanescent and dispersive travelling waves. For these reasons we choose to employ the Bernoulli-Euler model for axial waves in rods which does allow wave motion in its basic constituents, but do not support evanescent and dispersive travelling waves. Fortunately, the Bernoulli-Euler model is the low frequency asymptotical reduction of plane symmetric waves in an elastic layer, see [22]. The acoustic analogy to this model is the somewhat unrealistic model for plane acoustic waves in a duct with a multi-component periodic gas. Such a periodic waveguide was in fact also considered by [1] as a special case of problems governed by Hill's equation, but this reference did not present results and provide physical interpretations similar to those given in this paper. A similar problem was also studied in [23], but here attention was given to topology optimisation of a two material compound rod with the objective to maximise eigenfrequency gaps.

Our aim is to highlight the underlying mechanisms involved in the generation of stop bands in a periodic Bernoulli-Euler rod. In Section 2 results from Floquet analysis and the reflection and transmission coefficients at an interface are provided. Already here an advantage of the model chosen arises since all waveguide properties are condensable to just two principle parameters both having a clear physical meaning. In Section 3 we provide some important details of the physics behind stop bands obtained through asymptotic analysis of the results reported in Section 3. Section 4 discusses the topology of the stop band pattern and its relation to the waveguide parameters. In Section 5 the *Phase-closure Principle* is applied in order to link resonance criteria for a unit cell and the individual segments to the location of stop band borders and pass band locations. The results obtained so far are discussed in Section 6 where emphasis is put on physical interpretation of the findings made throughout preceding Sections. Lastly, in Section 7, steady-state forced response of a rod with periodic insert is considered in two alternative formulations. The numerical analysis of transients in a rod is also presented and energy accumulation/transmission is discussed. Conclusions are given in Section 8.

2. The model

The model employed is shown in Figure 1 where a unit cell from an infinite structure is sketched. We initially define the unit cell as a rod consisting of two segments whose uniaxial stress wave speeds are given by $c_j = \sqrt{E_j/\rho_j}$, where E_j is the elastic modulus and ρ_j is density. If the unit cell is viewed as a strip cut from a plate, then the plane strain wave speeds

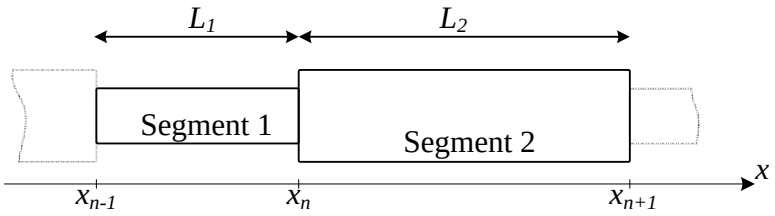

Figure 1: Unit cell of present study consisting of segment 1 and segment 2. x_n indicates the location of interfaces.

are $c_j = \sqrt{\frac{E_j}{\rho_j(1-\nu_j^2)}}$ where ν_j are Poisson's ratios. We designate lengths and cross sectional areas as L_j and A_j (for a plate strip of height h_j then $A_j = 1 \cdot h_j$, i.e. height per unit width) where the subscript $j = 1, 2$ denote the segment number within the unit cell. The governing equation for axial waves in non-dimensional form is:

$$\frac{\partial^2 u_j}{\partial x^2} - \frac{1}{c_j^2/c_1^2}\frac{\partial^2 u_j}{\partial t^2} = 0 \tag{1}$$

where lengths have been scaled by L_1, speeds by c_1, and time by L_1/c_1. If furthermore, a non-dimensional frequency ω is introduced as $\omega = \Omega L_1/c_1$ a general solution to equation (1) is presented as:

$$u_j(x,t) = \alpha_j \mathrm{e}^{\mathrm{i}k_j x - \mathrm{i}\omega t} + \beta_j \mathrm{e}^{-\mathrm{i}k_j x - \mathrm{i}\omega t} \tag{2}$$

where $k_j = \frac{\omega c_1}{c_j}$ is the non-dimensional wavenumber. The first term, the α-term, represents a right going wave and the second term, the β-term, represents a left going wave. Consequently, α and β shall henceforth be used to designate right and left going waves.

2.1. Floquet analysis

The matching conditions and Floquet periodicity conditions are formulated, according to the unit cell shown in Figure 1, see also [1, Ch. 8]:

$$u_1(1,t) = u_2(1,t) \tag{3a}$$

$$u_1'(1,t) = \frac{E_2 A_2}{E_1 A_1} u_2'(1,t) \tag{3b}$$

$$u_1(0,t) = u_2(1 + L_2/L_1, t)\lambda \tag{3c}$$

$$u_1'(0,t) = \frac{E_2 A_2}{E_1 A_1} u_2'(1 + L_2/L_1, t)\lambda \tag{3d}$$

where primes denote derivatives wrt. x and the parameter λ is the propagation constant. The nontrivial solution to the above system of equations exists when λ is a root of the characteristic equation:

$$\lambda^2 + q(\omega)\lambda + 1 = 0 \tag{4}$$

where:

$$q(\omega) = -2\cos(\omega)\cos(\tau\omega) + \left(\frac{1}{\kappa} + \kappa\right)\sin(\omega)\sin(\tau\omega) \tag{5}$$

in which $\tau = \frac{L_2}{c_2}\frac{c_1}{L_1}$ and $\kappa = \frac{E_2A_2/c_2}{E_1A_1/c_1} = \frac{\rho_2 c_2 A_2}{\rho_1 c_1 A_1}$ have been introduced. The parameter τ can be interpreted as the ratio of propagation times. It is defined at the outset that $\tau \leq 1$, since any waveguide configuration where $\tau \geq 1$ can be inverted to $\tau \leq 1$ simply by interchanging the segment numbering. The coefficient κ is the ratio of impedances of the two segments analog as the acoustic impedance $Z = \rho c$. We shall henceforth refer to κ as *impedance mismatch parameter*. Throughout the subsequent discussion the advantage of collecting all waveguide parameters in just the two quantities κ and τ becomes clear.

Inspection of the solution to the quadratic equation (4) reveals that $|q(\omega)| > 2$ (when the discriminant is positive) leads to $|\lambda| \neq 1$ and therefore defines a stop band. For an impedance matched rod, i.e. $\kappa = 1$, it is immediately noticed that $q(\omega)$ will never be larger than two and stop bands will therefore not be present.

3. Asymptotic analysis of stop band borders

The inequality $|q(\omega)| > 2$ is what predicts the formation of stop bands and this Section is devoted to gaining some understanding of this. We do this by establishing asymptotic results of stop band borders for small and large impedance mismatches, respectively.

3.1. Small impedance mismatch asymptotic approximations

First, we conveniently notice that for an impedance matched unit cell ($\kappa = 1$) $q(\omega)$ simplifies to:

$$q(\omega) = -2\cos(\omega + \tau\omega) \tag{6}$$

Thus $|q(\omega)| = 2$ at the frequencies:

$$\omega_{\text{crit}} = \frac{n\pi}{\tau + 1} \tag{7}$$

which we throughout the paper refer to as *critical frequencies*. Suppose now the rod has a small impedance mismatch, say $\kappa = 1+\epsilon$, then $q(\omega)$ breaks the barrier $|q(\omega)| = 2$ and a relatively narrow stop band is therefore generated in the vicinity of the critical frequency. This suggests asymptotic analysis of equation (5) for small perturbations of perfectly matched impedance.

Let us first define that ϵ is a small positive parameter and take $\kappa = 1+\epsilon$. Insertion of this in (5) and expanding leads to the relation

$$\pm 2 \sim -2\cos(\omega)\cos(\tau\omega) + \left(2 + \epsilon^2 - \epsilon^3 + \epsilon^4 + O(\epsilon^5)\right)\sin(\omega)\sin(\tau\omega)\ ,\ \epsilon \to 0 \tag{8}$$

The frequency is now expanded in the usual way:

$$\omega \sim \omega_0 + \epsilon\omega_1 + \epsilon^2\omega_2 + \epsilon^3\omega_3 + O(\epsilon^4) \quad \text{as} \quad \epsilon \to 0 \tag{9}$$

After inserting this in equation (8) and expanding the trigonometric functions for small ϵ, we compare terms of the same order, and find to leading order:

$$\epsilon^0 : \qquad \pm 2 = -2\cos((1+\tau)\omega_0) \quad \Rightarrow \quad \omega_0 = \frac{n\pi}{\tau+1} \tag{10}$$

which was known in advance. The $O(\epsilon)$ terms turn out to be identically zero when employing (10), but by balancing terms of $O(\epsilon^2)$, $O(\epsilon^3)$, and $O(\epsilon^4)$ the following is obtained:

$$\omega_1 = \pm(\tau+1)^{-1}\sqrt{\frac{1}{2} - \frac{1}{2}\frac{\cos\left(n\pi\frac{1-\tau}{1+\tau}\right)}{\cos(n\pi)}} \tag{11}$$

$$\omega_2 = \frac{\cos(\omega_0(1-\tau)) - \cos(n\pi) + (1-\tau)\omega_1\sin(\omega_0(1-\tau))}{4(1+\tau^2)\omega_1\cos(n\pi)} \tag{12}$$

$$\begin{aligned}\omega_3 = \Big[&\left(6 - 3(1+\tau)^2\omega_1^2 + (1+\tau)^4\omega_1^4 - 12(1+\tau)^2\omega_2^2\right)\cos(n\pi) + \\ &3\left((\tau-1)^2\omega_1^2 - 2\right)\cos((1-\tau)\omega_0) + 6(\tau-1)(\omega_1-\omega_2)\sin((1+\tau)\omega_0)\Big] \\ &/\left(24(1+\tau)^2\omega_1\cos(n\pi)\right)\end{aligned} \tag{13}$$

Further terms in the expansion (9) are trivial, but cumbersome and therefore not presented here. The result is consequently two versions of (9), stemming from the $\pm$ in (11), representing the left and right boundary of the stop

bands. The results are valid for any n each corresponding to a critical frequency from where a stop band develops.

The result of this analysis including up to $O(\epsilon^3)$ terms in (9) is shown in Figure 2 along with the direct numerical results obtained from (5) for $\tau = 1/3$. One may remark that for this value of τ it turns out that $\omega_1 = 0$ when $n = 4$ which effectively corresponds to a stop band of zero width. In fact for integral values of $1/\tau$ the $n = 1/\tau + 1$ critical frequency has a zero width stop band.

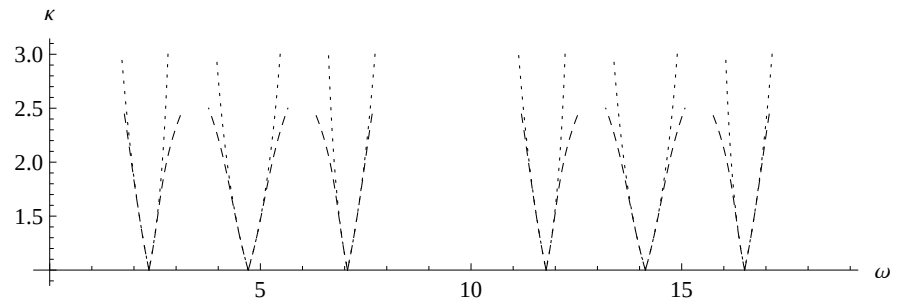

Figure 2: Borders of stop bands for $n = 1, 2, 3, 5, 6, 7$ for small impedance mismatch and $\tau = 1/3$. Dotted curve: exact results, Dashed curve: asymptotic results.

We may interpret the critical frequencies as the 'seeds' from where stop bands emerge when κ increases. This also means that the centre of a stop band will be found in the vicinity of $n\pi/(1+\tau)$, it can however be seen from Figure 2 that the stop bands at $n = 1, 3, 5, 7$ grow slightly asymmetric around their critical frequencies. But the critical frequency will always be contained in the stop band.

3.2. Large impedance mismatch asymptotic approximations

Similar to the above analysis it is possible to obtain some approximations for stop band borders when κ is large. Specifically we prescribe that $\kappa \sim 1/\epsilon$ as $\epsilon \to 0$. Again we expand the frequency by $\omega \sim \omega_0 + \epsilon\omega_1 + \epsilon^2\omega_2 + O(\epsilon^3)$ as $\epsilon \to 0$, and compare terms of same order. These yields:

$$O(\epsilon^{-1}): \qquad \sin(\omega_0)\sin(\tau\omega_0) = 0 \quad \Rightarrow \quad \omega_{0,1} = n\pi \quad \text{and} \quad \omega_{0,2} = m\pi/\tau \tag{14}$$

where n and m are integers. The leading order term $\omega_{0,2} = m\pi/\tau$ relates to the location of zero width stop bands in Figure 2. The other leading order term $\omega_{0,1}$ are the locations of the pass bands that are not adjacent to a zero

width stop band. It shall be demonstrated later that a different expansion of the frequency is required for $\omega_0 = \omega_{0,2}$ when $1/\tau$ is integral. For now we proceed as before and compare higher order terms and find:

$$O(1)\colon \omega_1 = \frac{\pm 2 + 2\cos(\omega_0)\cos(\tau\omega_0)}{\tau\cos(\tau\omega_0)\sin(\omega_0) + \cos(\omega_0)\sin(\tau\omega_0)} \tag{15}$$

$$\begin{aligned} O(\epsilon)\colon \omega_2 = {} & \frac{-2\tau\omega_1\cos(\omega_0)(\omega_1\cos(\tau\omega_0) + 2\sin(\tau\omega_0))}{2\tau\cos(\tau\omega_0)\sin(\omega_0) + \cos(\omega_0)\sin(\tau\omega_0)} \\ & + \frac{\sin(\omega_0)\left((1+\tau^2)\omega_1^2 - 2\right)\sin(\tau\omega_0) - 4\omega_1\cos(\tau\omega_0)}{\tau\cos(\tau\omega_0)\sin(\omega_0) + \cos(\omega_0)\sin(\tau\omega_0)} \end{aligned} \tag{16}$$

This approximation, including up to $O(\epsilon^2)$ terms in ω, are compared to the direct numerical results in Figure 3. A very appreciable correspondence is observed between the two results. The above expressions for ω_1 and ω_2 are seen to fail when $\omega_0 = \omega_{0,2}$ and $1/\tau$ is integral due to division by zero. The cause of the failure is seen from (14) where $\omega_0 = \omega_{0,2}$ turns out to be a double root. The encounter of double roots is often a sign of a challenging problem [24]. To overcome this difficulty we suggest an alternative expansion of ω:

$$\omega \sim \omega_{0,2} + \epsilon^{1/2}\omega_1 + \epsilon\omega_2 + \epsilon^{3/2}\omega_3 + O\left(\epsilon^2\right) \quad \text{as} \quad \epsilon \to 0 \tag{17}$$

Again by expanding the equation for $q(\omega)$ and compare terms of equal order do we find:

$$O(\epsilon^{-1/2}) \quad :0 \tag{18}$$

$$O(\epsilon^0)\colon \omega_1 = \pm\sqrt{\frac{\pm 2 + \cos(\omega_{0,2})\cos(\tau\omega_{0,2})}{\tau\cos(\omega_{0,2})\cos(\tau\omega_{0,2})}} \tag{19}$$

$$O(\epsilon^{1/2})\colon \omega_2 = 0 \tag{20}$$

$$O(\epsilon^1)\colon \omega_3 = \frac{(1+\tau^2)\omega_1(\tau\omega_1^2 - 6)}{12\tau} \tag{21}$$

These are valid only when $1/\tau$ is integral. The result is compared to the direct numerical solution in Figure 4 where terms of $O(\epsilon^{3/2})$ is included. Again, a very appreciable match is observed between the asymptotic approximations and the direct numerical solution.

In case the parameter $1/\tau$ is non-integral the stop band borders are all captured by the results in (14)-(16). Some of them, however, diverges from the correct result even for relatively large values of κ. This is illustrated in

Figure 5 where $1/\tau = 1/3.3$ is taken. Values of n and m corresponding to each leading order term in (14) are indicated as well. The left most stop band in the Figure have both $m = n = 0$ and ω_0 is therefore again a double root of (14) and this stop band border is therefore approximated by (17).

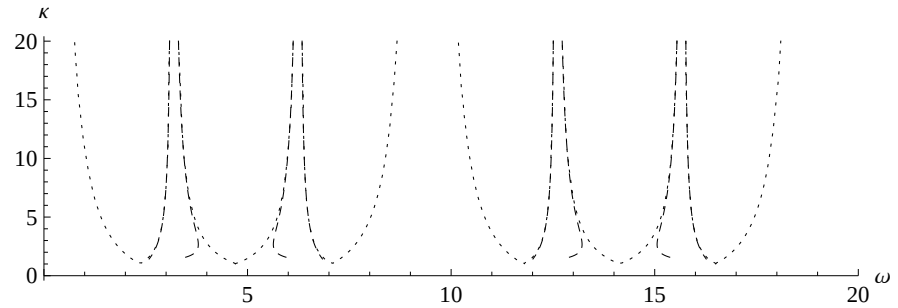

Figure 3: Borders of stop bands for $n = 1, 2, 4, 5$ for large impedance mismatch and $\tau = 1/3$. Dotted curve: exact results, Dashed curve: asymptotic results.

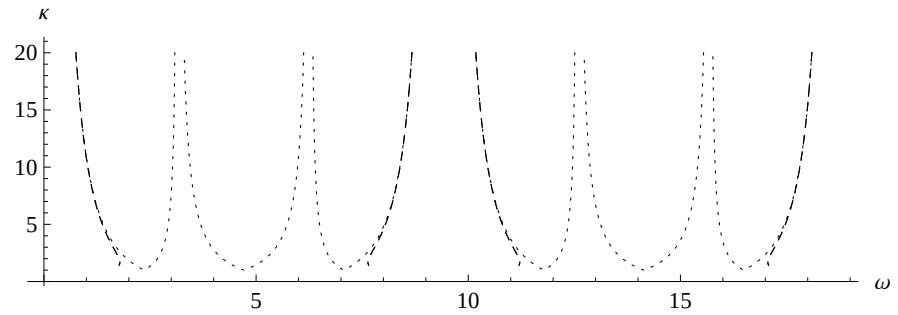

Figure 4: Borders of stop bands for $m = 0, 1, 2$ for large impedance mismatch and $\tau = 1/3$. Dotted curve: exact results, Dashed curve: asymptotic results.

We shall return to a more physical interpretation of the asymptotic formulae in Section 6.

4. Topology of stop band pattern

In this Section the topology of the stop band pattern is discussed. The solid and dashed lines in the subsequent plots correspond to the two roots of (4).

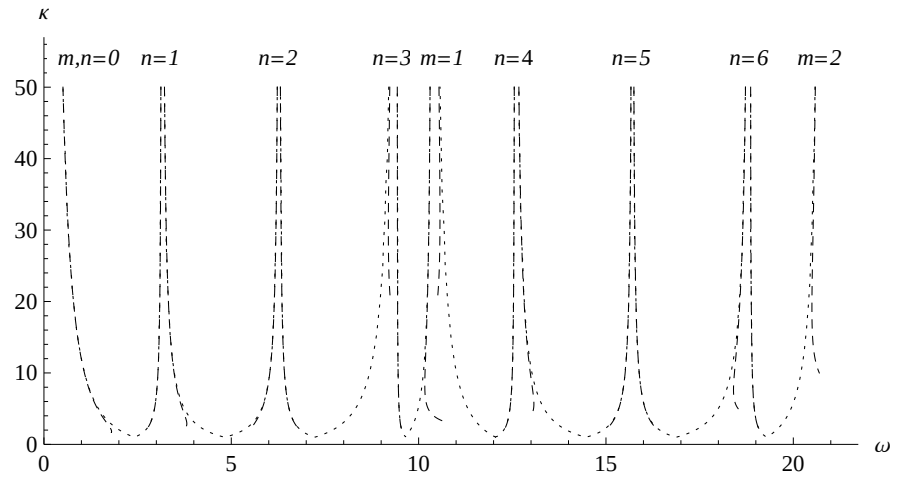

Figure 5: Borders of stop bands for large impedance mismatch with $\tau = 1/3.3$. Dotted curve: exact results, Dashed curve: asymptotic results. Parameters n and m are indicated.

4.1. Groups and group width

From parameter studies it is clear that for the model selected the stop bands form groups. We choose to define the width of such a group by

$$\Delta\omega_g = \frac{2\pi}{\tau} = 2\pi\frac{c_2}{L_2}\frac{L_1}{c_1} \tag{22}$$

Illustrations are provided in Figure 6-9 where the groups are clearly seen. Equation (22) is obtainable by considering the relative magnitude of the terms in (5). Unless $\kappa = 1$ the term $(1/\kappa+\kappa)\sin(\omega)\sin(\tau\omega)$ is the largest of $q(\omega)$ and furthermore since $\tau < 1$ then $(1/\kappa+\kappa)\sin(\tau\omega)$ forms an envelope of $\sin(\omega)$. The wave length of this envelope is $2\pi/\tau$.

There is an essential difference between the cases where $1/\tau$ is integral (Figure 6-8) compared to the case where $1/\tau$ is non-integral, shown in Figure 9. The size and location is preserved when comparing stop bands in the two halves of the groups for integral $1/\tau$. This is not the case when $1/\tau$ is non-integral. Consequently, the stop band groups are visually less obvious when $1/\tau$ is non-integral.

4.2. Number of stop bands in a group

In Section 3 it was discussed how the stop bands originate from the critical frequencies when an impedance mismatch is introduced. This effectively predicts the number of stop bands in a group from the simple inequality

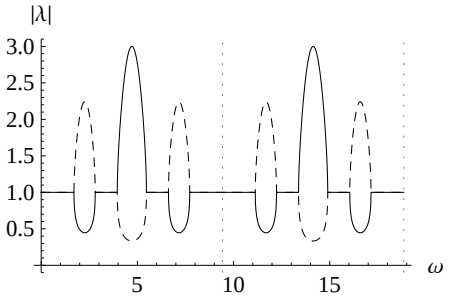

Figure 6: Stop band pattern with $\tau = 1/3$ and $\kappa = 1/3$. $\Delta\omega_g = 6\pi$. Vertical grid lines at 3π and 6π.

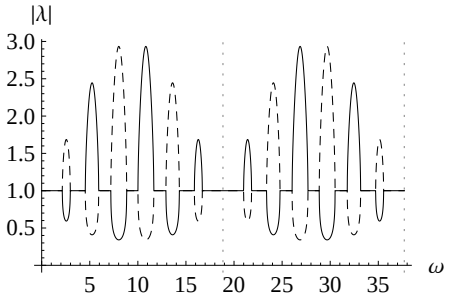

Figure 7: Stop band pattern with $\tau = 1/6$ and $\kappa = 1/3$. $\Delta\omega_g = 12\pi$. Vertical grid lines at 6π and 12π.

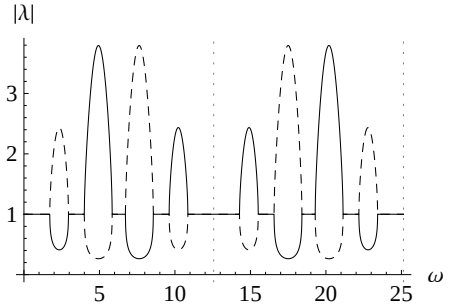

Figure 8: Stop band pattern with $\tau = 1/4$ and $\kappa = 1/4$. $\Delta\omega_g = 8\pi$. Vertical grid lines at 4π and 8π.

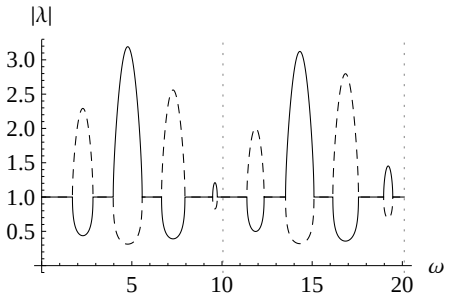

Figure 9: Stop band pattern with $\tau = 1/3.2$ and $\kappa = 1/3.2$. $\Delta\omega_g \approx 20.1$. Vertical grid lines at π/τ and $2\pi/\tau$.

$\omega_{\text{crit}} < \Delta\omega_g$. Thus, the number of stop bands in a group is the largest n satisfying:

$$n < 2\left(\tfrac{1}{\tau} + 1\right) \tag{23}$$

We know furthermore that these are found in the vicinity of the critical frequencies predicted by (7). It was ascertained earlier that some stop bands disappear when $1/\tau$ is integral. In this case the formula for the number of stop bands is:

$$n = \frac{2}{\tau} \tag{24}$$

5. Eigenfrequencies and Phase-closure Principle for periodic rods

Several papers have demonstrated the close relation between stop band borders and the eigenfrequencies of a single unit cell provided this is symmetric, see Figure 10. This matter is, for instance, discussed in [14] and [15], the former described the complicated wave motion in a beam with periodic supports, and the latter derived eigenfrequency formulae for the same structure incorporating the propagation constant. Considerations along these lines are expedient in the discussions of the topics in this paper. The rela-

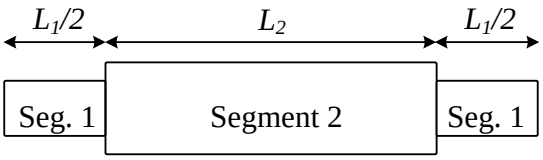

Figure 10: Symmetric configuration of unit cell.

tion between eigenfrequencies and the Floquet plot becomes apparent when comparing the discriminant of equation (4) to the eigenfrequency equations for the symmetric unit cell with free-free and fixed-fixed boundary conditions. By designating these eigenfrequency equations $f_{\text{free}}(\omega)$ and $f_{\text{fixed}}(\omega)$, it turns out that the following relation holds:

$$q^2(\omega) - 4 = \frac{-1}{16\kappa^2} f_{\text{free}}(\omega) f_{\text{fixed}}(\omega) \tag{25}$$

More details may be found in AppendixA. So the relation between eigenfrequencies and stop bands observed by [14] is therefore also present for the current model.

5.1. Determination of critical frequencies by phase-closure principle

An attractive method for determining eigenfrequencies of a unit cell is the *phase-closure principle*, as this likely leads to an important insight in the physics at the transition from stop to pass band. Before doing so, we shortly discuss the applicability of the method to the problem at hand. It is clear that the actual wave motion of a unit cell cannot be seen as a single harmonic due to the difference in wave speeds. Thus, the motion will either have to be interpreted as a superposition of a number of harmonics valid for all x, this view was adopted in [14]. Or alternatively, the wave motion can be rendered as consisting of piecewise harmonic waves pertaining to a certain segment. In the first case, it is not immediately obvious how the total phase

of the waves should be defined, but in the latter interpretation the notion of phase change over a segment is quite obvious. Consequently the total phase change can be established by summation of phase changes in each segment. In the following utilisation of the phase-closure principle we adopt the latter view of piecewise harmonic waves to construct the actual wave motion in a unit cell and shall refer to such a wave as a *compound wave*. In AppendixB we show the Fourier content of an eigenmode as a complementary view of how the wave motion is interpreted in this Section.

The phase-closure principle states that when the total phase change a wave experiences after completing a full circuit in a rod equals a multiple of 2π resonance occurs (see [25]). A simple way of stating the total phase change for, say, a free-free rod is $2K_1L_1 + 2K_2L_2$ where $K_j = k_j \frac{c_1}{L_1}$ is the dimensional wave number. This implicitly assumes an impedance match between the segments since any internal reflections at interfaces are ignored. Thus, the result must be expected to relate to the critical frequencies. The resonance condition in non-dimensional form therefore becomes:

$$2\omega \left(\frac{L_1 c_1}{c_1 L_1} + \frac{L_2 c_1}{c_2 L_1} \right) = 2\pi n \quad \Rightarrow \tag{26}$$

$$\omega = \frac{n\pi}{1+\tau} \tag{27}$$

So this way of stating the resonance condition of a unit cell leads to the critical frequencies and this is indeed an interesting result since it points out a simple way of determining where the stop bands appear. This also provides some understanding of the critical frequencies. From equation (26) we understand that the critical frequencies are those where n half compound waves fits into a unit cell and, therefore, there is a πn phase change after traversing the unit cell once. So basically the critical frequencies is the eigenfrequencies of a compound wave when $\kappa = 1$. This is basically the Bragg resonance condition, but with the wavelength defined with reference to the compound wave. Thus, the stop bands arise around the frequencies where reflections of waves are in phase and therefore will interference.

5.2. Determination of stop band borders by phase-closure principle

The concept behind the phase-closure principle can be used, however, in a slightly different way where account is taken of internal reflections. To do so we apply the systems of equations from AppendixA representing the free-free and fixed-fixed rods and remove the boundary equation concerning the left hand end of the rod. This results in two systems of five equations in the six unknowns $\alpha_{1,2,3}$ and $\beta_{1,2,3}$. When the reflected wave β_1 returns

back perfectly in phase with the incident wave α_1 (with the proper account of a possible phase change at the left edge of the rod) resonance occurs. The result for a free boundary condition is conveniently stated in terms of the parameters κ and τ:

$$\left(\frac{\beta_1}{\alpha_1}\right)_{\text{free}} = \frac{\mathrm{e}^{\mathrm{i}\omega}\left(1-\kappa^2-\mathrm{e}^{\mathrm{i}\omega}(-1+\kappa)^2+\mathrm{e}^{\mathrm{i}(1+2\tau)\omega}(1+\kappa)^2+\mathrm{e}^{2\mathrm{i}\tau\omega}\left(-1+\kappa^2\right)\right)}{(1+\kappa)^2+\mathrm{e}^{\mathrm{i}\omega}\left(-1+\kappa^2\right)-\mathrm{e}^{2\mathrm{i}\tau\omega}(-1+\kappa)\left(-1+\kappa+\mathrm{e}^{\mathrm{i}\omega}(1+\kappa)\right)} \tag{28}$$

A similar result for a fixed boundary condition can be determined as well. The quantities $\phi_{\text{free}} = \text{phase}(\beta_1/\alpha_1)_{\text{free}}$ and $\phi_{\text{fixed}} = \text{phase}(\beta_1/\alpha_1)_{\text{fixed}} - \pi$ (to account for the phase shift at the left boundary of the unit cell) are plotted in Figure 11 and 12. This enables the simple reading of eigenfrequencies being the locations where the curves pass the abscissa. One can remark in the latter Figure that the curves are lie on top of each other.

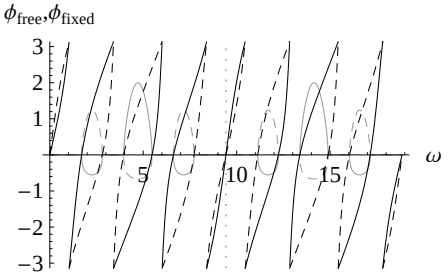

Figure 11: Solid line: ϕ_{free}, Dashed Line: ϕ_{fixed}. $\kappa = \tau = 1/3$. Grid line is located at 3π. Stop bands are shown in the background. Eigenfrequencies are located where the curves crosses zero.

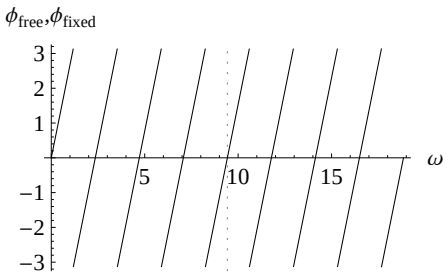

Figure 12: Solid line: ϕ_{free}, Dashed Line: ϕ_{fixed}. $\kappa = 1$ and $\tau = 1/3$. Grid line is located at 3π.

A skew symmetric behaviour is apparent from Figure 11 in the following way: a stop band in the first half of the group, i.e. below $\omega = \pi/\tau = 3\pi$, having a free-free eigenfrequency on its left border has a similar stop band in the upper half of the group, but with a free-free eigenfrequency on its right boundary - and vice versa. In fact what happens is that eigenfrequencies merge at $\omega = \pi/\tau$, as earlier mentioned, swap places between π/τ-$2\pi/\tau$ compared with 0-π/τ, merge and swap back when crossing $2\pi/\tau$. This pattern repeats itself for each multiple of $2\pi/\tau$. The quantities ϕ_{free} and ϕ_{fixed} of the impedance matched rod (Figure 12) are seen to be linear with frequency, and the eigenfrequencies are therefore evenly spaced and are predictable by formula (27).

6. Interpretation of results

As stated in Subsection 2.1 the origin of a stop band is due to an impedance mismatch between the segments and the width of the stop band increases with increasing impedance mismatch which was demonstrated in Section 3, see equation (5).

The results from the asymptotic analysis of small impedance mismatch hint at some finer details of the physics involved in the stop band creation. By means of the first two terms in the expansion of ω scaled to dimensional frequency we find stop bands in the intervals $\Omega_1 < \Omega < \Omega_2$ where

$$\Omega_{1,2} = \Omega_{\text{crit}} \left(1 \pm (\kappa - 1) \sqrt{\frac{1}{2} - \frac{1}{2} \frac{\cos\left(\Omega_{\text{crit}} \Delta t\right)}{\cos(\Omega_{\text{crit}} T)}} + O((\kappa - 1)^2) \right) \tag{29}$$

in which we have introduce $T = L_1/c_1 + L_2/c_2$, the time for a disturbance to traverse a unit cell, and $\Delta t = L_1/c_1 - L_2/c_2$ being the difference in propagation time in the two segments. The parameter Δt has the following physical significance: From a scattering process at the interface at x_n, see Figure 1, one wave will travel towards the x_{n-1} interface, reflect again and travel back towards x_n. Meanwhile will a wave travel from x_n to x_{n+1} and reflect back to x_n. In general there will be a time delay between arrival back to the x_n interface and Δt is exactly half this time delay or simply the time difference between arrival of the left and right going wave to the x_{n-1} and x_{n+1} interfaces, respectively. So we may interpret the quantity $\Omega_{\text{crit}} \Delta t$ as a 'phase loss' due to the time delay between waves reflecting back to an interface. So, what drives the creation of a stop band is the mismatch of impedances, $\kappa - 1 \neq 0$, alongside with this phase loss. With this in mind it is not difficult to imagine what happens physically in the case of zero width stop bands as discussed in Section 3. Since the phase loss grows with n the phase loss may add up to a complete circuit and no stop band is created.

From the large impedance mismatch asymptotic results we also get a hint of why the pass bands are maintained as $\kappa \to \infty$. As κ grows the width of the pass bands decreases like $2/\kappa$ and becomes just 'pass points' (rather than pass bands) in the limit, and are located at $\omega_{0,1} = n\pi$ and $\omega_{0,2} = \frac{m\pi}{\tau}$. By scaling these to dimensional quantities we find:

$$\Omega_{0,1} = n\pi \frac{c_1}{L_1} \tag{30}$$

$$\Omega_{0,2} = m\pi \frac{c_2}{L_2} \tag{31}$$

It is rapidly obtained that these are the eigenfrequencies, with boundaries either free or fixed, of segment 1 and segment 2, respectively. So when the impedance mismatch is large the relatively narrow pass bands appear around the eigenfrequencies of the individual segments. Opposite the interpretation of critical frequencies may we interpret the eigenfrequencies of the individual segments as the seeds from where a pass band emerges when κ decreases from infinity. This furthermore points out the reason for creation of groups as explained in Section 4. These are formed by the eigenfrequencies of the segment with the fastest propagation time, and the stop bands in such a group are hence constrained between the eigenfrequencies of the other segment.

It is expedient to discuss the reflection and transmission process at an interface in the case of a large impedance mismatch. Generally will a wave designated α_1 which is incident on an interface reflect a wave with amplitude $\beta_1 = -\frac{\kappa-1}{\kappa+1}\alpha_1$ and transmit a wave of amplitude $\alpha_2 = (1 - \frac{\kappa-1}{\kappa+1})\alpha_1$. In the case when $\kappa >> 1$ a wave propagating in segment 1 will be almost fully reflected, i.e. $\beta_1/\alpha_1 \approx -1$, when it is incident on the interface to segment 2. Consequently, the transmitted wave will be very small, $\alpha_2/\alpha_1 \approx 0$. I.e. the result basically corresponds to a fixed boundary condition. Explained in words, a wave becomes trapped in the small, compliant, and fast segment as it propagates back and forth and keeps being reflected when it meets the large, stiff, and slow segment.

From the above discussions we now know that it is a trivial matter to apply the phase-closure principle to determine:

- Locations of stop bands for small impedance mismatches as the critical frequencies.
- Locations of pass bands for large impedance mismatches as the eigenfrequencies of the individual segments.
- Borders of stop bands for any value of κ as the eigenfrequencies of the symmetric unit cell.

So the creation of stop and pass bands as explained above all correspond to creation of resonances of either the compound structure or the individual segments. As a final comment it is argued that higher stop band groups are just higher harmonic versions of the lowest stop band group. The reasoning behind this statement is that the stop bands are bounded by eigenfrequencies where the successive occurrences of these are higher harmonic phenomena compared to the first.

7. Steady-state and transient forced response of a rod with the periodic insert

The analysis reported in the previous Sections has been restrained to steady-state free waves in an infinitely long periodic waveguide. For any application, however, it is necessary to account for the finite length of a periodic segment, to specify its loading conditions, and to consider transients in its performance. These issues are tackled in this Section.

The attenuation levels predicted for the stop bands by means of the Floquet theory are known to be in an excellent agreement with the insertion losses for structures containing a few periodicity cells [26]. The insertion losses are commonly estimated as the ratio of the power flow into a structure without and with the periodic segment, $IL = 10\log(P_0/P_n)$. This formulation implies that the same force is applied at the same place and the same frequency on a structure with/without the insert and only the steady-state response is accounted for. Such a concept differs from the idea of solving the equation (4) to determine propagation constants for free waves. These constants, by definition, specify the ratio between the complex-valued axial displacements at two arbitrary cross-sections in a periodic rod provided that the distance between them equals the length of a periodicity cell. No forcing is involved in this definition.

Therefore, it is of interest to derive a transfer matrix for free incident waves of unit amplitude traversing an array of a finite number of periodicity cells, extended further out as a homogeneous rod, and to compare to the propagation constants for an infinite periodic structure. For consistency, the comparison should be extended to the stationary forcing problem for the same layout of a rod with the periodic insert. The transfer function in this case is derived as the complex-valued amplitude of the outgoing wave driven by a force of the unit amplitude at the inlet.

The derivation of transfer matrices is a straightforward matter, and the end results are illustrated in Figure 13 for the insert consisting of two periodicity cells. The parameters of these cells are the same as those used to in Figure 6. The complex-valued amplitudes of outgoing waves have been obtained in the closed analytical form by means of symbolic manipulator Mathematica, but the formulae are rather cumbersome, and, therefore, not presented here. The same holds true for the propagation constants found from equation (4), squared to account for traversing two periodicity cells. These constants are dependent only upon κ and τ, whereas their counterparts found from transfer matrices feature dependence upon κ, L_2/L_1 and c_1/c_2. However, the shapes of curves obtained for different L_2/L_1 and c_1/c_2

with τ being preserved are almost the same in the stop bands regions.

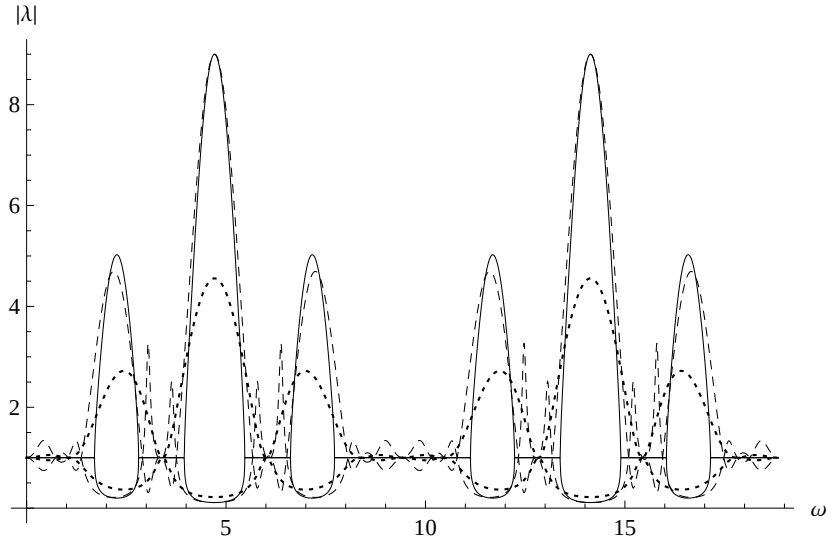

Figure 13: Solid lines: The Floquet propagation constants found for an insert consisting of two periodicity cells, Dashed lines: the transfer function from the forcing problem, Dotted lines: the transfer function for an incident wave of unit amplitude.

As seen from Figure 13, the solution of the forcing problem for just two periodicity cells agrees with predictions of the Floquet theory much better than the solution of the 'incident wave' problem. This result suggests that an assumption of the perfect source, employed in the forcing problem, mimics the interaction pattern of free waves in an infinite periodic structure quite accurate. The analysis of a structure of the transfer matrix of a single unit cell inserted in an infinite homogeneous waveguide lies beyond the scope of this paper.

Though substantial effort has been given to analysis of stationary wave motion in periodic structures, much less efforts have been made to study transient effects in such structures. The remaining part of this Section is devoted to such a study. As seen from Figure 13, the solution of the steady-state forcing problem agrees fairly well with results obtained for an infinite periodic structure. Therefore, it is reasonable to expect that the transients observed in solving the forcing problem in time domain with initial conditions represent their counterpart in an infinite periodic structure.

The Newmark integration scheme has been implemented in a finite element (FE) code with Newmark parameters $\gamma = 1/2$ and $\beta = 1/4$. The

element length is chosen so there are at least 10 elements per wave length, and the size of the time step is based on a Courant number of 1/5. The model, which is shown in Figure 14, is made with 6 symmetric unit cells connected to a semi-infinite rod in the right hand end modelled as an impedance boundary condition tuned to give no reflection when a wave is incident on it. The structure is excited at the left end by a harmonic force. All parameters are taken as unity, but with $c_2 = 3\text{m/s}$ corresponding to the stop band pattern in Figure 6. The excitation force is defined as $P(t) = \cos(\Omega t)$.

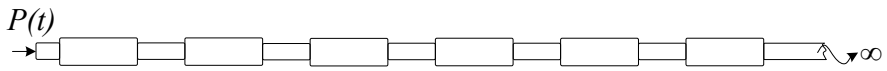

Figure 14: Periodic waveguide applied in the transient model.

To illustrate the wave attenuation from excitation in a stop band we provide in Figure 15 a plot of deflections determined from the FE code and the corresponding Floquet modes, determined from (3). The axial deflections are shown on the vertical axis and scaled with the deflections at $x = 0$. There is an appreciable similarity between the transient FE result and the Floquet mode in Figure 15 despite the fact that the Floquet mode assumes an infinite periodic structure and the FE results only includes six unit cells. The attenuation effect is also seen to arise even with a fairly small number of periodicity cells and already after traversing three unit cells is the attenuation significant.

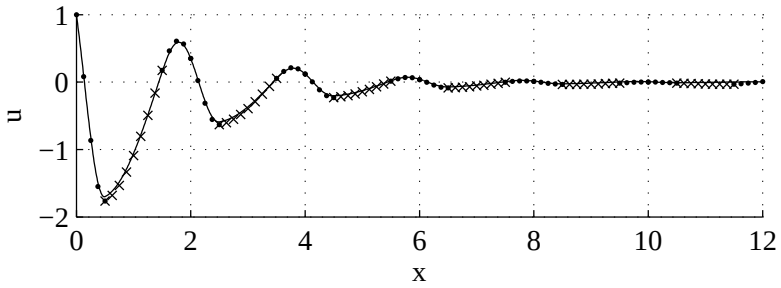

Figure 15: Deflections at $\Omega = 4.5046\text{rad/s}$ (a stop band) at $t = 250\text{s}$. Dots: segment 1, Crosses: segment 2, Solid line: deflections determined from Floquet analysis. SI units are used.

It is of interest to trace the work done by the excitation force, the energy flowing out of the structure, and thereby also the energy accumulated in the structure. This is done exactly at an eigenfrequency and in its near

proximity. Specifically, the eigenfrequency $\Omega_n = 5.5046$rad/s corresponding to a stop band border as seen in Figure 6, is selected. The results are provided in the Figures 16-18. As a first observation it is noticed that the solution becomes stationary which is achieved when the accumulated energy, the crosses, becomes constant. The largest amount of energy can be injected into the structure when excited at the eigenfrequency which leads to the largest energy accumulation. It seems intuitive that when the excitation is in the pass band more energy can leak out of the non-reflecting boundary condition since waves can now propagate through the structure. As a consequence hereof is the amount of accumulated energy smaller in Figure 18 compared to 17.

The underlying mechanism of the small energy injection when excitation is in a stop band, Figure 16, becomes clear when tracing the phase shift history between the velocity of the first node and the excitation force. These are given in Figure 19 and 20. Apparently the phase shift closes in on $-\pi/2$ and the excitation force can therefore not inject energy into the structure. One remarks that the power injection is:

$$P_{\text{in}} = \frac{1}{2} P V_1 \cos(\theta) \tag{32}$$

where θ is the phase angle between the excitation force P and nodal velocity V_1. So at phase shifts in the vicinity of $\pm\pi/2$ only very little power can be injected.

8. Conclusions

In this paper axial waves in a periodic Bernoulli-Euler rod have been analysed in order to facilitate the understanding of periodicity effects and stop bands. This has been done by Floquet analysis, asymptotic analysis, and by the phase-closure principle.

Two principle parameters, namely, the impedance mismatch and the ratio of propagation times, are introduced, and the relation of the stop band pattern with these parameters is explained and quantified. It is found, by application of the phase-closure principle, that the stop band locations are linked to the eigenfrequencies of an impedance matched symmetrical unit cell with symmetrical boundary conditions. It is also found that pass bands are always located at the eigenfrequencies of the individual segments with symmetrical boundary conditions regardless of the impedance mismatch. The

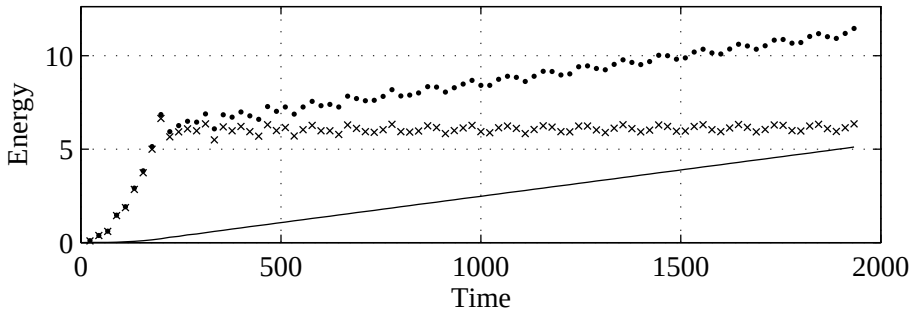

Figure 16: Energies when excited inside the stop band (at $\Omega = (5.5046 - 0.1)$rad/s). Dots: Energy in, Crosses: Energy accumulated, Solid line: Energy out. SI units are used.

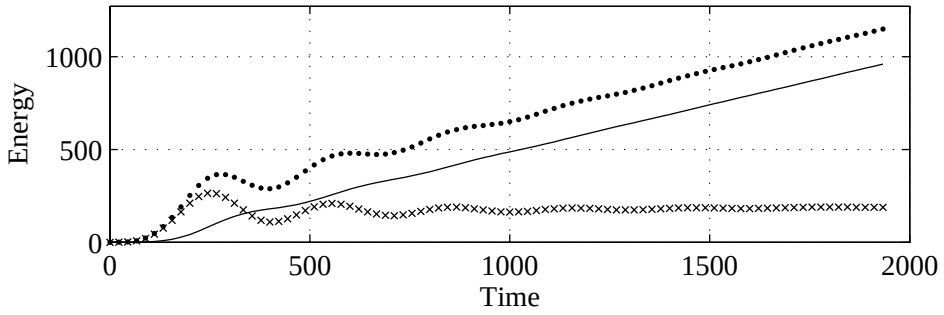

Figure 17: Energies when excited exactly at an eigenfrequency (at $\Omega = 5.5046$rad/s). Symbols are the same as in Figure 16.

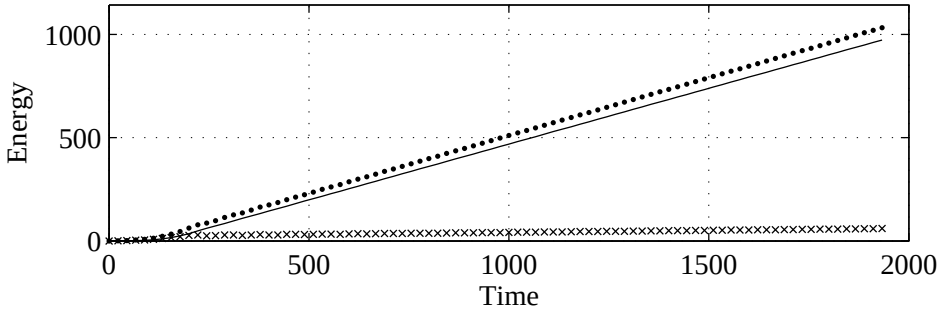

Figure 18: Energies when excited inside the pass band (at $\Omega = (5.5046 + 0.1)$rad/s). Symbols are the same as in Figure 16.

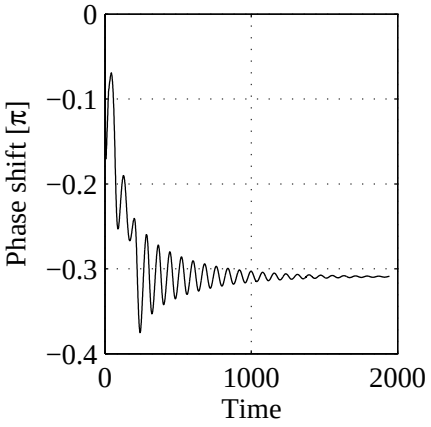

Figure 19: Phase shift between velocity of first node and excitation force at $\Omega = (5.5046 + 0.1)$rad/s (pass band).

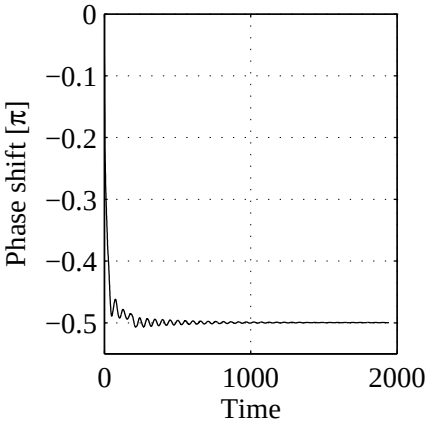

Figure 20: Phase shift between velocity of first node and excitation force at $\Omega = (5.5046 - 0.1)$rad/s (stop band).

exact location of stop band borders is determined numerically by the phase-closure principle applied in an untraditional manner, and simple asymptotic formulae for small and large impedance mismatch are derived.

The steady-state forcing problem for a rod with a periodic insert is solved in two formulations, and results are shown to be in agreement with Floquet analysis for an infinite rod. By transient FE analysis of harmonic forcing of a rod with the periodic insert it has been demonstrated that there is a significantly smaller energy injection into the structure when it is excited in a stop band compared to in a pass band. The reason for this is shown to be a $-\pi/2$ phase shift between excitation force and velocity response of the structure at the excitation point.

The relations given relating τ to the topology of stop band pattern backed up with the formulae from the asymptotic analysis points out a simple way of choosing the unit cell parameters to have stop bands where desired. Since only few unit cells are needed to have an appreciable wave attenuation, it is reasonable to suggest that broad band mechanical filters can be designed by combining different unit cells with overlapping stop band patterns. Such a design is achievable from the simple formulae presented in this paper.

Acknowledgement

The Research is funded by *The Danish Council for Independent Research, Technology and Production Sciences* Grant number: UK 95 OS63822 PO83004.

AppendixA. Derivation of eigenfrequency equations

Here we derive the frequency equations for the symmetric unit cell with free-free and fixed-fixed boundary conditions, and prove its relation to the Floquet discriminant. Referring to Figure 10 the matching equations at the interfaces are setup as

$$u_1(1/2) = u_2(1/2) \tag{A.1}$$

$$u_1'(1/2) = \frac{E_2A_2}{E_1A_1}u_2'(1/2) \tag{A.2}$$

$$u_2(1 + L_2/L_1) = u_3(1 + L_2/L_1) \tag{A.3}$$

$$\frac{E_2A_2}{E_1A_1}u_2'(1 + L_2/L_1) = u_3'(1 + L_2/L_1) \tag{A.4}$$

valid regardless of boundary condition. The boundary conditions are simply:

$$\text{free-free:} \qquad u_1'(0) = 0 \quad u_3'\left(1 + \tfrac{L_2}{L_1}\right) = 0 \tag{A.5}$$

$$\text{fixed-fixed:} \qquad u_1(0) = 0 \quad u_3\left(1 + \tfrac{L_2}{L_1}\right) = 0 \tag{A.6}$$

From here two systems of equations are setup and the frequency equations are then found as the nontrivial solutions of these. Specifically they read:

$$f_{\text{free}} = -4\mathrm{i}\left(2\kappa\cos(\tau\omega)\sin(\omega) + \left(-1 + \kappa^2 + \left(1 + \kappa^2\right)\cos(\omega)\right)\sin(\tau\omega)\right) \tag{A.7}$$

$$f_{\text{fixed}} = 4\mathrm{i}\left(2\kappa\cos(\tau\omega)\sin(\omega) + \left(1 - \kappa^2 + \left(1 + \kappa^2\right)\cos(\omega)\right)\sin(\tau\omega)\right) \tag{A.8}$$

The relation to stop bands may now be identified from the fact that:

$$\frac{q(\omega)^2 - 4}{f_{\text{free}}f_{\text{fixed}}} = \frac{-1}{16\kappa^2} \tag{A.9}$$

which is frequency independent and therefore do the two transcendental equations $q(\omega)^2 - 4$ and $f_{\text{free}}f_{\text{fixed}}$ share the same roots.

AppendixB. Fourier Decomposition

The analysis throughout the paper strongly implies that the complicated eigenfrequency spectrum in a unit cell arises due to the reflections happening at the interfaces between the segments. So, as earlier mentioned the resulting wave motion may be interpreted as a superposition of a large number of waves. This may be quantified by a Fourier decomposition on the mode shape. Such an analysis leads to the results in Figure B.21 where the first 10 Fourier coefficients are plotted for each wave number for the unit cell configuration in Figure 6. We choose to do this at the eigenfrequency located at $\omega_n \approx 5.47$. The mode shape, which is seen in Figure B.22, is symmetric about $x = (1 + L_2/L_1)/2$ and consequently is it necessary to extract only the cosine coefficients. The spatial frequency content now becomes clear.

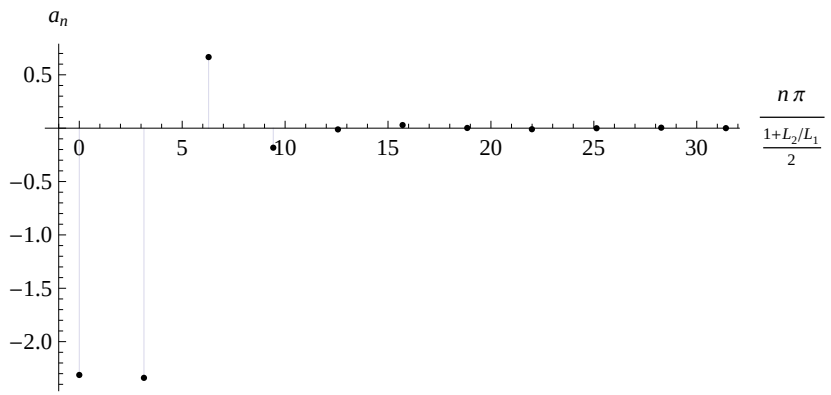

Figure B.21: Fourier cosine coefficient (a_n) at eigenfrequency $\omega_n = 5.47$ for free-free rod.

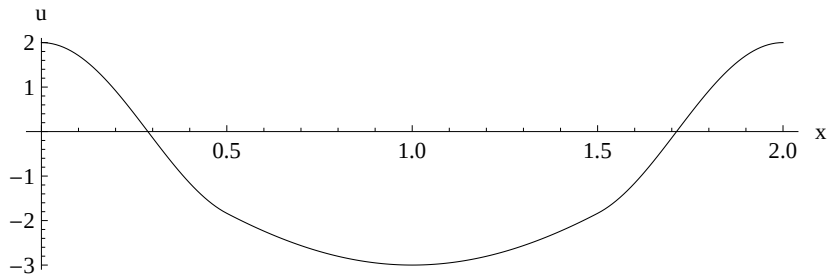

Figure B.22: Mode shape of free-free rod at $\omega_n = 5.47$

Firstly we notice that, as expected, the Fourier coefficients approach zero

rapidly as the wavenumber increases. The two actual wavenumbers at this frequency in the individual segments are $k_1 = 5.47$ and $k_2 = 1.82$ which is recognisable from the plot since the largest Fourier coefficients are found around these wavenumbers.

References

[1] L. Brillouin, Wave propagation in periodic structures, Dover Publications, 1946.

[2] O. R. Asfar, A. H. Nayfeh, The application of the method of multiple scales to wave propagation in periodic structures, Society for Industrial and Applied Mathematics 25 (1983) 455–480.

[3] Z.-Y. Tao, W.-Y. He, X. Wang, Resonance-induced band gaps in a periodic waveguide, Journal of Sound and Vibrations 313 (2008) 830–840. doi:10.1016/j.jsv.2007.11.055.

[4] Z. Tao, W. He, Y. Xiao, W. Zhang, X. Wang, Sound transmission within the bragg gap via the high-order modes in a waveguide with periodically corrugated walls, Journal of Applied Physics 105 (2009) 830–840. doi:10.1016/j.jsv.2007.11.055.

[5] V. A. Pogrebnyak, Non-bragg reflections in a periodic waveguide, Optics Communications 232 (2004) 201–207. doi:10.1016/j.optcom.2003.12.067.

[6] C. Elachi, Acoustic microwave generation in a periodic piezoelectric medium with drifting charges, Applied Physics 5 (1974) 159–164.

[7] P. Langlet, A.-C. Haldky-Hennion, J.-N. Decarpigny, Analysis of the propagation of plane acoustic waves in passive periodic materials using the finite element method, J. Acoust. Soc. Am. 98 (1995) 2792–2800. doi:10.1121/1.413244.

[8] C. G. Poulton, A. B. Movchan, R. C. McPhedran, N. A. Nicorivici, Y. Antipov, Eigenvalue problems for doubly periodic structures and phononic band gaps, Proc. R. Soc. Lond. A. 456 (2000) 2543–2559. doi:10.1098/rspa.2000.0624.

[9] A. El-Bahrawy, Stopbands and passbands for symmetric rayleigh-lamb modes in a plate with corrugated surface, Journal of Sound and Vibration 170 (1994) 145–160.

[10] S. Seshadri, Effect of periodic surface corrugation in the propagation of rayleigh waves, J. Acoust. Soc. Am. 65 (1978) 687–694.

[11] A. Boström, Surface waves on the periodic boundary of an elastic half space, Applied Scientific Research 39 (1982) 129–142. doi:10.1007/BF00457015.

[12] A. Boström, Acoustic waves in a cylindrical duct with periodically varying cross section, Wave Motion 5 (1983) 59–67. doi:10.1016/0165-2125(83)90007-0.

[13] J. S. Jensen, Phononic band gaps and vibrations in one- and two-dimensional mass-spring structures, Journal of Sound and Vibration 266 (2003) 1053–1078. doi:10.1016/S0022-460X(02)01629-2.

[14] D. J. Mead, Free wave propagation in periodically supported, infinite beams, Journal of Sound and Vibration 11 (1970) 181–197. doi:10.1016/S0022-460X(70)80062-1.

[15] G. S. Gupta, Natural flexural waves and the normal modes of periodically-supported beams and plates, Journal of Sound and Vibration 13 (1970) 89–101. doi:10.1016/S0022-460X(70)80082-7.

[16] A. Søe-Knudsen, S. Sorokin, Modelling of linear wave propagation in spatial fluid filled pipe systems consisting of elastic curved and straight elements, Journal of Sound and Vibration 329 (2010) 5116–5146. doi:10.1016/j.jsv.2010.06.015.

[17] S. G. Haslinger, N. V. Movchan, A. B. Movchan, R. C. McPhedran, Transmission, trapping and filterring of waves in periodically constrained elastic plates, Proc. R. Soc. Lond. A. 468 (2012) 76–93. doi:10.1098/rspa.2011.0318.

[18] M. M. Sigalas, E. N. Economou, Elastic and acoustic wave band structure, Journal of Sound and Vibration 158 (1992) 377–382. doi:10.1016/0022-460X(92)90059-7.

[19] D. J. Mead, Wave propagation in continuous periodic structures: Research contributions from southampton, 1964-1995, Journal of Sound and Vibration 190 (1996) 495–524. doi:10.1006/jsvi.1996.0076.

[20] N. Olhoff, B. Nui, G. Cheng, Optimum design of band-gap beam structures, International Journal of Solids and Structures 49 (2012) 3158–3169. doi:10.1016/j.ijsolstr.2012.06.014.

[21] A. Søe-Knudsen, Design of stop-band filter by use of curved pipe segments and shape optimization, Struct Multidisc Optim 44 (2011) 863–874. doi:10.1007/s00158-011-0691-2.

[22] R. D. Mindlin, An Introduction to the Mathematical Theory of Vibrations of Elastic Plates, World Scientific, 2006.

[23] J. S. Jensen, N. L. Pedersen, On maximal eigenfrequency separation in two-material structures: the 1d and 2d scalar cases, Journal of Sound and Vibration 289 (2006) 967–986. doi:10.1016/j.jsv.2005.03.028.

[24] E. J. Hinch, Perturbation Methods, Cambridge University Press, 1991.

[25] D. J. Mead, Waves and modes in finite beams: Application of the phase-closure principle, Journal of Sound and Vibration 171 (1994) 695–702. doi:10.1006/jsvi.1994.1150.

[26] A. Søe-Knudsen, S. Sorokin, R. Darula, Theoretical and experimental analysis of the stop-band behaviour of elastic springs with periodically discontinuous curvature, J. Acoust. Soc. Am. 132 (2012) 1378–1383. doi:10.1121/1.4740480.